Chapter 10

Negative Conductance Oscillators (Lasers)

Negative conductance oscillators are employed for amplifying and generating coherent electromagnetic fields in various frequency regions. The essential components of a negative conductance oscillator are a frequency-selective circuit, a device showing a negative differential conductance (gain), and a device with a nonlinear gain-saturation or amplitude-limiting function. Various frequency-selective circuits are used to form a high-Q cavity depending on an operation frequency, i.e., an LC circuit, delayed feedback loop, Fabry-Perot cavity, ring cavity, distributed feedback cavity, and many others. Usually, the negative differential conductance and the nonlinear characteristics are provided by the same device. Solid-state devices such as tunnel (Esaki) diodes, IMPATT diodes, Gunn diodes, and Josephson junctions are employed for a radio wave and microwave oscillators. Accelerated electron beams and inverted media are used as a negative differential conductance and nonlinear element for higher-frequency regions, including millimeter, sub-millimeter, infrared, optical, and XUV spectra.

In a typical coherent communication system, a transmitter consists of an oscillator, modulator, and post-amplifier. An oscillator generates a low-noise and frequency-stabilized electromagnetic wave. Information is encoded onto either the amplitude, frequency, or phase of the coherent carrier wave emitted from the oscillator. A post-amplifier compensates for the loss of the modulator and/or to boost the transmitted signal power. If frequency or phase modulation is employed, an injection-locked oscillator can be used as a post-amplifier. For example, a low-noise Gunn diode is used as an oscillator and a high-power IMPATT diode is used as an injection-locked oscillator (post-amplifier). The received signal is fed into a mixer with a coherent local oscillator wave in order to translate the carrier wave into an intermediate frequency (IF) signal or directly into a baseband signal. This mixing process has a frequency and mode filtering function and rejects background noise and cross-talk from other channels. A local oscillator is frequency stabilized and often phase-locked to the received signal. A phase-locked-loop (PLL) oscillator is employed for homodyne detection. Negative conductance oscillators can be used as free-running oscillators, injection-locked oscillators, and phase-locked-loop local oscillators in such a coherent communication system.

A negative conductance oscillator is described by the circuit shown in Fig. 10.1. An LC

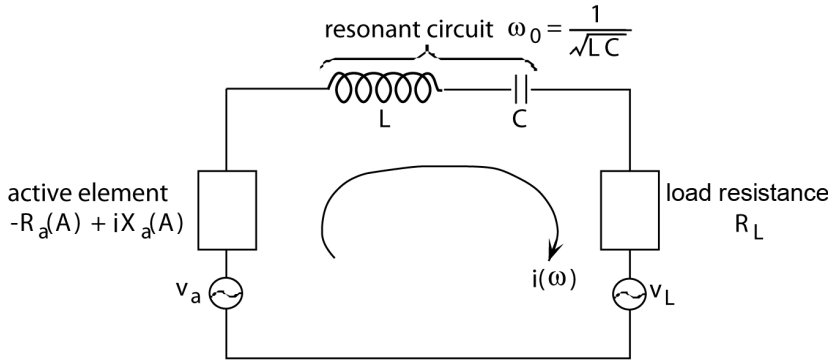

Figure 10.1: An electrical circuit model of a negative conductance oscillator.

series circuit represents a frequency-selective element. An active element with a negative differential conductance (gain) and a nonlinear gain saturation characteristic is represented by a complex impedance $-R_a + jX_a$, where the negative resistance $-R_a$ represents a saturable gain and the reactance X_a represents an associated dispersion. The active element should have an internal noise source represented by the noise voltage v_a. A positive resistance R_L represents a load resistance, which accounts for the output coupling loss from the oscillator. An external noise is fed into the oscillator through this load resistance and is represented by the noise voltage v_L. Finally, the oscillation field is represented by an internal AC current $i(\omega)$. van der Pol was the first to study the noise properties of such a negative conductance oscillator; thus, it is often referred to as the van der Pol oscillator.[1] Note that the circuit representation of the negative conductance oscillator in Fig. 10.1 is quite general. This simple model covers the fundamental performance and noise property of almost all negative conductance oscillators, including a laser oscillator.

10.1 Master Equation of a Laser Oscillator

Figure 10.2 shows a typical laser oscillator. Two high reflection mirrors constitute a Fabry-Perot cavity. The photon decay rate is expressed by $\frac{\omega}{Q} = \frac{c}{2L} \ln \frac{1}{R_1 R_2}$, where Q is a cavity Q-value, L is a cavity length and R_1, R_2 are the mirror reflectivities. An oscillation field and inverted medium are represented by the electric field $E(z,t)$ and the ensemble of atomic polarizations $P(z,t)$:

$$E(z,t) = \frac{1}{2} \sum_n E_n(t) e^{i(\omega_n t + \phi_n)} u_n(z) + C.C. \quad , \tag{10.1}$$

$$P(z,t) = \frac{1}{2} \sum_n P_n(t) e^{i(\omega_n t + \phi_n)} u_n(z) + C.C. \quad , \tag{10.2}$$

where n designates a longitudinal mode with a spatial mode function $u_n(z)$. We assume a single transverse mode operation. The Maxwell equation with a driving term is given

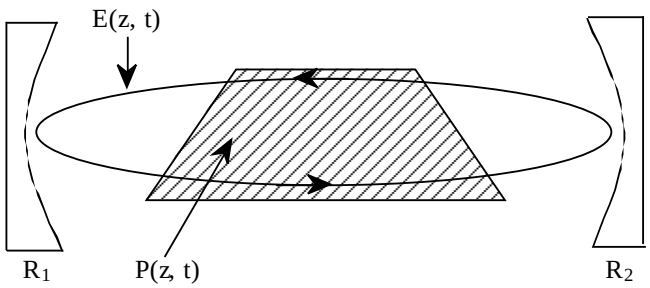

Figure 10.2: A laser oscillator with a Fabry-Perot cavity.

by[2],[3]

$$-\frac{\partial^2 E}{\partial z^2} + \mu_0\sigma\frac{\partial E}{\partial t} + \mu_0\varepsilon_0\frac{\partial^2 E}{\partial t^2} = -\mu_0\frac{\partial^2 P}{\partial t^2} \quad . \tag{10.3}$$

Using Eqs. (10.1) and (10.2) in Eq. (10.3), we have the equations of motion for the amplitude and phase of the oscillation field:

$$\dot{E}_n = -\frac{1}{2}\left(\frac{\omega_n}{Q}\right)E_n - \frac{1}{2}\left(\frac{\omega_n}{\varepsilon_0}\right)I_m(P_n) \quad , \tag{10.4}$$

$$\dot{\phi}_n = (\Omega_n - \omega_n) - \frac{1}{2}\left(\frac{\omega_n}{\varepsilon_0}\right)\frac{1}{E_n}Re(P_n) \quad , \tag{10.5}$$

where $\frac{\omega_n}{Q} = \frac{\sigma}{\varepsilon_0}$ is the photon decay rate, Ω_n is an empty cavity resonant frequency, and ω_n is an actual oscillation frequency. Equations (10.4) and (10.5) show that the in-phase component $Re(P_n)$ of the induced atomic dipole causes a dispersion and the quadrature-phase component $Im(P_n)$ of the dipole provides a gain. It is convenient to introduce an electric susceptibility $\chi_n = \chi_{nr} + i\chi_{ni}$ to represent a dipole,

$$P_n = \varepsilon_0\chi_n E_n = \varepsilon_0(\chi_{nr} + j\chi_{ni})E_n \quad . \tag{10.6}$$

Using Eq. (10.6) in Eq. (10.4) and Eq. (10.5), we have the laser master equation:

$$\dot{E}_n = -\frac{1}{2}\left(\frac{\omega_n}{Q}\right)E_n - \frac{1}{2}\omega_n\chi_{ni}E_n \quad , \tag{10.7}$$

$$\dot{\phi}_n = (\Omega_n - \omega_n) - \frac{1}{2}\omega_n\chi_{nr} \quad . \tag{10.8}$$

The steady state solutions of Eqs. (10.7) and (10.8) provide the threshold condition (gain = loss) and the oscillation frequency,

$$\frac{\omega_n}{Q} = \omega_n\chi_{ni} \quad , \tag{10.9}$$

$$\omega_n = \Omega_n - \frac{1}{2}\omega_n\chi_{nr} \quad . \tag{10.10}$$

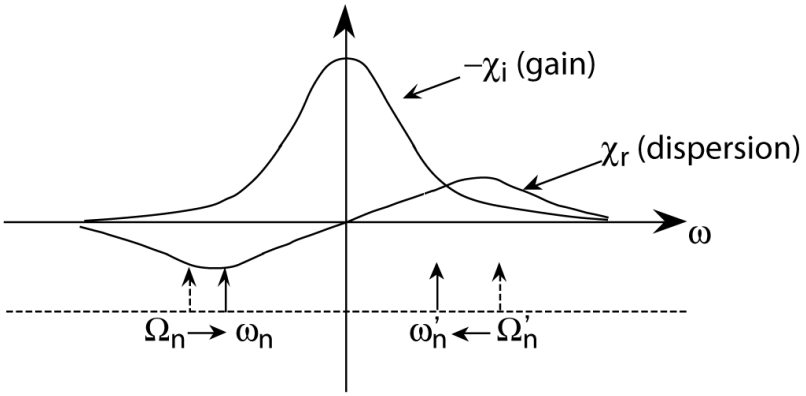

Figure 10.3: A complex electric susceptibility $\chi = \chi_r + i\ \chi_i$ of an inverted system.

The representative functions of χ_i and χ_r are shown in Fig. 10.3. Equation (10.10) indicates that the actual oscillation frequency ω_n is always pulled toward the gain center from an empty cavity frequency Ω_n due to the presence of the dispersion.

If the cavity internal electric field amplitude is normalized to represent a "photon amplitude", the stored energy is given by

$$E = \hbar\omega A_0^2 = \frac{1}{2} L A^2 \quad , \tag{10.11}$$

where A_0 is the photon field amplitude, $n = A_0^2$ is the photon number and A is the equivalent oscillation current amplitude in the LC circuit (Fig. 10.1), i.e. $I = A\cos(\omega t)$. From Eq. (10.11), the photon field amplitude A_0 and the equivalent current amplitude A are related by

$$A_0 = \sqrt{\frac{L}{2\hbar\omega}} A \quad . \tag{10.12}$$

The output optical power from the laser oscillator is given by

$$P_{\rm out} = \hbar\omega A_0^2 \left(\frac{\omega}{Q_{\rm ex}} \right) = \frac{1}{2} R_L A^2 \quad , \tag{10.13}$$

from which the photon decay rate is expressed as

$$\frac{\omega}{Q_{\rm ex}} = \frac{R_L}{L} \quad . \tag{10.14}$$

The internally generated optical power is given by

$$P_{\rm in} = \hbar\omega A_0^2 \omega\chi_i(A_0) = \frac{1}{2} R_a(A) A^2 \quad , \tag{10.15}$$

from which the photon amplification rate is expressed as

$$\omega\chi_i(A_0) = \frac{R_a(A)}{L} \quad . \tag{10.16}$$

The actual oscillation frequency is given by

$$\omega = \Omega - \frac{1}{2}\omega\chi_r(A_0) = \Omega - \frac{1}{2L}X_a(A) \quad , \tag{10.17}$$

from which the dispersion is expressed by

$$\omega\chi_r(A_0) = \frac{X_a(A)}{L} \quad . \tag{10.18}$$

Table 10.1 summarizes the one-to-one correspondence between the electrical circuit language and the quantum electronics language.

Table 10.1: Comparison of the electrical circuit language and quantum electronics language for a laser oscillator.

	Electrical circuit	Quantum electronics
Oscillation field amplitude	$\sqrt{\frac{L}{2}}A$	$\sqrt{\hbar\omega}A_0$
Photon decay rate	$\frac{R_L}{L}$	$\frac{\omega}{Q_{\text{ex}}}$
Photon amplification rate	$\frac{R_a(A)}{L}$	$\omega\chi_i(A)$
Dispersion	$\frac{X_a(A)}{L}$	$\omega\chi_r(A)$

10.2 Free-Running Van der Pol Oscillators

When the active element is pumped by an external energy source and a negative differential conductance is realized, the internal and external noise voltages, v_a and v_L, are amplified and the fluctuation frequency component of the current $i(\omega)$ near the LC circuit resonant frequency, $\omega_0 = \frac{1}{\sqrt{LC}}$, grows. This process is called "regenerative amplification." Once the negative resistance of the active element balances the positive load resistance, i.e. $R_a = R_L$, the circuit becomes unstable and the noise grows exponentially, purifying its spectral shape. The circuit starts to oscillate and the steady-state coherent field amplitude is established in the circuit. This steady-state condition is established by the gain-saturation

of the active element. In this way, the broadband noise, v_a and v_L, are transformed into a coherent wave with stabilized amplitude and a well-defined frequency. Frequency-selective amplification which purifies the spectral profile and gain saturation which stabilizes the amplitude are the two basic ingredients for a negative conductance oscillator.

The circuit equation (in complex representation) for the current $i(\omega)$ is given by[4],[5]

$$\left[R_L + i\left(\omega L - \frac{1}{\omega C}\right) - R_a + iX_a\right] i(\omega) = v_a(\omega) + v_L(\omega) \quad . \tag{10.19}$$

A time-dependent real current $i(t)$, which is a real part of $i(\omega)$, is expressed as

$$\begin{aligned} i(t) \equiv Re(i(\omega)) &= Re\left[(A + \Delta A)e^{i(\omega t + \Delta\phi)}\right] \\ &= [A + \Delta A(t)]\cos(\omega t + \Delta\phi(t)) \quad , \end{aligned} \tag{10.20}$$

where A and ω are the average amplitude and frequency of the oscillating current and $\Delta A(t)$ and $\Delta\phi(t)$ are slowly varying amplitude and phase fluctuations. The gain saturation of the active element is represented by

$$-R_a = \frac{-R_0}{1 + \beta A^2} \quad , \tag{10.21}$$

where $-R_0$ is the unsaturated negative differential resistance, which is proportional to the pump rate, and β is the saturation parameter.

If one assumes $\left|\frac{\Delta A}{A}\right| \ll 1$, one can linearlize R_a and X_a as follows:

$$R_a = R_a(A) + \frac{\partial R_a}{\partial A}\Delta A \quad , \tag{10.22}$$

$$X_a = X_a(A) + \frac{\partial X_a}{\partial A}\Delta A \quad . \tag{10.23}$$

Since an actual oscillation frequency ω is close to the LC circuit resonant frequency, one obtains

$$\omega L - \frac{1}{\omega C} = \frac{L}{\omega}\left(\omega^2 - \frac{1}{LC}\right) = \frac{L}{\omega}(\omega + \omega_0)(\omega - \omega_0) \simeq 2L(\omega - \omega_0) \quad . \tag{10.24}$$

Substituting Eqs. (10.20), (10.22), (10.23), and (10.24) into Eq. (10.19) and taking the real part of both sides of Eq. (10.19), one obtains

$$\begin{aligned} Re\Bigg\{\Bigg[&R_L - R_a(A) - \frac{\partial R_a}{\partial A}\Delta A + i2L(\omega - \omega_0) \\ &+ i\left(X_a(A) + \frac{\partial X_a}{\partial A}\Delta A\right)\Bigg](A + \Delta A)e^{i(\omega t + \Delta\phi)}\Bigg\} = v_a(t) + v_L(t) \quad . \end{aligned} \tag{10.25}$$

Replacing $i\Omega = i(\omega - \omega_0)$ by $\frac{d}{dt}$ and taking the time derivative $(A + \Delta A(t))e^{i(\omega t + \Delta\phi(t))}$, Eq. (10.25) is reduced to

$$\begin{aligned} Re\Bigg\{\Bigg[&R_L - R_a(A) + i2L\left(\omega - \omega_0 + \frac{X_a(t)}{2L}\right) + 2L\left(\frac{1}{A}\frac{d\Delta A}{dt} - \frac{1}{2L}\frac{\partial R_a}{\partial A}\Delta A\right) \\ &+ i2L\left(\frac{d\Delta\phi}{dt} + \frac{1}{2L}\frac{\partial X_a}{\partial A}\Delta A\right)\Bigg] Ae^{i(\omega t + \Delta\phi)}\Bigg\} = v_a(t) + v_L(t) \quad . \end{aligned} \tag{10.26}$$

If one ignores all fluctuation terms, i.e. $\Delta A(t) = \Delta\phi(t) = v_a(t) = v_L(t) = 0$, in Eq. (10.26), one has the following steady-state solutions:

$$R_L = R_a(A) = \frac{R_0}{1 + \beta A^2} \quad , \tag{10.27}$$

$$\omega = \omega_0 - \frac{X_a(A)}{2L} \quad . \tag{10.28}$$

From Eq. (10.27), the squared, steady-state oscillation amplitude is given by

$$A^2 = \frac{1}{\beta}\left(\frac{R_0}{R_L} - 1\right) \quad . \tag{10.29}$$

As shown in Fig. 10.4(a), the squared coherent oscillation amplitude builds up at an

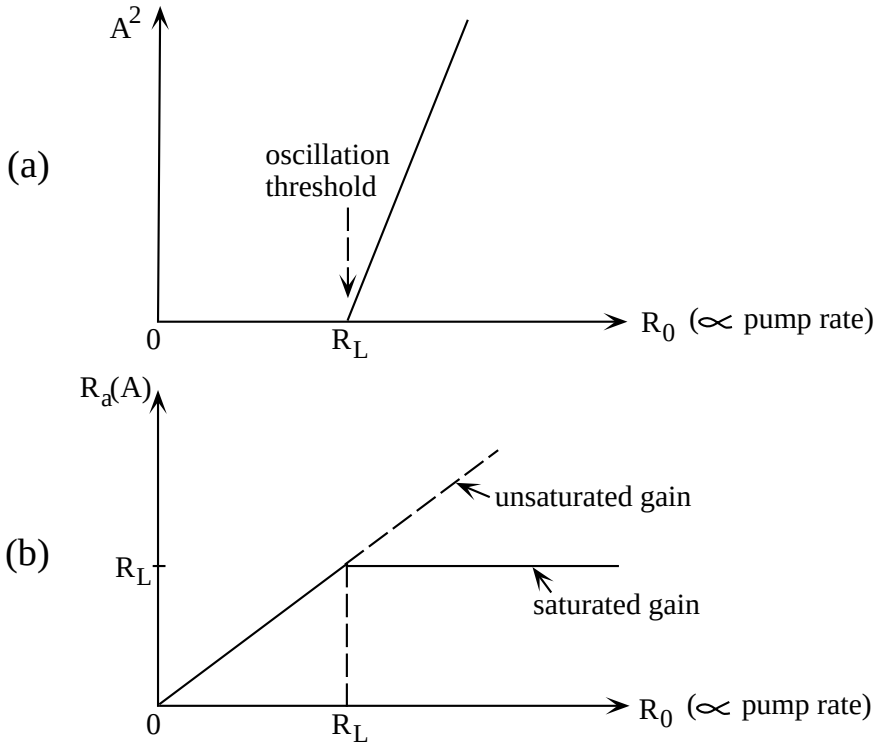

Figure 10.4: The oscillator power and saturated gain of a laser oscillator.

oscillation threshold, $R_0 = R_L$, and increases linearly with the pump rate (the unsaturated negative differential resistance R_0 is proportional to the pump rate). The negative differential resistance R_a linearly increases with the pump rate below the threshold and is clumped at the load resistance R_L above the threshold, as shown in Fig. 10.4(b). When the oscillation field increases above the steady-state value given by Eq. (10.29), the saturated gain decreases to below R_L and the circuit has a net loss. This results in the decrease in the oscillation field. On the other hand, when the oscillation field decreases below the

steady-state value, the saturated gain increases to above R_L. In this case, the circuit has a net gain and the oscillation field is amplified. In this way, the oscillation field amplitude and the saturated gain are simultaneously stabilized to their steady-state values. This nonlinear process is due to mutual coupling between the oscillation field and the active element and is termed "relaxation oscillation."

10.3 Amplitude and Phase Noise of an Internal Field

The small fluctuating parts in Eq. (10.26) are

$$\left(2L\frac{d}{dt}\Delta A - A\frac{\partial R_a}{\partial A}\Delta A\right)\cos(\omega t+\Delta\phi) - \left(2LA\frac{d}{dt}\Delta\phi + A\frac{\partial X_a}{\partial A}\Delta A\right)\sin(\omega t+\Delta\phi) = v_a(t)+v_L(t) \quad . \tag{10.30}$$

Multiplying Eq. (10.30) by $\cos(\omega t+\Delta\phi)$ or $\sin(\omega t+\Delta\phi)$ and integrating over one period of oscillation, $T=\frac{2\pi}{\omega}$, one has

$$2L\frac{d}{dt}\Delta A - A\frac{\partial R_a}{\partial A}\Delta A = \frac{\omega}{\pi}\int_{t-\frac{\pi}{\omega}}^{t+\frac{\pi}{\omega}}(v_a(t')+v_L(t'))\cos(\omega t'+\Delta\phi)dt' = v_{ac}+v_{Lc} \quad , \tag{10.31}$$

$$2LA\frac{d}{dt}\Delta\phi + A\frac{\partial X_a}{\partial A}\Delta A = -\frac{\omega}{\pi}\int_{t-\frac{\pi}{\omega}}^{t+\frac{\pi}{\omega}}(v_a(t')+v_L(t'))\sin(\omega t'+\Delta\phi)dt' = -(v_{as}+v_{Ls}) \quad . \tag{10.32}$$

Here, $v_{ac}(v_{Lc})$ and $v_{as}(v_{Ls})$ are the cosine and sine components of the internal (external) noise voltages,

$$v_a(t) = v_{ac}\cos(\omega t+\Delta\phi) + v_{as}\sin(\omega t+\Delta\phi) \quad ,$$

$$v_L(t) = v_{Lc}\cos(\omega t+\Delta\phi) + v_{Ls}\sin(\omega t+\Delta\phi) \quad .$$

A resistive saturation parameter s and reactive saturation parameter r are introduced and defined by

$$s \equiv -\frac{A}{R_a(A)}\frac{\partial R_a}{\partial A} \quad , \tag{10.33}$$

$$r \equiv \frac{A}{R_a(A)}\frac{\partial X_a}{\partial A} \quad . \tag{10.34}$$

If one uses Eq. (10.21) for saturated gain, the resistive saturation parameter is given by

$$s = \frac{2\beta A^2}{1+\beta A^2} = \begin{cases} 0 & : \beta A^2 \ll 1 \quad \text{(just above threshold)} \\ 2 & : \beta A^2 \gg 1 \quad \text{(far above threshold)} \end{cases} \quad . \tag{10.35}$$

Equations (10.31) and (10.32) are rewritten using Eqs. (10.33) and (10.34) as

$$\frac{d}{dt}\Delta A + \frac{sR_L}{2L}\Delta A = \frac{1}{2L}(v_{ac}+v_{Lc}) \quad , \tag{10.36}$$

$$\frac{d}{dt}\Delta\phi + \frac{rR_L}{2LA}\Delta A = -\frac{1}{2LA}(v_{as}+v_{Ls}) \quad . \tag{10.37}$$

The amplitude noise ΔA is caused by the cosine components of the internal and external noise voltages and is suppressed with the decay rate $\frac{s}{2}\frac{R_L}{L} = \frac{s}{2}\left(\frac{\omega}{Q_e}\right)$, where Q_e is a Q factor due to output coupling loss and $\frac{\omega}{Q_e}$ is the associated photon decay rate. The gain saturation represented by the resistive saturation parameter s operates as a restoring force for the amplitude. On the other hand, there is no restoring force for the phase. The phase noise $\Delta\phi$ is caused by the sine components of the internal and external noise voltages and also driven by the amplitude noise via the reactive saturation parameter. Therefore, the phase of a free-running oscillator diffuses via a random walk, while the amplitude is stabilized to its steady-state value. This effect is shown schematically in Fig. 10.5.

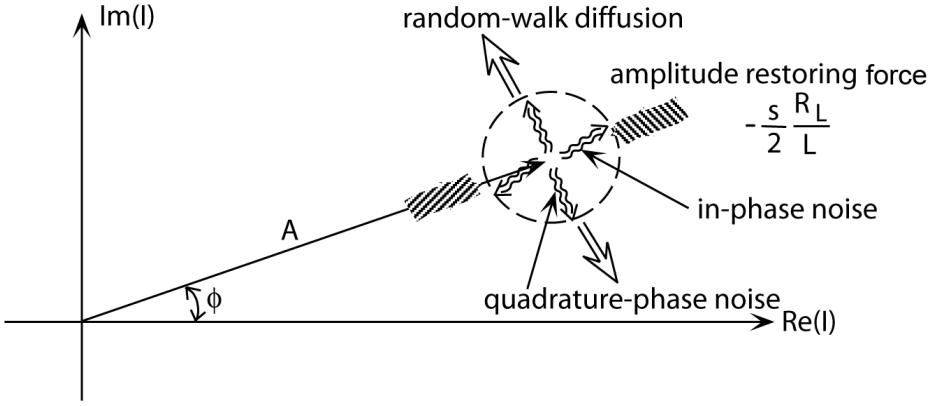

Figure 10.5: The noise driving forces of a laser oscillator.

Fourier analysis of Eqs. (10.36) and (10.37) results in the power spectral densities of ΔA and $\Delta\phi$:

$$S_{\Delta A}(\Omega) = \frac{1}{s^2 R_L^2} \cdot \frac{S_{ac}(\Omega) + S_{Lc}(\Omega)}{1 + (\Omega/\Omega_c)^2} \quad , \tag{10.38}$$

$$S_{\Delta\phi}(\Omega) = \frac{\left(\frac{\omega}{Q_e}\right)^2}{4A^2 R_L^2 \Omega^2} \left[S_{as}(\Omega) + S_{Ls}(\Omega)\right] + \frac{\left(\frac{r}{s}\right)^2 \left(\frac{\omega}{Q_e}\right)^2}{4A^2 R_L^2 \Omega^2} \cdot \frac{S_{ac}(\Omega) + S_{Lc}(\Omega)}{1 + (\Omega/\Omega_c)^2} \quad . \tag{10.39}$$

Here, the noise bandwidth Ω_c is given by

$$\Omega_c = \frac{s}{2}\left(\frac{\omega}{Q_e}\right) = \begin{cases} 0 & : \beta A^2 \ll 1 \qquad \text{(just above threshold)} \\ \dfrac{\omega}{Q_e} & : \beta A^2 \gg 1 \qquad \text{(far above threshold)} \end{cases} \quad . \tag{10.40}$$

Figure 10.6 shows the amplitude noise spectra for various pump rates. At far above threshold, the amplitude noise spectrum is reduced to

$$S_{\Delta A}(\Omega) = \frac{1}{4R_L^2} \cdot \frac{S_{ac}(\Omega) + S_{Lc}(\Omega)}{1 + \left(\Omega/\frac{\omega}{Q_e}\right)^2} \quad . \tag{10.41}$$

Let us consider the two limiting cases:

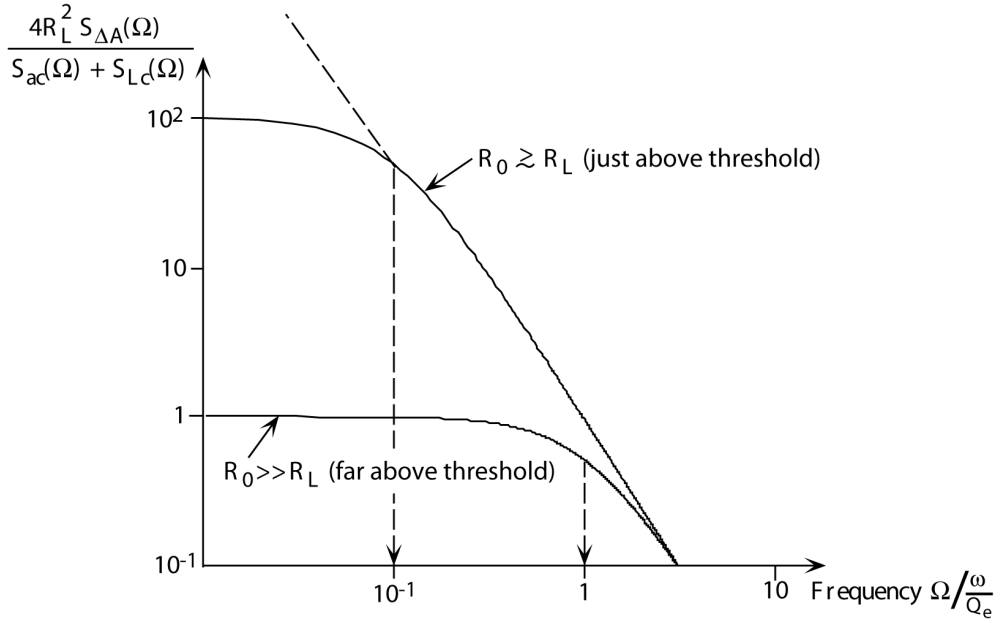

Figure 10.6: The amplitude noise spectra of a laser oscillator.

(1) Quantum Limit: $S_{ac}(\Omega) = S_{Lc}(\Omega) = 4\hbar\omega R_L$

Both internal and external noise voltages are limited by a quantum mechanical zero-point fluctuation. An ideal laser oscillator is such an example. The amplitude noise spectrum for this case is

$$S_{\Delta A}(\Omega) = \frac{\frac{2\hbar\omega}{R_L}}{1 + \left(\Omega / \frac{\omega}{Q_e}\right)^2} \quad . \tag{10.42}$$

(2) Thermal Limit: $S_{ac}(\Omega) = S_{Lc}(\Omega) = 8k_BTR_L$

Both internal and external noise voltages are limited by Johnson-Nyquist thermal noise. An ideal microwave oscillator is such an example. The amplitude noise spectrum for this case is

$$S_{\Delta A}(\Omega) = \frac{\frac{4k_BT}{R_L}}{1 + \left(\Omega / \frac{\omega}{Q_e}\right)^2} \quad . \tag{10.43}$$

The stored energy inside the LC circuit is given by

$$\frac{1}{2}LA^2 = \hbar\omega n \quad , \tag{10.44}$$

where n is the number of oscillator photons. Therefore, the spectrum of the photon number

is

$$S_{\Delta n}(\Omega) = \left(\frac{LA}{\hbar\omega}\right)^2 S_{\Delta A}(\Omega) = \begin{cases} 4n \cdot \dfrac{\left(\frac{\omega}{Q_e}\right)^{-1}}{1+\left(\Omega/\frac{\omega}{Q_e}\right)^2} & : \text{Quantum limit} \\ 4n\left(\dfrac{2k_BT}{\hbar\omega}\right)\dfrac{\left(\frac{\omega}{Q_e}\right)^{-1}}{1+\left(\Omega/\frac{\omega}{Q_e}\right)^2} & : \text{Thermal limit} \end{cases} . \tag{10.45}$$

Therefore, the variance in the photon number $\langle \Delta n^2 \rangle$ is calculated by the Parseval theorem:

$$\langle \Delta n^2 \rangle \equiv \int_0^\infty S_{\Delta n}(\Omega)\frac{d\Omega}{2\pi} = \begin{cases} n & : \text{Quantum limit} \\ 2nn_{\text{th}} & : \text{Thermal limit} \end{cases} . \tag{10.46}$$

The van der Pol oscillator in the quantum limit has a Poissonian photon number distribution at far above threshold, for which the variance $\langle \Delta n^2 \rangle$ is equal to the mean n. On the other hand, the variance of the photon number in the thermal limit is larger than the Poisson limit by a factor of $2n_{\text{th}} = 2\,(k_BT/\hbar\omega)$, where n_{th} is the number of thermal photons.

Figure 10.7 shows the phase noise spectra for various pump rates. The phase noise

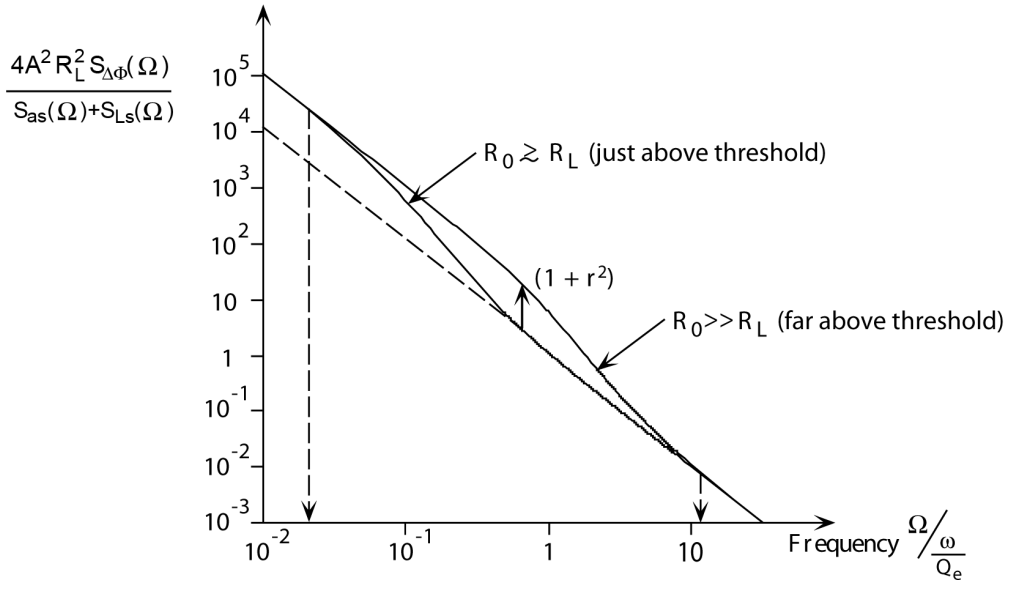

Figure 10.7: The phase noise spectra of a laser oscillator.

spectral density diverges in the zero frequency limit, $S_{\Delta\phi}(\Omega \to 0) \to \infty$, which is the characteristic of a Wiener-Lévy process and originates from the fact that there is no restoring force for a phase. When $r = 0$ and at a quantum limit, the phase noise spectral

density is

$$S_{\Delta\phi}(\Omega) = \frac{\left(\frac{\omega}{Q_{\rm ex}}\right)}{A_0^2\Omega^2} \quad . \tag{10.47}$$

A laser has a coherent photon field A_0 inside a cavity, into which a random-phase spontaneous emission is coupled. The rate of spontaneous emission coupling into a laser mode is equal to $A = \frac{\omega}{Q_{\rm ex}}$, because the stimulated emission rate B per photon must be equal to the cavity decay rate $\frac{\omega}{Q_{\rm ex}}$ at above the threshold and the spontaneous emission rate A into a laser mode must be equal to the stimulated emission rate B for one photon (Einstein's relation). One-half of the spontaneous photons have a quadrature phase with respect to the laser field and causes a phase diffusion. The phase jump per one spontaneous photon with a quadrature phase is equal to $\Delta\phi = 1/A_0$ and the rate of such a phase jump is given by $\frac{1}{2}\left(\frac{\omega}{Q_{\rm ex}}\right)[1/s]$. From this simple argument, we obtain the expression for a random walk phase diffusion over a time interval t:

$$\overline{\Delta\phi^2} = \frac{1}{A_0^2} \times \frac{1}{2}\left(\frac{\omega}{Q_{\rm ex}}\right) t \equiv 2D_\phi t \quad , \tag{10.48}$$

from which we have the phase diffusion constant,

$$D_\phi = \frac{\left(\frac{\omega}{Q_{\rm ex}}\right)}{4A_0^2} = \frac{1}{4}\lim_{\Omega\to 0}\left[\Omega^2 S_{\Delta\phi}(\Omega)\right] \quad . \tag{10.49}$$

If we define an instantaneous frequency by

$$\Delta\omega(t) = \frac{d}{dt}\Delta\phi(t) \quad , \tag{10.50}$$

the frequency noise spectrum is given by

$$\begin{aligned} S_{\Delta\omega}(\Omega) &= \Omega^2 S_{\Delta\phi}(\Omega) \\ &= \frac{\left(\frac{\omega}{Q_{\rm ex}}\right)^2}{4A^2R_L^2}\left[S_{as}(\Omega) + S_{Ls}(\Omega)\right] + \frac{\left(\frac{r}{s}\right)^2\left(\frac{\omega}{Q_{\rm ex}}\right)^2}{4A^2R_L^2}\cdot\frac{\left[S_{ac}(\Omega) + S_{Lc}(\Omega)\right]}{1+(\Omega/\Omega_c)^2} \quad . \end{aligned} \tag{10.51}$$

In contrast to the phase noise, the frequency noise is a statistically stationary process and has a finite spectral density at $\Omega = 0$.

The frequency noise enhancement factor appeared in Eq. (10.51) is expressed by

$$\begin{aligned} \frac{r}{s} &\equiv \left(\frac{A}{R_a(A)}\frac{\partial X_a}{\partial A}\right) / \left(-\frac{A}{R_a(A)}\frac{\partial R_a}{\partial A}\right) \\ &= -\left(\frac{\partial X_a}{\partial A}\right) / \left(\frac{\partial R_a}{\partial A}\right) \\ &= -\left(\frac{\partial \chi_r}{\partial A_0}\right) /. \left(\frac{\partial \chi_i}{\partial A_0}\right) \quad . \end{aligned} \tag{10.52}$$

This parameter is often referred to as a linewidth enhancement factor or Henny's α parameter.[3],[5]

10.4 Spectral Linewidth

The oscillator circuit impedance is calculated from Eq. (10.19) as

$$Z(\omega) = 2L\left[\frac{1}{2}\frac{\omega}{Q} + i(\omega - \omega_0^{'})\right] \quad , \tag{10.53}$$

where $\omega_0^{'} = \omega_0 - \frac{X_a(A)}{2L}$ is the actual oscillation frequency, ω_0 is the cold cavity resonant frequency, and Q is the effective (or active) Q value defined by

$$\frac{\omega}{Q} \equiv \frac{\omega}{Q_e} - \frac{\omega}{Q_a} = \frac{R_L}{L} - \frac{R_a(A)}{L} \quad . \tag{10.54}$$

The spectral profile of the oscillating current $i(\omega)$ is calculated by

$$\overline{|i(\omega)|^2} = \frac{S_{v_a}(\omega_0^{'}) + S_{v_L}(\omega_0^{'})}{4L^2\left[\frac{1}{4}\left(\frac{\omega}{Q}\right)^2 + (\omega - \omega_0^{'})^2\right]} \quad . \tag{10.55}$$

Since $S_{v_a}(\omega_0^{'})$ and $S_{v_L}(\omega_0^{'})$ are slowly-varying functions of $\omega_0^{'}$ and can be considered constant where the denominator is not very large, the spectral profile Eq. (10.55) is Lorentzian with a full-width at half-maximum (FWHM)

$$\Delta\omega_{1/2} = \frac{\omega}{Q} \quad . \tag{10.56}$$

(1) Below the Oscillation Threshold

In this case, gain saturation is negligible, $R_a(A) \simeq R_0$, and thus one obtains

$$\Delta\omega_{1/2} = \frac{\omega}{Q_e}\left(1 - \frac{R_0}{R_L}\right) \quad . \tag{10.57}$$

The spectral linewidth decreases linearly with the difference $(R_L - R_0)$ between the threshold pump rate and the actual pump rate.

(2) Above the Oscillation Threshold

In the earlier discussion about the steady-state solution, the saturated gain $R_a(A)$ was made equal to the loss R_L. This is not exactly the case because an actual oscillator has internal and external noise sources. The saturated gain $R_a(A)$ is always slightly smaller than the loss R_L; that is, an actual oscillator has a small "net loss" even above the threshold, as shown in Fig. 10.8. The steady-state oscillation field is maintained in spite of a "net loss" because the internal and external noise powers are coupled into the oscillator and compensate for the net loss. By increasing the noise powers coupled into the oscillator, the "net loss," $R_L - R_a(A)$, increases and the spectral linewidth becomes broader.

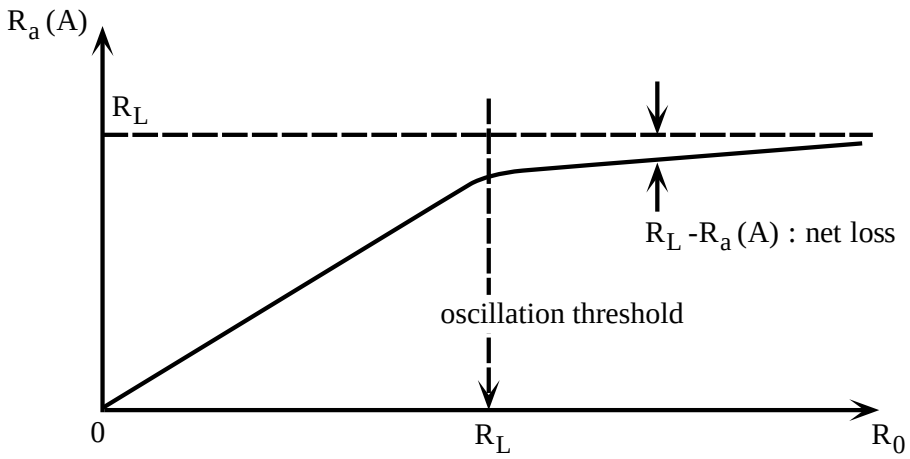

Figure 10.8: The saturated gain $R_a(A)$ vs. pump rate R_0 of a laser oscillator.

In order to evaluate the saturated gain and the linewidth, let us calculate the total emitted power by

$$\begin{aligned} P_e &= R_L \int_0^\infty \overline{|i(\omega_0')|^2} \frac{d\omega}{2\pi} \\ &= \frac{R_L}{4L^2\left(\frac{\omega}{Q}\right)} \left[S_{v_a}(\omega_0') + S_{v_L}(\omega_0')\right] \quad . \end{aligned} \tag{10.58}$$

Let us consider the two limiting cases:

(2-A) Quantum Limit: $S_{v_a}(\omega_0') = S_{v_L}(\omega_0') = 2\hbar\omega_0' R_L$

$$\Delta\omega_{1/2} \equiv \frac{\omega}{Q} = \frac{\hbar\omega_0' \left(\frac{\omega}{Q_e}\right)^2}{P_e} \quad . \tag{10.59}$$

If one uses $\Delta\nu_{1/2} = \frac{1}{2\pi}\Delta\omega_{1/2}$ and $\Delta\nu_c = \frac{1}{2\pi}\left(\frac{\omega}{Q_e}\right)$, one obtains

$$\Delta\nu_{1/2} = \frac{2\pi h\nu_0'(\Delta\nu_c)^2}{P_e} \quad . \tag{10.60}$$

This is the Schawlow-Townes linewidth for a laser oscillator.[6]

(2-B) Thermal Limit: $S_{v_a}(\omega_0') = S_{v_L}(\omega_0') = 4k_BTR_L$

$$\Delta\omega_{1/2} = \frac{2k_BT\left(\frac{\omega}{Q_e}\right)^2}{P_e} \quad , \tag{10.61}$$

$$\Delta\nu_{1/2} = \frac{4\pi k_BT(\Delta\nu_c)^2}{P_e} \quad . \tag{10.62}$$

This is the Shimoda-Takahashi-Townes linewidth for a maser oscillator.[7]

10.5 Spontaneous Emission Coupling Efficiency

The spectral linewidth $\Delta\omega_{1/2}$ in the quantum limit is rewritten using Eqs. (10.29) and (10.13) as

$$\Delta\omega_{1/2} = \left(\frac{\omega}{Q_e}\right) \frac{2\beta\frac{\hbar\omega_0^{'}}{L}}{\left(\frac{R_0}{R_L}-1\right)} \quad . \tag{10.63}$$

The linewidth drops by a factor of $2\beta\hbar\omega_0^{'}/L$ at the threshold and decreases linearly with the relative pump rate $(R_0/R_L - 1)$, as shown in Fig. 10.11. The physical meaning of the factor $2\beta\hbar\omega_0^{'}/L$ can be elucidated in the following way. According to the saturated gain model Eq. (10.27), the gain is decreased to one-half at the saturation intensity:

$$A_s^2 = \frac{1}{\beta} \quad . \tag{10.64}$$

This saturation intensity A_s^2 is converted to the saturation photon number by Eq. (10.44)

$$n_s = \frac{L}{2\hbar\omega_0^{'}\beta} \quad . \tag{10.65}$$

The transition from the upper state to the lower state in an efficient laser oscillator is achieved by the two processes: spontaneous emission with a rate A and stimulated emission with a rate Bn, where A and B are Einstein's spontaneous A and stimulated B coefficients and n is the photon number of a laser mode. When $A \gg Bn$, $R_a(A) \simeq R_0$ (unsaturated gain), wherease if $A \ll Bn$, $R_a(A) \ll R_0$ (highly saturated gain). The gain decreases to one-half of the unsaturated gain, $R_a(A) = \frac{1}{2}R_0$, at $n = n_s$, where we should have

$$A = Bn_s \quad . \tag{10.66}$$

The total spontaneous emission rate A is equal to the product of the spontaneous emission rate into a single laser mode B and the total number of modes M within the gain bandwidth,

$$A = BM \quad . \tag{10.67}$$

The spontaneous emission coupling efficiently ξ is defined by the fractional rate of spontaneous emission coupled into a single laser mode out of the total spontaneous emission rate. Based on this definition, we can express ξ in terms of the effective mode number M or the saturation photon number n_s:

$$\xi = \frac{1}{M} = \frac{1}{n_s} = \frac{2\hbar\omega_0^{'}\beta}{L} \quad . \tag{10.68}$$

Laser threshold

A laser threshold is defined as the condition that the average photon number of a laser mode is equal to one, where the stimulated emission rate is equal to the spontaneous emission rate into the same mode. The average photon number at a threshold is

$$n = \xi P_{\rm th}\tau_{\rm ph} = 1 \quad , \tag{10.69}$$

from which the threshold pump rate is given by

$$P_{\rm th} = \frac{1}{\xi \tau_{\rm ph}} = \frac{\left(\frac{\omega}{Q_e}\right)}{\xi} \quad . \tag{10.70}$$

A minimum possible laser threshold is equal to $\frac{\omega}{Q_e}$, which is achieved when $\xi = 1$, and a laser threshold increases with decreasing ξ.

Photon number

The photon number at below threshold is

$$n = \xi P \tau_{\rm ph} = \xi \frac{P}{\left(\frac{\omega}{Q_e}\right)} \quad , \tag{10.71}$$

while that at above threshold is

$$n = n_s \left(P/P_{\rm th} - 1\right) = \frac{1}{\xi}\left(P/P_{\rm th} - 1\right) \quad . \tag{10.72}$$

The photon number jumps from $n = 1$ at $P = P_{\rm th}$ to $n = 1/\xi$ at $P = 2P_{\rm th}$ as shown in Fig. 10.9.

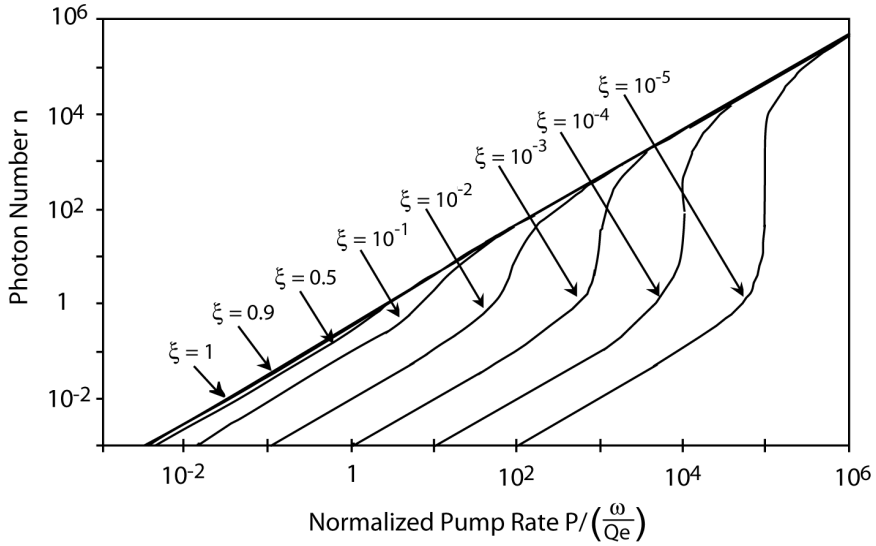

Figure 10.9: Average photon number n vs. normalized pump rate $P/\left(\frac{\omega}{Q_e}\right)$.

Spectral linewidth

The spectral linewidth at below threshold is

$$\Delta\omega_{1/2} = \frac{\omega}{Q_e}\left(1 - P/P_{\rm th}\right) \quad , \tag{10.73}$$

while that at above threshold is

$$\Delta\omega_{1/2} = \frac{\left(\frac{\omega}{Q_e}\right)}{n} = \xi\left(\frac{\omega}{Q_e}\right)\frac{1}{P/P_{\rm th}-1} \quad . \tag{10.74}$$

The spectral linewidth abruptly drops from the cold cavity linewidth $\frac{\omega}{Q_e}$ to $\xi\left(\frac{\omega}{Q_e}\right)$ at $P/P_{\rm th}=2$, as shown in Fig. 10.11. The abrupt change of the spectral linewidth is absent for $\xi = 1$.

Gain saturation

The total spontaneous emission rate A increases linearly with the pump rate at below the threshold, but is saturated at above the threshold due to the onset of the stimulated emission,

$$A = \begin{cases} P & : \text{bellowsthreshold} \\ P_{\rm th} = \dfrac{\left(\frac{\omega}{Q_e}\right)}{\xi} & : \text{above threshold} \end{cases} \quad . \tag{10.75}$$

Figure 10.10 shows the normalized total spontaneous emission rate $\frac{A}{\left(\frac{\omega}{Q_e}\right)}$ vs. normalized pump rate $P/\left(\frac{\omega}{Q_e}\right)$.

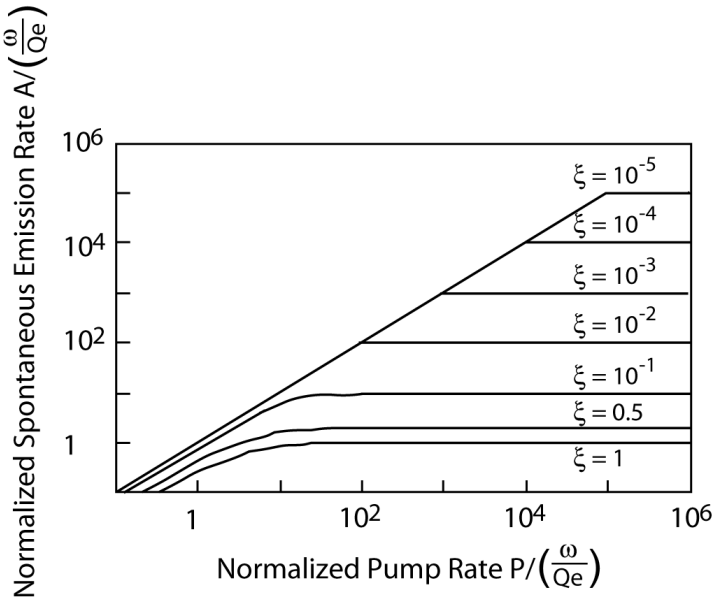

Figure 10.10: Normalized spectral linewidth $\frac{\Delta\omega_{1/2}}{\left(\frac{\omega}{Q_e}\right)}$ vs. normalized pump rate $P/\left(\frac{\omega}{Q_e}\right)$

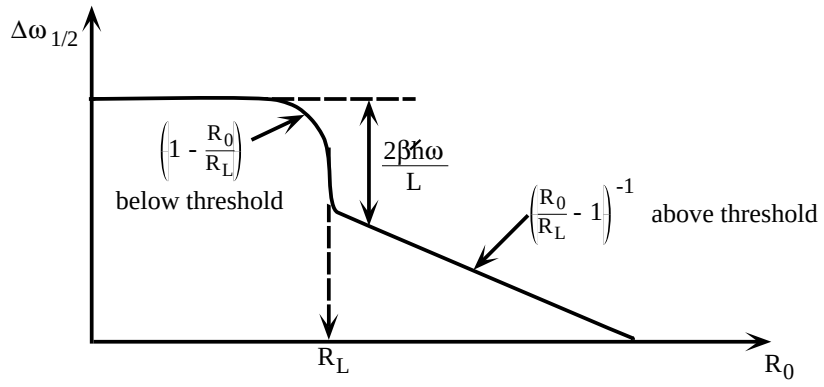

Figure 10.11: The spectral linewidth $\Delta\omega_{1/2}$ vs. pump rate R_0 of a laser oscillator.

10.6 Amplitude and Phase Noise of an Output Wave

The amplitude and phase noise studied thus far is those of the internal field of an oscillator. In most practical cases, however, one needs to know the noise of an output wave rather than that of an internal field, and these two are not identical.[4],[5]

Consider a negative conductance oscillator with a circulator as the output coupling element, as shown in Fig. 10.12. The circulator separates the input and output ports and simultaneously serves as the load resistance R_L for an oscillator internal circuit as shown in Fig. 10.1. Therefore, as far as the internal current I is concerned, this configuration is identical to the oscillator model shown in Fig. 10.1.

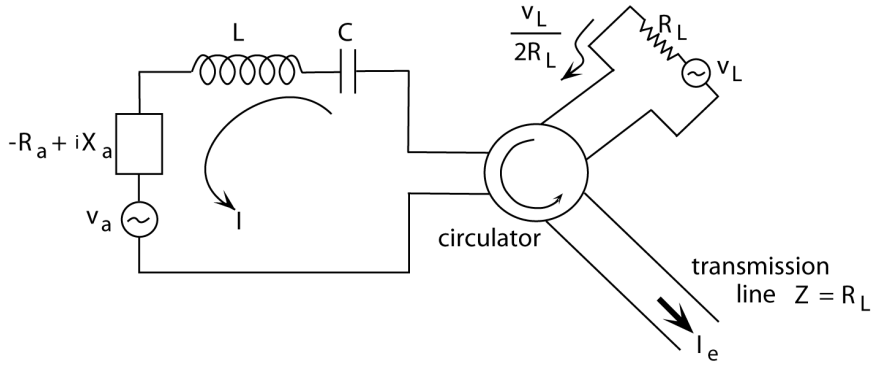

Figure 10.12: A negative conductance oscillator with an output coupling circuit.

The output current I_e consists of the reflected noise current $v_L/2R_L$ and the internal current I:

$$I_e = I - \frac{v_L}{2R_L} \quad , \tag{10.76}$$

where

$$I = (A + \Delta A)\cos(\omega t + \Delta\phi) \quad , \tag{10.77}$$

$$I_e = (A_e + \Delta A_e)\cos(\omega t + \Delta\phi_e) \quad , \tag{10.78}$$

$$v_L = v_{Lc}\cos(\omega t + \Delta\phi) + v_{Ls}\sin(\omega t + \Delta\phi) \quad . \tag{10.79}$$

From the above relations, the amplitude noise of the output wave is

$$\begin{aligned} \Delta A_e(\Omega) &= \Delta A(\Omega) - \frac{v_{Lc}(\Omega)}{2R_L} \\ &= \left(\frac{1}{i2L\Omega + sR_L} - \frac{1}{2R_L}\right) v_{Lc}(\Omega) + \frac{1}{i2L\Omega + sR_L} v_{ac}(\Omega) \quad . \end{aligned} \tag{10.80}$$

The power spectral density of ΔA_e is thus given by

$$S_{\Delta A_e}(\Omega) = \frac{\left(\frac{2}{s} - 1\right)^2 + (\Omega/\Omega_c)^2}{4R_L^2[1 + (\Omega/\Omega_c)^2]} S_{Lc}(\Omega) + \frac{1}{s^2 R_L^2} \cdot \frac{1}{1 + (\Omega/\Omega_c)^2} S_{ac}(\Omega) \quad . \tag{10.81}$$

At just above the oscillation threshold ($s \ll 1$), the spectrum Eq. (10.81) is close to that of the internal field Eq. (10.38) except for the white noise in the high-frequency regime, $\Omega > \frac{\omega}{Q_e}$, (Fig. 10.13). This white noise comes from the reflected external noise $-v_{Lc}/2R_L$ in Eq. (10.80).

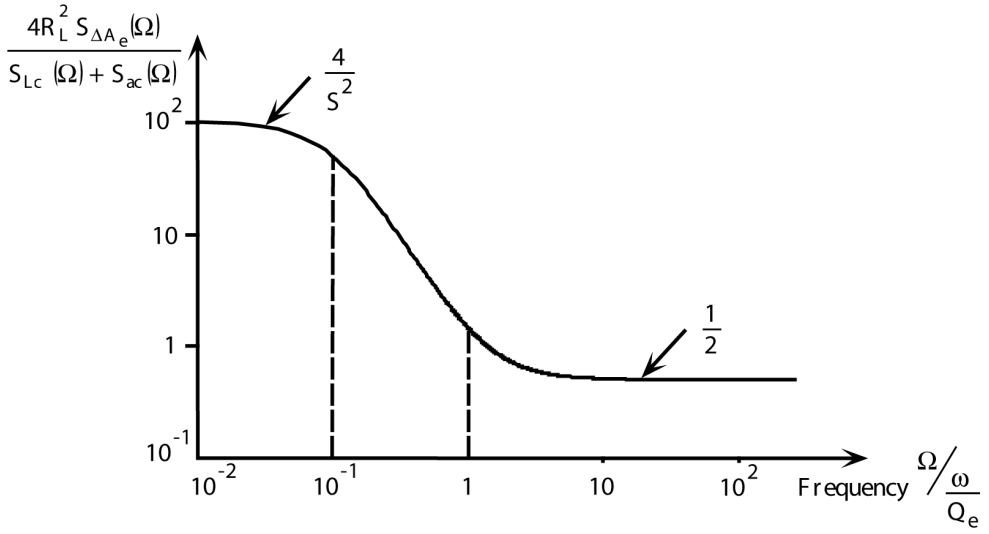

Figure 10.13: Normalized amplitude noise spectrum of an output field.

At far above threshold ($s \simeq 2$), Eq. (10.81) is reduced to

$$S_{\Delta A_e}(\Omega) = \frac{1}{4R_L^2}\left[\frac{\left(\Omega/\frac{\omega}{Q_e}\right)^2}{1 + \left(\Omega/\frac{\omega}{Q_e}\right)^2} S_{Lc}(\Omega) + \frac{1}{1 + \left(\Omega/\frac{\omega}{Q_e}\right)^2} S_{ac}(\Omega)\right] \quad . \tag{10.82}$$

Consider the following two cases. When both internal and external noise sources are quantum limited, i.e., $S_{Lc}(\Omega) = S_{ac}(\Omega) = 4\hbar\omega R_L$, one has a white noise spectrum:

$$S_{\Delta A_e}(\Omega) = \frac{\hbar\omega}{R_L} \quad . \tag{10.83}$$

The output photon flux N is given by

$$N = \frac{1}{2} R_L A_e^2/\hbar\omega \quad , \tag{10.84}$$

and its spectrum is

$$\begin{aligned} S_{\Delta N}(\Omega) &= \left(\frac{R_L A_e}{\hbar\omega}\right)^2 S_{\Delta A_e}(\Omega) \\ &= \frac{R_L A_e^2}{\hbar\omega} \\ &= 2N \quad . \end{aligned} \tag{10.85}$$

If this photon flux fluctuation is converted to photocurrent fluctuation by a photodetector with 100% quantum efficiency, the current spectrum is

$$S_{\Delta I}(\Omega) = q^2 S_{\Delta N}(\Omega) = 2q^2 N = 2qI \quad , \tag{10.86}$$

where $I = qN$ is the average dc current. This is the full-shot noise. As shown in Fig. 10.14, the origin of this (quantum) shot noise is the internal noise v_{ac} in the low-frequency regime, $\Omega < \frac{\omega}{Q_e}$, and the external noise v_{Lc} in the high-frequency regime, $\Omega > \frac{\omega}{Q_e}$. The (originally white) internal noise v_{ac} is transformed into a Lorentzian spectrum due to the storage (averaging) function of the resonator. A rapid fluctuation component of v_{ac} is averaged by the storage effect of the field inside the resonator. On the other hand, the (originally white) external noise v_{Lc} is transformed into the opposite spectral shape because a fluctuation component of v_{Lc} near the cavity resonance $\left(\Omega < \frac{\omega}{Q_e}\right)$ is absorbed and suppressed by the gain saturation of a laser oscillator. A fluctuation component of v_{Lc} far from the cavity resonance $\left(Q > \frac{\omega}{Q_e}\right)$ is simply reflected. A highly saturated oscillator behaves as a "matched load" near resonance and behaves as an "infinite impedance reflector" far from resonance.

The phase noise of an output wave is given by

$$\begin{aligned} &\Delta\phi_e(\Omega) = \Delta\phi(\Omega) - \frac{v_{Ls}(\Omega)}{2R_L A} \\ &= -\frac{1}{i\Omega 2LA}\left[v_{as} + \left(1 + i\Omega\frac{L}{R_L}\right) v_{Ls}\right] - \frac{rR_L}{i\Omega 2LA} \cdot \frac{1}{i\Omega 2L + sR_L}(v_{ac} + v_{Lc}) \quad . \end{aligned} \tag{10.87}$$

The power spectral density of $\Delta\phi_e$ is

$$\begin{aligned} S_{\Delta\phi_e}(\Omega) = &\frac{1}{4L^2A^2\Omega^2} S_{as}(\Omega) + \left(\frac{1}{4L^2A^2\Omega^2} + \frac{1}{4R_L^2A^2}\right) S_{Ls}(\Omega) \\ &+ \frac{\left(\frac{r}{s}\right)^2}{4L^2A^2\Omega^2} \cdot \frac{1}{1 + (\Omega/\Omega_c)^2} \left[S_{ac}(\Omega) + S_{Lc}(\Omega)\right] \quad . \end{aligned} \tag{10.88}$$

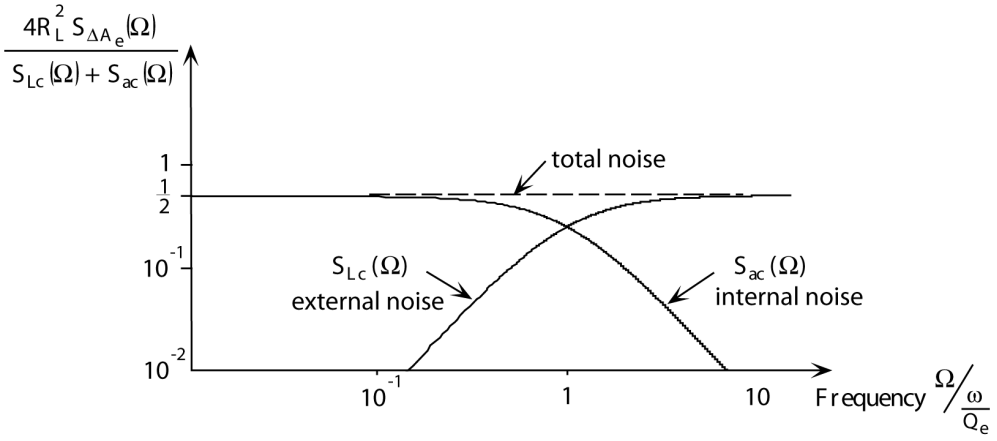

Figure 10.14: Normalized amplitude noise spectrum of an output field at far above threshold.

The phase noise spectrum $S_{\Delta\phi_e}(\Omega)$ is shown in Fig. 10.15 and is different from the internal phase noise spectrum $S_{\Delta\phi}(\Omega)$ only in the high-frequency region, i.e. white-noise spectrum. The internal phase noise due to v_{Ls} and the directly reflected noise wave v_{Ls} are 90° out-of-phase, as indicated in Eq. (10.87), so they are simply added. On the other hand, the internal amplitude noise due to v_{Lc} and the directly reflected noise wave v_{Lc} are 180° out-of-phase, as indicated in Eq. (10.80), and thus cancel each other out.

In the special case of no internal noise, $S_{ac}(\Omega) = S_{as}(\Omega) = 0$, and quantum-limited external noise, $S_{Lc}(\Omega) = S_{Ls}(\Omega) = 4\hbar\omega R_L$, the amplitude and phase noise spectra are

$$\left.\begin{aligned} S_{\Delta A_e}(\Omega) &= \frac{\hbar\omega}{R_L}\cdot\frac{\left(\Omega/\frac{\omega}{Q_e}\right)^2}{1+\left(\Omega/\frac{\omega}{Q_e}\right)^2} \quad \searrow \\ A^2 S_{\Delta\phi_e}(\Omega) &= \frac{\hbar\omega}{R_L}\frac{1+\left(\Omega/\frac{\omega}{Q_e}\right)^2}{\left(\Omega/\frac{\omega}{Q_e}\right)^2} \quad \nearrow \end{aligned}\right\} \quad S_{\Delta A_e}(\Omega)\cdot A^2 S_{\Delta\phi_e}(\Omega) = \left(\frac{\hbar\omega}{R_L}\right)^2 \quad . \qquad (10.89)$$

This is often referred to as the spectral Heisenberg uncertainty principle. A saturated oscillator suppresses the amplitude noise to below the shot-noise value (standard quantum limit: SQL) and enhances the phase noise to above the SQL within the resonator bandwidth, $\Omega < \frac{\omega}{Q_e}$. Such a field with reduced amplitude noise and enhanced phase noise is called an amplitude-squeezed state, which satisfies the minimum uncertainty product. On the other hand, a field with the amplitude and phase noise equal to the SQL is called a coherent state. An ideal saturated oscillator without internal noise produces an amplitude-squeezed state in the low-frequency regime and a coherent state in the high-frequency regime, as shown in Fig. 10.16. An example of such an ideal laser without an internal noise (pump noise) is a constant-current-driven semiconductor laser.

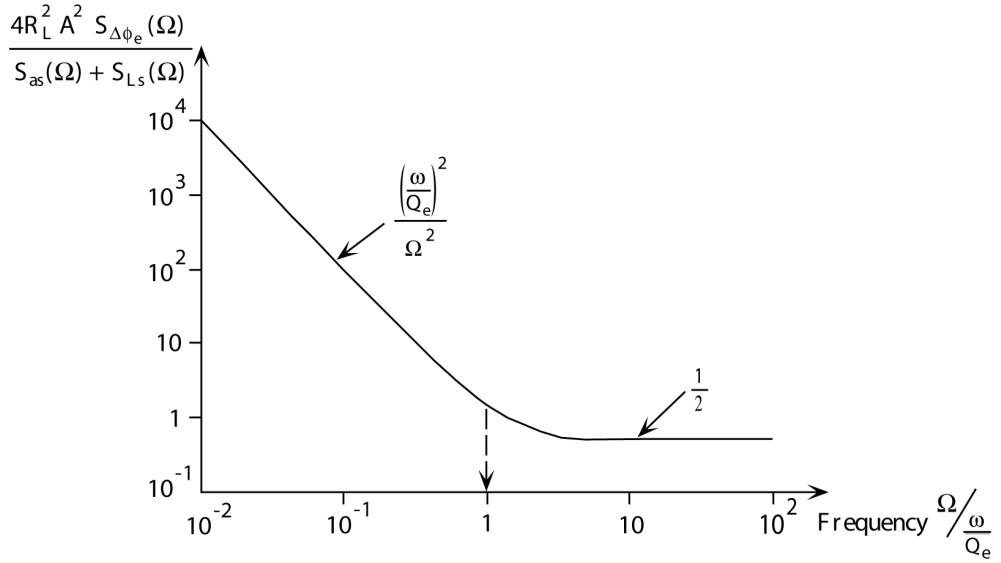

Figure 10.15: Normalized phase noise spectrum of an output field.

10.7 Injection-Locked Oscillators

Consider a negative conductance oscillator, which is injection-locked by an external coherent signal v_e, as shown in Fig. 10.17. The circuit equation (in complex representation) is[8]

$$\left[R_L + i\left(\omega L - \frac{1}{\omega C}\right) - R_a + iX_a\right] i(\omega) = v_a(\omega) + v_L(\omega) + v_e(\omega) \quad . \tag{10.90}$$

Assume that the internal current $i(t)$ is phase-locked by the injection signal $i_e(t) = \frac{v_e}{2R_L}$,

$$i_e(t) = Re\left(\frac{v_e(\omega)}{2R_L}\right) = Re(A_e\ e^{i\omega t}) \quad , \tag{10.91}$$

$$i(t) \equiv Re\left[i(\omega)\right] = Re\left[(A + \Delta A)e^{i(\omega t + \phi + \Delta\phi)}\right] \quad . \tag{10.92}$$

The amplitude and phase noise of the injection signal are attributed to the external noise voltage v_L. Using Eqs. (10.91) and (10.92) in Eq. (10.90), one obtains

$$\begin{aligned}\Big\{R_L - R_a(A) - \frac{\partial R_a}{\partial A}\Delta A + 2L\frac{1}{A}\frac{d}{dt}\Delta A \\ +i2L\left[\omega - \omega_0 + \frac{X_a(A)}{2L} + \frac{1}{2L}\frac{\partial X_a}{\partial A}\Delta A + \frac{d}{dt}\Delta\phi\right]\Big\} \\ \times(A + \Delta A)e^{i(\omega t + \phi + \Delta\phi)} = v_a + v_L + 2R_L A_e e^{i\omega t} \quad .\end{aligned} \tag{10.93}$$

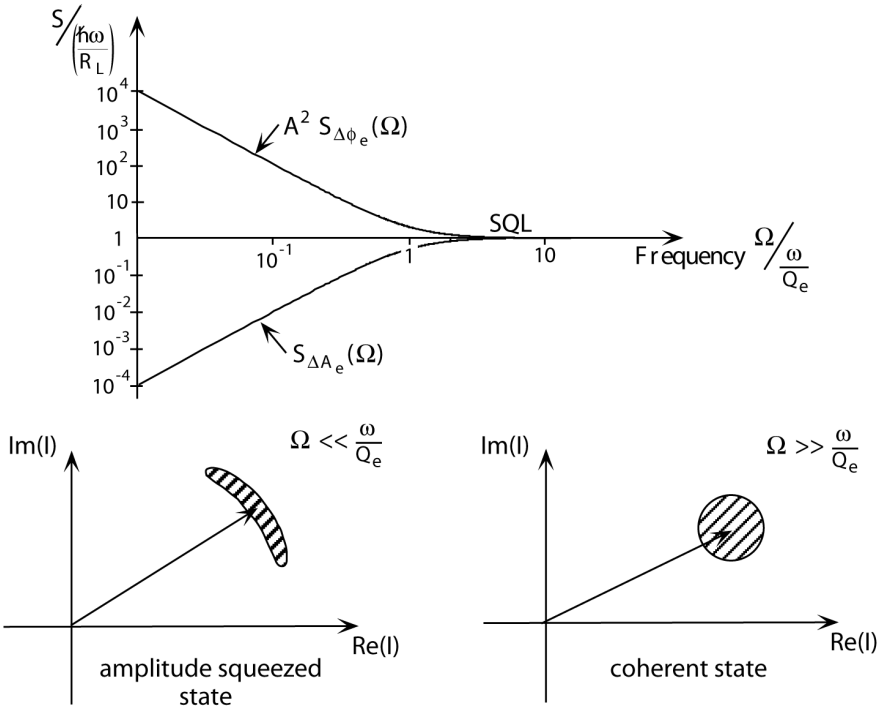

Figure 10.16: The spectral uncertainty relation between the amplitude and phase noise of an output field from an ideal laser.

The steady-state solution is obtained by neglecting all fluctuating terms:

$$\left[R_L - R_a(A) + i2L(\omega - \omega_0^{'})\right] A = 2R_L A_e(\cos\phi - i\sin\phi) \quad . \tag{10.94}$$

Here, $\omega_0^{'} = \omega_0 - \frac{X_a(A)}{2L}$ is a free-running oscillation frequency. The real part of Eq. (10.88) is

$$[R_L - R_a(A)]A = 2R_L A_e \cos\phi \quad . \tag{10.95}$$

We expand the oscillation amplitude A in terms of a free-running oscillation amplitude A_0 and small change of amplitude ΔA due to the injection signal:

$$A = A_0 + \Delta A \quad , \tag{10.96}$$

where A_0 satisfies the gain clamping condition

$$R_L = \frac{R_0}{1 + \beta A_0^2} \quad . \tag{10.97}$$

Using Eqs. (10.96) and (10.97) in Eq. (10.95), one obtains

$$\Delta A = A_e \left(\frac{1 + \beta A_0^2}{\beta A_0^2}\right) \cos\phi \quad . \tag{10.98}$$

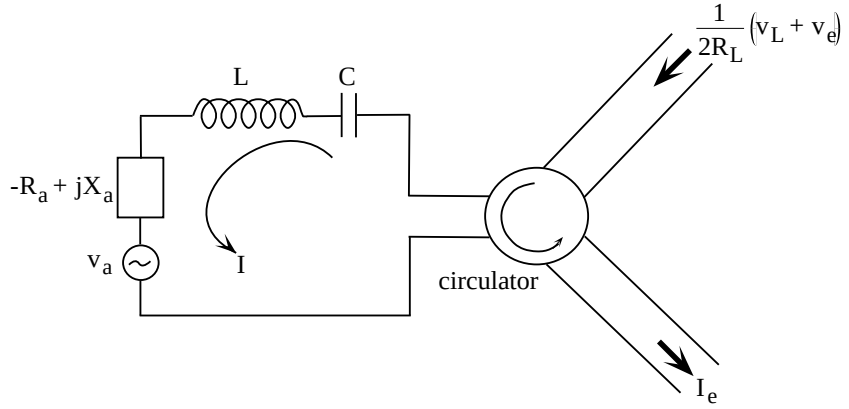

Figure 10.17: An electrical circuit model of an injection-locked laser oscillator.

This increase in the internal oscillation amplitude is converted to the change in the output wave amplitude by using the boundary condition, $\Delta A_e = \Delta A - A_e$:

$$\Delta A_e = \frac{(1 + \beta A_0^2)\cos\phi - \beta A_0^2}{\beta A_0^2} A_e \quad . \tag{10.99}$$

When the oscillator is pumped just above threshold, $\beta A_0^2 \ll 1$, the conversion from the input to output amplitude, a reflection coefficient, is given by

$$\frac{\Delta A_e}{A_e} \simeq \frac{\cos\phi}{\beta A_0^2} > 1 \quad \text{(amplification)} \quad . \tag{10.100}$$

On the other hand, when the oscillator is pumped far above threshold, $\beta A_0^2 \gg 1$, the reflection coefficient is

$$\frac{\Delta A_e}{A_e} \simeq \cos\phi - 1 \quad \text{(attenuation)} \quad . \tag{10.101}$$

As will be shown later, if the injection signal frequency ω and the free-running oscillation frequency $\omega_0^{'}$ are identical, the phase shift ϕ is equal to zero. In such a case, the injection-locked oscillator at far above threshold completely suppresses the amplitude signal and, therefore, the injection-locked oscillator operates as a matched load with complete amplitude limiting function.

The imaginary part of Eq. (10.94) is

$$L(\omega - \omega_0^{'})A = -R_L A_e \sin\phi \quad . \tag{10.102}$$

In order to have a real value of the phase shift ϕ in Eq. (10.102), one has the constraint for the allowed frequency detuning $\left|\omega - \omega_0^{'}\right|$:

$$\left|\omega - \omega_0^{'}\right| = \left|\frac{R_L}{L}\frac{A_e}{A}\sin\phi\right| \leq \frac{\omega}{Q_e} \cdot \frac{A_e}{A} = \Delta\omega_L \quad . \tag{10.103}$$

This gives the Adler's equation for a locking bandwidth $\Delta\omega_L$. When the frequency detuning $\omega - \omega_0^{'}$ is within this bandwidth, the oscillator frequency is locked to the injection signal frequency ω. The phase shift ϕ is now given by

$$\sin\phi = -\frac{\omega - \omega_0^{'}}{\left(\frac{\omega}{Q_e}\right)\frac{A_e}{A}} = \frac{\omega_0^{'} - \omega}{\Delta\omega_L} \quad . \tag{10.104}$$

Figure 10.18 shows the oscillation frequency ω_a, phase shift ϕ, internal amplitude modulation ΔA, and output wave amplitude modulation ΔA_e of the injection-locked oscillator as a function of the frequency detuning $\omega - \omega_0^{'}$.

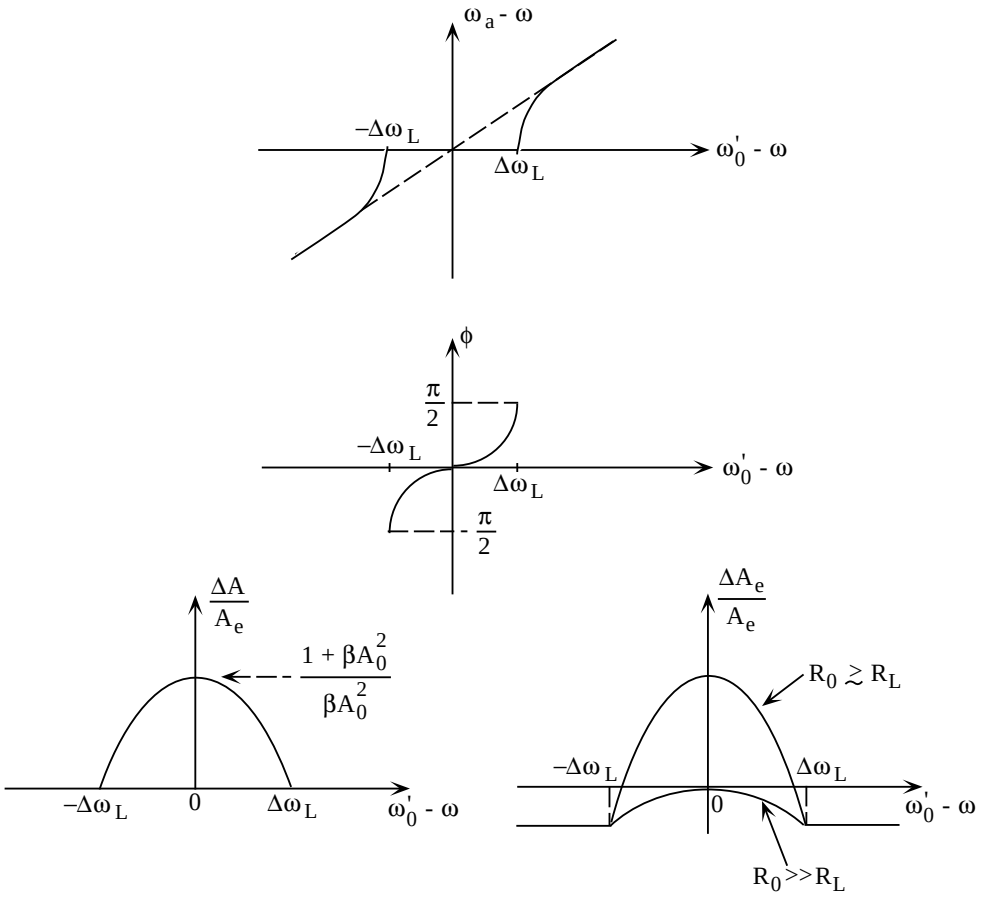

Figure 10.18: The oscillation frequency ω_a, phase shift ϕ, internal amplitude change $\frac{\Delta A}{A_e}$ and reflection coefficient $\frac{\Delta A_e}{A_e}$ of an injection-locked oscillator.

Consider the amplitude and phase noise of an injection-locked oscillator. Assuming $\omega = \omega_0^{'}$ and $\phi = 0$ in Eq. (10.93), one obtains

$$\left(2L\frac{d}{dt}\Delta A - A\frac{\partial R_a}{\partial A}\Delta A\right)\cos(\omega t) - 2LA\left(\frac{d}{dt}\Delta\phi + \frac{1}{2L}\frac{\partial X_a}{\partial A}\Delta A\right)\sin(\omega t)$$
$$= v_a + v_L + 2R_L A_e \Delta\phi \sin(\omega t) \quad . \tag{10.105}$$

Multiplying $\cos\omega t$ and $\sin\omega t$ and integrating over one period of oscillation, one has the following equations for the amplitude noise $\Delta A(t)$ and phase noise $\Delta\phi(t)$:

$$2L\frac{d}{dt}\Delta A - A\frac{\partial R_a}{\partial A}\Delta A = v_{ac} + v_{Lc} \quad , \tag{10.106}$$

$$-2LA\left(\frac{d}{dt}\Delta\phi + \frac{1}{2L}\frac{\partial X_a}{\partial A}\Delta A\right) = v_{as} + v_{Ls} + 2R_L A_e \Delta\phi \quad . \tag{10.107}$$

The resistive saturation parameter s is now given by

$$\begin{aligned} s &\equiv -\frac{A}{R_a(A)}\frac{\partial R_a}{\partial A} \\ &= -\frac{A}{R_L}\frac{\partial R_a}{\partial A}\left(1 - \frac{2A_e}{A}\right)^{-1} \quad , \end{aligned} \tag{10.108}$$

where Eq. (10.95) with $\phi = 0$ is used to derive the second equality. Equation (10.106) is rewritten as

$$\frac{d}{dt}\Delta A + \frac{s}{2}\left(\frac{\omega}{Q_e}\right)\left(1 - \frac{2A_e}{A}\right)\Delta A = \frac{1}{2L}(v_{ac} + v_{Lc}) \quad . \tag{10.109}$$

The Fourier-transformed internal and external amplitude noise are

$$\Delta A(\Omega) = \frac{\frac{1}{2L}\left[v_{ac}(\Omega) + v_{Lc}(\Omega)\right]}{i\Omega + \Delta\omega_a} \quad , \tag{10.110}$$

$$\begin{aligned} \Delta A_e(\Omega) &= \Delta A(\Omega) - \frac{v_{Lc}(\Omega)}{2R_L} \\ &= \frac{\frac{\omega}{Q_e} - \Delta\omega_a - i\Omega}{2R_L(i\Omega + \Delta\omega_a)} v_{Lc}(\Omega) + \frac{\frac{\omega}{Q_e}}{2R_L(i\Omega + \Delta\omega_a)} v_{ac}(\Omega) \quad . \end{aligned} \tag{10.111}$$

Here, $\Delta\omega_a = \frac{s}{2}\left(\frac{\omega}{Q_e}\right)\left(1 - \frac{2A_e}{A}\right)$ is the amplitude noise bandwidth. At far above threshold and for a relatively small injection signal, $\frac{\omega}{Q_e} - \Delta\omega_a \simeq 2\Delta\omega_L$. Since $\frac{\omega}{Q_e} \gg \Delta\omega_L$ in a practical situation, $\Delta\omega_a \simeq \frac{\omega}{Q_e}$ and one thus has the amplitude noise spectrum:

$$S_{\Delta A_e}(\Omega) = \frac{1}{4R_L^2}\left[\frac{\Omega^2 + 4\Delta\omega_L^2}{\Omega^2 + \left(\frac{\omega}{Q_e}\right)^2} S_{Lc}(\Omega) + \frac{\left(\frac{\omega}{Q_e}\right)^2}{\Omega^2 + \left(\frac{\omega}{Q_e}\right)^2} S_{ac}(\Omega)\right] \quad . \tag{10.112}$$

When the internal noise voltage is negligible, $S_{ac}(\Omega) = 0$, the normalized amplitude noise spectrum is shown schematically in Fig. 10.19.

On the other hand, Eq. (10.107) is rewritten as

$$\frac{d}{dt}\Delta\phi + \Delta\omega_L\Delta\phi = \frac{r\left(\frac{\omega}{Q_e}\right)}{2A}\Delta A - \frac{1}{2LA}(v_{as} + v_{Ls}) \quad . \tag{10.113}$$

The Fourier-transformed internal and external phase noise for the negligible reactive saturation parameter $r = 0$ are

$$\Delta\phi(\Omega) = \frac{-[v_{as}(\Omega) + v_{Ls}(\Omega)]}{(i\Omega + \Delta\omega_L)2LA} \quad , \tag{10.114}$$

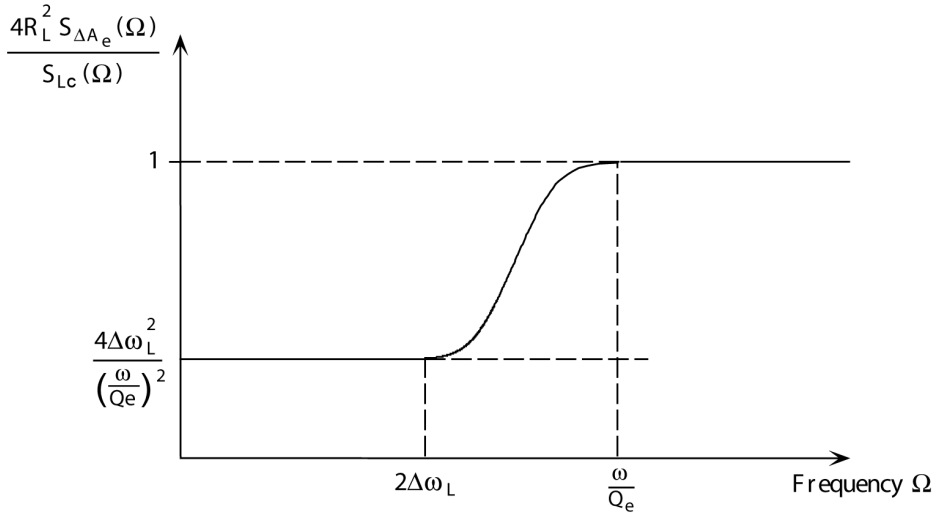

Figure 10.19: Normalized amplitude noise spectrum of an injection-locked oscillator.

$$\begin{aligned}\Delta\phi_e(\Omega) &= \Delta\phi(\Omega) + \frac{v_{Ls}(\Omega)}{2R_L A} \\ &= -\frac{1}{2LA(i\Omega + \Delta\omega_L)} \left\{ v_{as}(\Omega) + \left[1 - \frac{i\Omega + \Delta\omega_L}{\left(\frac{\omega}{Q_e}\right)} \right] v_{Ls}(\Omega) \right\} \quad .(10.115)\end{aligned}$$

The phase noise spectrum is given by

$$S_{\Delta\phi_e}(\Omega) = \frac{S_{as}(\Omega)}{4L^2A^2(\Omega^2 + \Delta\omega_L^2)} + \frac{S_{Ls}(\Omega)}{4L^2A^2} \frac{\Omega^2 + \left(\frac{\omega}{Q_e} - \Delta\omega_L\right)^2}{(\Omega^2 + \Delta\omega_L^2)\left(\frac{\omega}{Q_e}\right)^2} \quad . \tag{10.116}$$

When the internal noise voltage is negligible, $S_{as}(\Omega) = 0$, the normalized phase noise spectrum is shown schematically in Fig. 10.20.

If the internal noise is negligible, $S_{ac}(\Omega) = S_{as}(\Omega) = 0$, and the external noise is quantum-limited, $S_{Lc}(\Omega) = S_{Ls}(\Omega) = 4\hbar\omega R_L$, the amplitude and phase noise spectra are reduced to

$$S_{\Delta A_e}(\Omega) = \frac{\hbar\omega}{R_L} \left[\frac{\Omega^2 + 4\Delta\omega_L^2}{\Omega^2 + \left(\frac{\omega}{Q_e}\right)^2} \right] \quad , \tag{10.117}$$

$$A^2 S_{\Delta\phi_e}(\Omega) \simeq \frac{\hbar\omega}{R_L} \left[\frac{\Omega^2 + \left(\frac{\omega}{Q_e}\right)^2}{\Omega^2 + \Delta\omega_L^2} \right] \quad . \tag{10.118}$$

When $\Delta\omega_L \ll \frac{\omega}{Q_e}$, the product of the amplitude and phase noise spectra satisfies the uncertainty relationship:

$$S_{\Delta A_e}(\Omega) \cdot A^2 S_{\Delta\phi_e}(\Omega) \simeq \eta \left(\frac{\hbar\omega}{R_L} \right)^2 \quad , \tag{10.119}$$

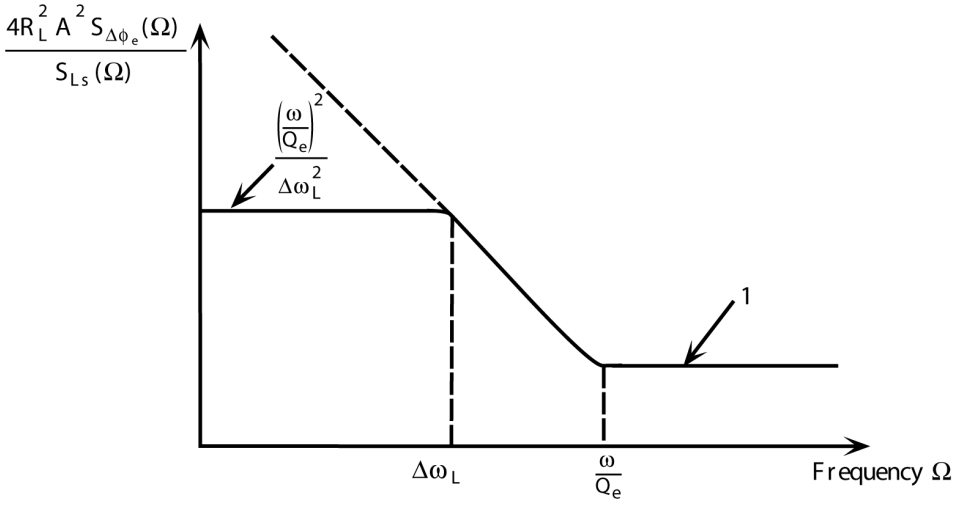

Figure 10.20: Normalized phase noise spectrum of an injection-locked laser oscillator.

where $\eta = 4$ for $\Omega \ll \Delta\omega_L$ and $\eta = 1$ (minimum uncertainty product) for $\Omega \gg \Delta\omega_L$. As shown in Fig. 10.21, an injection-locked oscillator has a localized phase distribution due to a phase-restoring force, while a free-running oscillator has a completely random phase distribution due to the absence of a phase-restoring force.

If an external injection signal has a phase diffusion noise $\Delta\phi_{\rm ex}$ and excess amplitude noise $\Delta A_{\rm ex}$, the equation of motion for the phase noise of an injection-locked oscillator is

$$\frac{d}{dt}\Delta\phi = -\Delta\omega_L \cos\phi(\Delta\phi - \Delta\phi_{\rm ex}) + (\omega_0^{'} - \omega)\frac{\Delta A}{A} - \Delta\omega_L \sin\phi \cdot \frac{\Delta A_{\rm ex}}{A_{\rm ex}} + \frac{r\left(\frac{\omega}{Q_e}\right)}{2A}\Delta A - \frac{1}{2LA}(v_{as} + v_{Ls}) \quad . \tag{10.120}$$

When there is a frequency detuning between $\omega_0^{'}$ and ω, the amplitude noise of the external injection signal, $\Delta A_{\rm ex}$, and that of the injection-locked laser, ΔA, contribute to the phase noise. When $\omega_0^{'} = \omega$, those excess noise contributions are suppressed but the phase diffusion noise $\Delta\phi_{\rm ex}$ of the external injection signal is not suppressed, and we have

$$S_{\Delta\phi_e}(\Omega) = \frac{\Omega^2}{\Omega^2 + \Delta\omega_L^2} S^0_{\Delta\phi_e}(\Omega) + \frac{\Delta\omega_L^2}{\Omega^2 + \Delta\omega_L^2} S_{\Delta\phi_{\rm ex}}(\Omega) \quad , \tag{10.121}$$

where $S_{\Delta\phi_e}(\Omega)^0$ is the external phase noise spectrum of a free-running oscillator Eq. (10.88) and $S_{\Delta\phi_{\rm ex}}(\Omega)$ is the phase diffusion noise spectrum of an external injection signal.

10.8 Frequency Modulation Feedback and Phase-Locked-Loop Oscillators

The frequency and/or phase noise of a laser oscillator is suppressed alternatively by a hybrid optoelectronic feedback control. Figures 10.22(a) and (b) show a frequency modu-

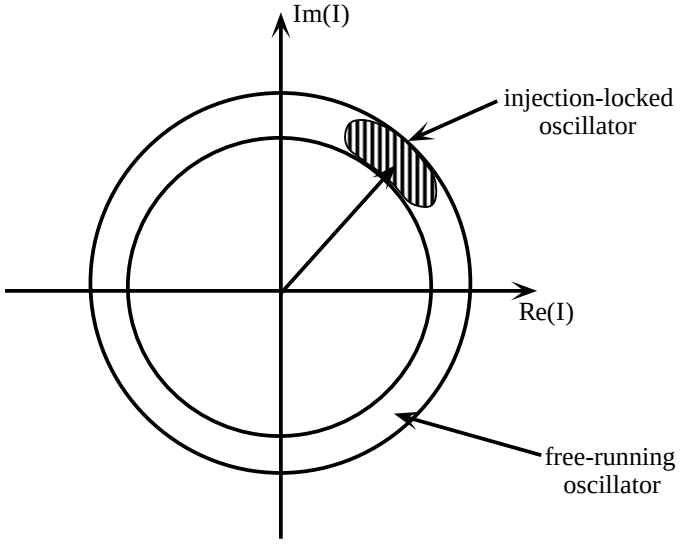

Figure 10.21: Phase noise distributions of a free-running laser and injection-locked laser.

lation feedback (FMFB) and phase locked loop (PLL) oscillator. In the FMFB oscillator, the output field from a slave laser is mixed with the output field of a (frequency standard) master laser and the beat note at a difference frequency $\omega_{IF} = \omega_s - \omega_m$ is fed into the frequency discriminator. The discriminator output reports the instantaneous frequency noise of the slave laser and is fedback to the slave laser to counter-modulate the oscillation frequency of the slave laser via the dispersion term χ_r (or reactance X_a) of the active medium or the empty cavity resonant frequency ω_0. This negative feedback loop can suppress the frequency noise spectrum of the slave laser within the loop bandwidth in addition to the center frequency stabilization to the master laser frequency.

In the PLL oscillator, the output field from a slave laser is mixed with the output field of a (phase standard) master laser with an identical frequency $\omega_m = \omega_s$. This optical homodyne detection output reports the instantaneous phase noise of the slave laser and is fedback to the slave laser to counter-modulate the oscillation phase of the slave laser via χ_r or ω_0. This negative feedback loop can suppress the phase noise spectrum of the slave laser within a loop bandwidth. If the slave laser output is replaced by a weak phase-modulated signal, the same PLL circuit operates as a high-gain noise-free amplifier for a weak incident signal, that is, the strong master output is just a replica of the weak phase-modulated signal wave.

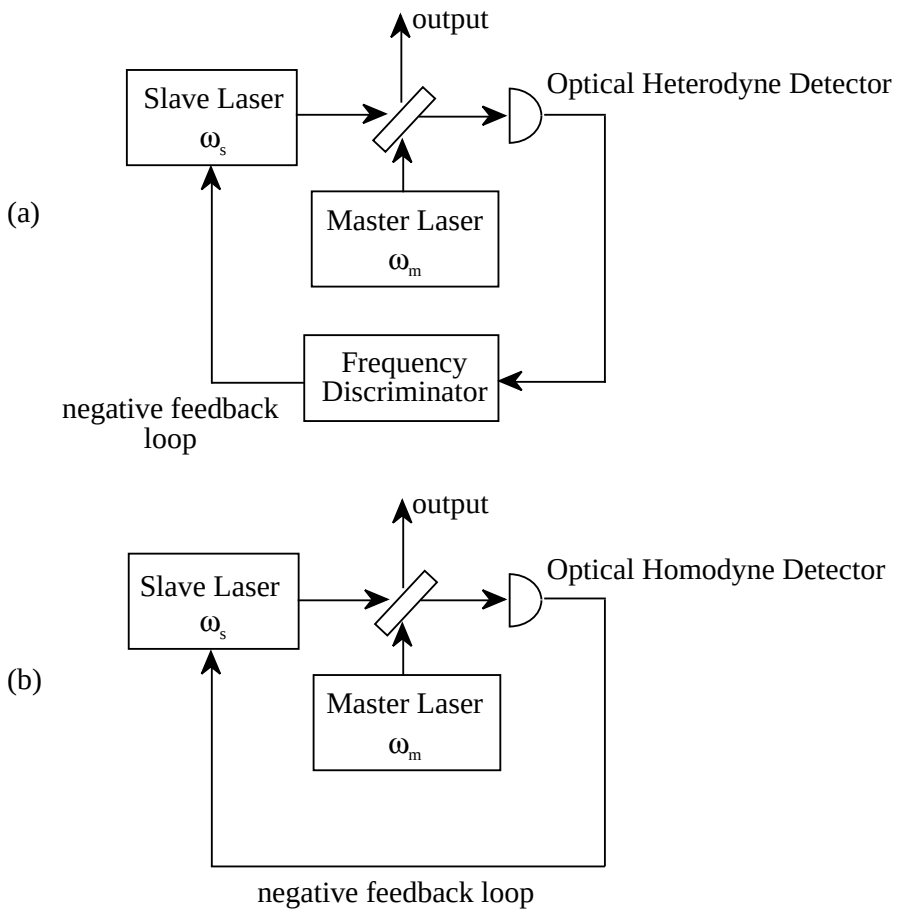

Figure 10.22: (a) Frequency modulation feedback (FMFB) laser oscillator and (b) phase-locked-loop (PLL) laser oscillator.

10.9 Quantum Noise Theory of Free-Running Lasers

IEEE J. Quantum Electron. QE-19, 34 (1983)
IEEE J. Quantum Electron. QE-19, 47 (1983)

10.10 Quantum Noise Theory of Injection-Locked Lasers

Phys. Rev. A29, 1261 (1984)

Bibliography

[1] B. van der Pol, *Phil. Mag. Series 7*, **3**, 65 (1927).

[2] M. Sargent III, M. O. Scully, and W. E. Lamb, Jr., *Laser Physics* (Addison-Wesley, London, 1974).

[3] A. E. Siegman, *Lasers* (University Science Books, Mill Valley, 1986).

[4] K. Kurokawa, *Bell Syst. Tech. J.* **48**, 1937 (1969).

[5] O. Nilsson, Y. Yamamoto, and S. Machida, *IEEE J. Quantum Electron* **QE-22**, 2043 (1986).

[6] A. Schawlow and C. H. Townes, *Phys. Rev.* **112**, 1940 (1958).

[7] K. Shimoda, H. Takahasi, and C. H. Townes, *J. Phys. Soc. Jpn.* **12**, 686 (1957).

[8] K. Kurokawa, *IEEE Trans. Microwave Theory Tech.* **MTT-16**, 234 (1968).

AM and FM Quantum Noise in Semiconductor Lasers—Part I: Theoretical Analysis

YOSHIHISA YAMAMOTO, MEMBER, IEEE

Abstract—**AM and FM quantum noise properties of semiconductor lasers have been studied theoretically. Theoretical formulations for the AM noise spectrum, photon number probability density, FM noise spectrum, instantaneous frequency probability density, and power spectrum are presented here as functions of semiconductor laser material, structural, and pumping parameters. Two theoretical approaches are employed: one is based on the quantum mechanical Langevin equation, and the other on the density matrix equation. Starting from the quantum mechanical Langevin equation, three different formulations, that is, the rate equation, Fokker-Planck equation, and van der Pol equation, are derived. The parameters which represent stimulated emission, spontaneous emission, and refractive-index dispersion are obtained by using the Kane function interpolated to Halperin-Lax bandtail and the Stern's improved matrix element. The above four different theoretical formulations are related to each other, and the applicability for each method is discussed.**

I. Introduction

DETAILED understanding of quantum noise properties in semiconductor lasers is important for coherent optical fiber communication systems [1] and sensor systems. Applications of semiconductor lasers as such principal devices in coherent optical fiber systems as transmitters, modulators, local oscillators, and optical amplifiers will give rise to great advantages in system performance and efficiency. Quantum noise in semiconductor lasers is one of the most important problems to be encountered in these applications, since semiconductor lasers have a low cavity Q and large quantum noise when compared with gaseous and solid-state lasers.

Five values that represent quantum noise characteristics for lasers, and that can be measured experimentally, are illustrated in Fig. 1. They are: 1) AM noise (or intensity fluctuation) spectrum $W_{\Delta p}(\omega)$; 2) photon number probability density Prob(n); 3) FM noise spectrum $W_{\delta\Omega}(\omega)$; 4) instantaneous frequency probability density Prob(Ω); and 5) power spectrum $W_0(\Omega)$.

The AM noise spectrum of a local oscillator is of practical significance in determining the carrier-to-noise ratio in an optical heterodyne detection system. The bit error rate depends on the photon number probability density in the local oscillator. The primary concern of the present study is: how does the actual AM noise power and photon number probability density in semiconductor lasers differ from the shot noise level and the Poisson distribution that is obtained with a completely coherent wave?

Manuscript received February 22, 1982; revised August 10, 1982.

The author is with the Musashino Electrical Communication Laboratory, Nippon Telegraph and Telephone Public Corporation, Musashino-shi, Tokyo, Japan.

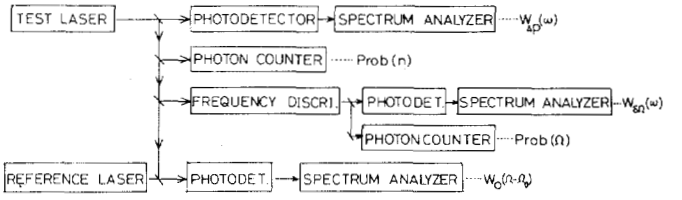

Fig. 1. Block diagrams for measuring observable quantum noise properties of semiconductor lasers. $W_{\Delta p}(\omega)$: AM noise spectrum; Prob(n): photon number probability density; $W_{\delta\Omega}(\omega)$: FM noise spectrum; Prob(Ω): instantaneous frequency probability density; and $W_0(\Omega - \Omega_0)$: power spectrum.

The FM noise spectrum is important in relation to the baseband signal-to-noise ratio in optical frequency shift keying (FSK) and phase shift keying (PSK) systems. This is because the FM noise spectrum appears as an additive noise in the final demodulation output. The instantaneous frequency probability density causes an excess bit error in the FSK system when the frequency shift between two signal states decreases and the tails of both signals' frequency probability densities overlap. This is also the case in a PSK system, when phase diffusion due to the FM noise approaches the phase shift between two signal states.

Two kinds of theoretical bases have been employed so far for quantum noise analyses of lasers. They are the quantum mechanical Langevin equation method and the density matrix method. The former method has been studied extensively by Haken and his colleagues [2], [3]. Quantum mechanical rate equations with fluctuation terms [4], [5], the Fokker-Planck equation for photon amplitude probability density [6], [7], and the classical van der Pol equation with a noise driving source [8], [9] belong to this category. The density matrix method has been studied by Lamb and his colleagues [10]-[12]. The pioneering work by Shimoda *et al.* on maser amplifier analysis (STT theory) [13] corresponds to the linear version of this theory. Lax and his co-workers have established that these two formulations are equivalent when the photon number in the cavity is large enough [14], [15]. Smith discussed the corrections for a small photon number [16]. Photon count statistics are studied experimentally [17] and theoretically [18].

Most of these theoretical studies have been devoted to gaseous and solid-state lasers. To the author's knowledge, however, these different theoretical approaches have not yet been systematically studied for semiconductor lasers. The relationship between the five values presented above that represent quantum noise properties of lasers have not fully been clarified either. The relation between AM and FM quantum noise is de-

0018-9197/83/0100-0034$01.00 © 1983 IEEE

picted in Fig. 2. Spontaneous emission coupled to a lasing mode directly causes intensity fluctuation and phase diffusion of the laser field. These processes can be described by the equation only for field variables. However, the actual quantum noise properties of semiconductor lasers are deeply affected by the different processes, such as the competition between carrier and photon fluctuation, carrier noise induced refractive-index change, and current noise induced diode temperature change.

The purpose of this paper is to describe the relations between these quantum noise properties in terms of the semiconductor laser material, structural, and pumping parameters, through the four different theoretical approaches.

It is well known that gain saturation is of key importance in laser noise characteristics. Spontaneous emission coupled to a lasing mode is, on the other hand, a direct origin of quantum noise. The relation between these two facts can be understood by refering to one of the important results of this paper. This result clarifies that the saturation parameter, which appears in the van der Pol equation and in the photon density matrix equation, is equivalent to the spontaneous emission coefficient which appears in the rate equation.

The flowchart of theoretical analyses in this paper is shown in Fig. 3. Numerical comparisons between the different theoretical approaches will be described in an accompanying paper [19]. Experimental results for several types of AlGaAs lasers will also be presented there.

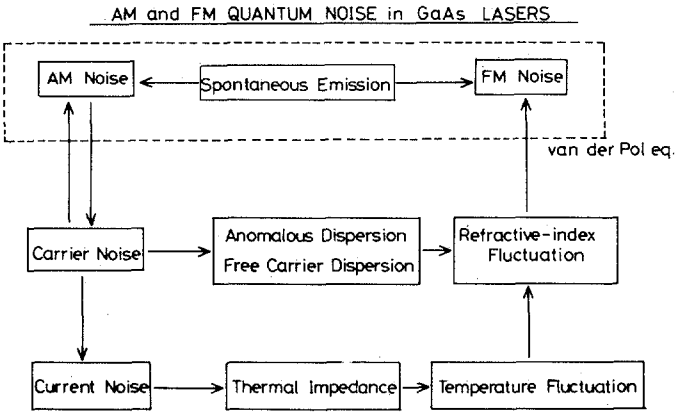

Fig. 2. Relations between quantum noise in semiconductor lasers.

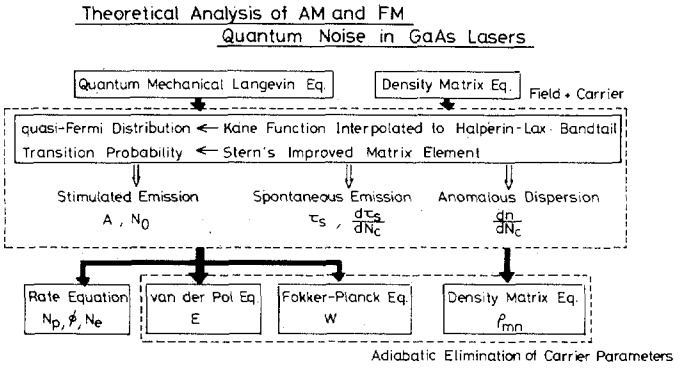

Fig. 3. Framework of theoretical formulation.

II. Quantum Mechanical Langevin Equation

The quantum mechanical Langevin equations for a photon amplitude operator b^+, a dipole moment operator $a^+_{kc}a_{k'v}$, and an electron number operator n_{kc}, will first be briefly described [20]. The van der Pol equation and rate equation to be used in Sections IV–VI are derived from the Langevin equation.

The photon amplitude operator b^+ of a single lasing mode obeys

$$\frac{d}{dt}\,b^+ = (j\omega - K)\,b^+ + j\sum_{kk'} g_{kk'}a^+_{kc}a_{k'v} + F(t). \tag{1}$$

Here ω is a cold cavity resonant frequency, $K = 1/2\tau_p$ is a loss constant including both the end mirror loss and free carrier absorption loss, and $g_{kk'}$ is the optical matrix element between the conduction band state with wave number k and the valence band state with wave number k'. The correlation function of the Marcovian fluctuation operator F is

$$\langle F(t)\,F^+(s)\rangle = \delta(t-s)\,\langle FF^+\rangle \tag{2}$$

where

$$\langle FF^+\rangle = 2Kn_{\text{th}},\ \langle F^+F\rangle = 2K(n_{\text{th}}+1),\ \langle FF\rangle = \langle F^+F^+\rangle = 0.$$

$n_{\text{th}} = [\exp(\hbar\omega/kT) - 1]^{-1}$ is the number of thermal photons.

The equation for the dipole moment operator $a^+_{kc}a_{k'v}$ is

$$\frac{d}{dt}\,a^+_{kc}a_{k'v} = (j\epsilon_{kk'} - \gamma_{kk'})\,a^+_{kc}a_{k'v} - jg_{kk'}b^+(n_{kc} - n_{k'v}) + F_{kck'v}(t). \tag{3}$$

Here $\epsilon_{kk'} = (E_{kc} - E_{k'v})/\hbar$ is the frequency separation between state kc and state $k'v$, and $\gamma_{kk'}$ is the phase decay constant between the two states. The fluctuation operator satisfies

$$\langle F_{kck'v}F_{k'vkc}\rangle + \langle F_{k'vkc}F_{kck'v}\rangle = 2\gamma_{kk'}\,[f_{kc}(1-f_{k'v}) + f_{k'v}(1-f_{kc})], \tag{4}$$

$$\langle F_{kck'v}F_{kck'v}\rangle + \langle F_{k'vkc}F_{k'vkc}\rangle = 0 \tag{5}$$

where $f_{kc} = [1 + \exp\{(E_{kc} - \xi_c)/k_BT\}]^{-1}$ is the quasi-Fermi distribution for the expected value of $n_{kc} = a^+_{kc}a_{kc}$ in the conduction band, ξ_c is the corresponding quasi-Fermi level, $f_{k'v} = [1 + \exp\{(\xi_v - E_{k'v})/k_BT\}]^{-1}$ is the quasi-Fermi distribution for the expected value of $n_{kv} = a^+_{kv}a_{kv}$ in the valence band, and ξ_v is the corresponding quasi-Fermi-level.

The time development of the electron number operator n_{kc} is given by

$$\frac{d}{dt}\,n_{kc} = \sum_{k'}\,[-jbg_{kk'}a^+_{kc}a_{k'v} + \text{HC}] - r_{sp,k} + P_k + F_{kckc}(t) + \frac{d}{dt}\,n_{kc}|_{el-el} \tag{6}$$

where HC means the Hermitian conjugate and P_k is the pump rate. The spontaneous emission rate $r_{sp,k}$ into all continuum light modes except for the laser mode is given by

$$r_{sp,k} = 2\pi\hbar\sum_{k'}|g_{kk'}|^2\rho_L\,n_{kc}(1-n_{k'v}). \tag{7}$$

Here, $\rho_L = V_oE_g^2/2\pi^2\hbar^3C^3$ is the normalized density of states

for the light field, V_o is the optical mode volume, and E_g is the optical energy. The last factor in (6) describes the electron-electron scattering process. The relaxation time τ_{el} is of the order of 10^{-13}-10^{-12} s. This is smaller than the carrier lifetime shortened by the stimulated emission process except for the extremely high light field intensity. Therefore, the electrons always obey the quasi-Fermi distribution. An equation similar to (6) holds for n_{kv}.

Since the phase decay constant $\gamma_{kk'}$ is normally very large, the integration of (3) can be performed adiabatically [14], [20]

$$a^+_{kc}a_{k'v} = -j\frac{g_{kk'}\,b^+(n_{kc}-n_{k'v})}{j(\Omega-\epsilon_{kk'})+\gamma_{kk'}} + \int_0^t F_{kck'v}(\tau)\cdot\exp\left(j\epsilon_{kk'}-\gamma_{kk'}\right)(t-\tau)\,d\tau \quad (8)$$

where Ω is the oscillation frequency. By substituting (8) into (1), it is possible to obtain

$$\frac{d}{dt}b^+ = (j\omega-K)\,b^+ + \left[\sum_{kk'}\frac{|g_{kk'}|^2\,(n_{kc}-n_{k'v})}{j(\Omega-\epsilon_{kk'})+\gamma_{kk'}}\right]b^+ + F(t) + j\sum_{kk'}g_{kk'}\int_0^t F_{kck'v}(\tau)\cdot\exp\left(j\epsilon_{kk'}-\gamma_{kk'}\right)(t-\tau)\,d\tau. \quad (9)$$

The electron distribution function is, in general, a nonlinear function of the photon number operator $n = b^+b$. It is possible to write

$$\sum_{kk'}\frac{|g_{kk'}|^2\,(n_{kc}-n_{k'v})}{j(\Omega-\epsilon_{kk'})+\gamma_{kk'}} = G + j\delta\omega - S(n) \quad (10)$$

where G is the unsaturated gain, and the saturation $S(n)$ may be approximated by a linear function of photon number

$$S(n) = \frac{dS(n)}{dn}\cdot n. \quad (11)$$

By using (10) and (11) with (9), and introducing the slowly varying amplitude $B^+ = b^+e^{-j\Omega t}$, one obtains

$$\frac{d}{dt}B^+ + \left[K - G + \frac{dS(n)}{dn}B^+B\right]B^+ = \tilde{F}(t), \quad (12)$$

$$\tilde{F}(t) = \left[F(t) + j\sum_{kk'}g_{kk'}\int_0^t F_{kck'v}(\tau)\cdot\exp\left(j\epsilon_{kk'}-\gamma_{kk'}\right)\cdot(t-\tau)\,d\tau\right]e^{-j\Omega t}. \quad (12')$$

This is the generalized van der Pol equation with a noise driving source $\tilde{F}(t)$.

The photon number representation of the Langevin equation (9) is obtained by using the identity $(d/dt)\,n = [(d/dt)\,b^+]\,b + b^+[(d/dt)\,b]$ as follows:

$$\frac{d}{dt}n = -2K\cdot n + E_{cv} + (E_{cv}-E_{vc})\,n + F_n(t) \quad (13)$$

where

$$E_{cv} = \sum_{kk'}|g_{kk'}|^2\cdot\frac{2\gamma_{kk'}}{(\epsilon_{kk'}-\Omega)^2+\gamma^2_{kk'}}\cdot n_{kc}(1-n_{k'v}) \quad (14)$$

is the rate of spontaneous emission coupled into the laser mode and E_{vc} is obtained from (14) by interchanging kc and $k'v$. The correlation function for the fluctuation operator is given by

$$\langle F_n(t)\,F_n(s)\rangle = \delta(t-s)\,\langle 2Kn + E_{cv}(n+1) + E_{vc}n\rangle. \quad (15)$$

Because of the assumption that the electrons in a band are always in a quasi-equilibrium, it is sufficient to employ one equation for the total number of electrons $N_c = \Sigma_k\, n_{kc}$. By inserting (8) into (6), and summing the resulting equation over all k values, one obtains

$$\frac{d}{dt}N_c = P - R_{sp} - (E_{cv}-E_{vc})\,n - E_{cv} + F_c(t). \quad (16)$$

Here, $P = \Sigma_k\, P_k$ and $R_{sp} = \Sigma_k\, r_{sp,k}$. The correlation function for the fluctuation operator is given by

$$\langle F_c(t)\,F_c(s)\rangle = \delta(t-s)\,\langle P + R_{sp} + E_{cv}(n+1) + E_{vc}n\rangle. \quad (17)$$

The cross-correlation function between the photon and electron fluctuation operators satisfies

$$\langle F_n(t)\,F_c(s)\rangle = \langle F_c(t)\,F_n(s)\rangle = -\delta(t-s)\,\langle E_{cv}(n+1) + E_{vc}\cdot n\rangle. \quad (18)$$

Equations (13) and (16) are rate equations with fluctuation operators. The mean values of these equations, of course, can be reduced to a Statz-deMars type rate equation.

III. Parameters in the Langevin Equation

A. Stimulated Emission, Spontaneous Emission, and Anomalous Dispersion Parameters

The expressions for the stimulated emission rate $E_{cv}n$, the absorption rate $E_{vc}n$, and the spontaneous emission rate R_{sp}, require the evaluation of both the conduction and valence band densities of states and the transition matrix element.

The conduction and valence band densities of the states depend on the carrier concentration and have bandtails within the energy gap. Bandtail representation studies were reported by Kane [21], Halperin and Lax [22], and Stern [23].

The matrix element is frequently assumed to be based on the so-called k-selection rule [24]. For semiconductor lasers doped with impurities and operating at room temperature, however, the k-selection rule does not hold and the matrix element is energy-dependent. The matrix element for the no k-selection rule transition between a parabolic band and a shallow impurity level was derived by Dumke [25]. An improved, but more complex matrix element, considering the bandtail effect, was obtained by Stern [23].

Detailed calculation of the gain coefficient was performed for GaAs using the Stern's improved matrix element and the density of states with the Kane function interpolated to the Halperin-Lax bandtail. The numerical result for peak gain coefficient $g_{\max}$ versus the carrier density N_e gives the following simple expressions for E_{cv} and E_{vc}.

$$E_{cv} = A\Gamma N_e \quad (19)$$

$$E_{vc} = A\Gamma N_0. \quad (20)$$

Here, Γ is the optical mode confinement factor to an active layer, $N_e = N_c/V_e$ is the minority carrier density, and V_e is the active region volume. A and N_0 are important material parameters determining the gain and noise characteristics of semiconductor lasers, both of which depend on background doping level and injected minority carrier density.

The spontaneous emission rate R_{sp} is given by

$$R_{sp} = N_c/\tau_s \tag{21}$$

where τ_s is the spontaneous carrier lifetime which can be calculated by using the detailed-balance approach of van Roosbroeck and Shockley from the theoretical gain spectra.

The anomalous dispersion $\delta\omega$ appearing in (10) is determined by the refractive-index change due to carrier density. It is obtained by the Kramers-Kronig integral of theoretical gain spectra. Determination of these coefficients A, N_0, τ_s, and dn/dN_c will be discussed in an accompanying paper [19].

B. Saturation Parameter, Spontaneous Emission Coefficient, and Population Inversion Parameter

The saturated gain $G - S(n)$, appearing in (9)–(11), is expressed by using (19) and (20) as

$$G - S(n) = \sum_{kk'} \frac{|g_{kk'}|^2 \gamma_{kk'}(n_{kc} - n_{k'v})}{(\Omega - \epsilon_{kk'})^2 + \gamma_{kk'}^2} = \frac{1}{2} A\Gamma(N_e - N_0) \tag{22}$$

where N_e is the saturated carrier density. The unsaturated carrier density N_e^0 is, on the other hand, independent of the photon number n. This density is determined by the pumping rate P and the spontaneous lifetime τ_s to be

$$N_e^0 = P\tau_s/V_e. \tag{23}$$

The unsaturated gain G is given by using (23) in (22) as follows:

$$G = \frac{1}{2} A\Gamma\left(\frac{P\tau_s}{V_e} - N_0\right). \tag{24}$$

The oscillation threshold condition is given by

$$2G_{th} \equiv A\Gamma\left(\frac{P_{th}\tau_s}{V_e} - N_0\right) = \frac{1}{\tau_p} \tag{25}$$

where τ_p is a photon lifetime and P_{th} is the threshold pumping rate. By using (25) in (24), it is possible to obtain

$$G = \frac{1}{2\tau_p}(Rn_{sp} + 1). \tag{26}$$

Here, $R = P/P_{th} - 1$ is the relative pumping level, and $n_{sp} = 1 + A\Gamma\tau_p N_0$ is the population inversion parameter. This latter parameter is near unity in gaseous and solid-state lasers. The most striking feature of semiconductor laser noise is attributed to the fact that n_{sp} is larger than unity.

The saturated gain $G - S(n)$ is clamped to the cavity loss constant K at above the lasing threshold by

$$G - \frac{dS(n)}{dn} \cdot n \lesssim K. \tag{27}$$

At well above the threshold the internal quantum efficiency is safely assumed to be unity, and the photon number n is given by

$$n = (P - P_{th})\tau_p = \frac{Rn_{sp}V_e}{A\Gamma\tau_s}. \tag{28}$$

Here, the second equality is derived by using (25). By using (28) and (26) with (27), the saturation parameter $dS(n)/dn$ can be obtained as

$$\frac{dS(n)}{dn} = \frac{A\Gamma\tau_s}{2\tau_p V_e} = \frac{A\tau_s}{2\tau_p V_0} \tag{29}$$

where $V_0 = V_e/\Gamma$ is the optical mode volume.

The spontaneous emission coefficient β used in the rate equation analysis is defined as the ratio of the spontaneous emission rate E_{cv} coupled to a laser mode, and the total spontaneous emission rate R_{sp} as follows:

$$\beta = E_{cv}/R_{sp} = \frac{A\tau_s}{V_0}. \tag{30}$$

The spontaneous emission coefficient β has the same form as the saturation parameter $dS(n)/dn$ except for the normalizing factor $1/2\tau_p$.

The spontaneous emission coefficient β as well as the population inversion parameter n_{sp} plays a key role in the quantum noise properties of semiconductor lasers as will be seen in the subsequent sections.

IV. Classical Treatment of van der Pol Equation with Noise Driving Source

A. Derivation of the Equation

The generalized van der Pol equation (12) for the photon amplitude, $B^+(t)$, can be transformed into its classical form by introducing the classical electric field

$$E(t) = \frac{(\hbar\Omega)^{1/2}}{2}\left[B \exp(j\Omega t) + B^* \exp(-j\Omega t)\right]. \tag{31}$$

The van der Pol equation for $E(t)$ is given by

$$\frac{d^2E}{dt^2} + (r - \alpha + \gamma|E|^2)\frac{dE}{dt} + \Omega^2 E = N(t), \tag{32}$$

where

$$r = 2K = 1/\tau_p, \tag{33}$$

$$\alpha = 2G = [(R + \Delta R)n_{sp} + 1]/\tau_p, \tag{34}$$

$$\gamma = \frac{2}{\hbar\Omega} \cdot \frac{dS(n)}{dn} = \frac{\beta}{\tau_p \hbar\Omega}. \tag{35}$$

Here, ΔR represents the effective pumping level shift introduced to describe the finite photon number at the lasing threshold. This value is given in terms of the pumping level R in the following manner:

$$\Delta R = (\sqrt{\pi}\,\kappa)^{-1} \exp(-\kappa^2 R^2)\,[1 + \operatorname{erf}(\kappa R)]^{-1}, \tag{36}$$

$$\kappa = \sqrt{\frac{n_{sp}}{2\beta}}. \tag{37}$$

The term ΔR is introduced so that the van der Pol equation

can be applied near the threshold. Validity is confirmed by means of the Fokker-Planck equation, which will be discussed in Section V. The value ΔR is $\sqrt{2\beta/\pi n_{sp}}$ at the lasing threshold, and rapidly decreases to zero in the region well above the threshold. Therefore, the unsaturated gain (34) is consistent with (26) for well above the threshold region.

The noise driving source $N(t)$ is given by

$$N(t) = j\Omega(\hbar\Omega)^{1/2}\,\tilde{F}(t) + \text{c.c.} \tag{38}$$

where c.c. denotes the complex conjugate, and $\tilde{F}(t)$ is given by (12′). The spectral density function of the noise driving source is

$$W_N(\Omega) = \frac{4\Omega^2\hbar\Omega}{\pi\tau_p}\left[n_{\text{th}} + \frac{1}{2} + n_{sp}g_N(\Omega)\right]. \tag{39}$$

Here, the three terms in the bracket respectively indicate the thermal photon, the cavity loss constant (photon lifetime), and the spontaneous emission photon contributions to $N(t)$. $g_N(\Omega)$ is the gain envelope function normalized as $g_N(\Omega_0) = 1$.

The solution of the van der Pol equation (32) is assumed to be expressed as the sum of the completely coherent signal wave, and the in-phase and out-of-phase narrow band Gaussian random noise waves in this manner:

$$E = E_0 \cos \Omega t + C_n(t) \cos \Omega t + S_n(t) \sin \Omega t. \tag{40}$$

The noise driving source $N(t)$ is also expressed as the sum of the in-phase and out-of-phase Gaussian random noise components such that

$$N(t) = N_c(t) \cos \Omega t + N_s(t) \sin \Omega t. \tag{41}$$

By using (40) and (41) with (32) and equating cosine and sine terms separately, the equation below can be obtained.

$$\frac{dS_n}{dt} = N_c/2\Omega, \tag{42}$$

$$\frac{dC_n}{dt} + \frac{\gamma}{2}(E_0^2 + \overline{C_n^2})\,C_n = N_s/2\Omega. \tag{43}$$

Here, the assumptions for $\ddot{C}_n$, $\dot{S}_n \ll \Omega C_n$, ΩS_n and $\overline{C_n^2}$, $\overline{S_n^2} \ll E_0^2$ are used. Steady-state solutions of (32) give

$$\frac{1}{2}(E_0^2 + \overline{C_n^2}) = \frac{n_{sp}}{\beta}(R + \Delta R)\hbar\Omega. \tag{44}$$

This value corresponds to the total optical energy stored in a laser mode.

The simple equations (42) and (43), together with (39) and (44), are the basic formulations for the analysis to be followed in this section.

B. AM Noise Spectrum

The output power $P(t)$ emitted from one of the laser facets is given by

$$P(t) = [E_0 + C_n(t)]^2/2\tau_{PM}. \tag{45}$$

Here, $\tau_{PM} = [(C/2L) \ln (1/R_M)]^{-1}$ is the photon lifetime determined by the output coupling from the laser facet, L is cavity length, and R_M is the facet reflectivity. dc photocurrent, $\langle i \rangle$, generated in a photodetector is

$$\langle i \rangle = D\overline{P(t)} = D(E_0^2 + \overline{C_n^2})/2\tau_{PM} \tag{46}$$

where $D = e\eta/\hbar\Omega$ is the photodetector conversion factor, and η is the photodetector quantum efficiency.

The term proportional to $E_0C_n(t)$ does not contribute to the dc photocurrent, since $C_n(t)$ is the zero mean Gaussian random variable. However this term does contribute to the noise power, that is, the beat noise between signal and noise waves. The spectral density of the noise current $\langle i_n^2 \rangle$ is

$$\langle i_n^2 \rangle = \frac{D^2}{\tau_{PM}^2} E_0^2 W_{cn}(\omega) \tag{47}$$

where $W_{cn}(\omega)$ is the spectral density of $C_n(t)$. The Fourier transform of (43) gives

$$W_{cn}(\omega) = \frac{W_{NS}(\omega)}{4\Omega^2\left[\omega^2 + \left\{\frac{n_{sp}}{\tau_p}(R + \Delta R)\right\}^2\right]} = \frac{2\hbar\Omega n_{sp} g_N(\Omega_0 + \omega)}{\pi\tau_p\left[\omega^2 + \left\{\frac{n_{sp}}{\tau_p}(R + \Delta R)\right\}^2\right]} \tag{48}$$

where the following spectral density of $N_s(t)$ is used.

$$W_{NS}(\omega) = W_{NC}(\omega) = 2W_N(\Omega_0 + \omega) = \frac{8\Omega^2\hbar\Omega}{\pi\tau_p} \cdot n_{sp} g_N(\Omega_0 + \omega). \tag{49}$$

Here, the small contribution of the thermal photon is neglected.

The value of $C_n(t)$ is calculated by using the spectral density $W_{cn}(\omega)$ as follows:

$$\overline{C_n(t)^2} \equiv \lim_{T\to\infty} \frac{1}{T}\int_0^T |C_n(t)|^2\,dt = \int_0^\infty W_{cn}(\omega)\,d\omega = \hbar\Omega/(R + \Delta R). \tag{50}$$

The value of E_0^2 can be derived using (50) in (44) such that

$$E_0^2 = \hbar\Omega\left[\frac{2n_{sp}}{\beta}(R + \Delta R) - \frac{1}{R + \Delta R}\right]. \tag{51}$$

Using (48) and (51) with (47), one obtains

$$\langle i_n^2 \rangle = \frac{e^2\eta^2\tau_p g_N(\Omega_0 + \omega)}{\pi\tau_{PM}^2 n_{sp}(R + \Delta R)^2} \cdot \left[\frac{2n_{sp}}{\beta}(R + \Delta R) - \frac{1}{R + \Delta R}\right] \Big/ [1 + (\omega/\omega_c)^2] \tag{52}$$

where ω_c is the cutoff frequency of the AM noise, and is given by

$$\omega_c = \frac{n_{sp}}{\tau_p}(R + \Delta R). \tag{53}$$

This is the unsaturated gain $\alpha - r$ which indicates that the unsaturated gain is still effective for suppressing AM noise. The relative intensity noise RIN is defined as

$$\text{RIN} \equiv \frac{\langle i_n^2 \rangle}{\langle i \rangle^2} = \tau_p \beta^2 \left[\frac{2n_{sp}}{\beta} (R + \Delta R) - \frac{1}{R + \Delta R} \right] \cdot g_N(\Omega_0 + \omega) / [\pi n_{sp}^3 (R + \Delta R)^4 \{1 + (\omega/\omega_c)^2\}]. \quad (54)$$

This RIN originates in the beat noise between E_0 and $C_n(t)$. The additional shot noise due to the signal wave E_0 and the noise wave $C_n(t)$ are also generated in the photodetector. Therefore, total RIN is

$$\text{RIN} = \text{eq. (54)} + 2\tau_{PM}\beta / [\eta n_{sp}(R + \Delta R)]. \quad (55)$$

The small contribution of beat noise between the noise waves is ignored here, although it is important for laser amplifiers operating below the lasing threshold [26], [27].

At well above the threshold region, $\Delta R = 0$ and the beat noise is dominant. The RIN in this region is approximated by

$$\text{RIN} = 2\tau_p \beta g_N(\Omega_0 + \omega) / [\pi n_{sp}^2 R^3 \{1 + (\omega/\omega_c)^2\}]. \quad (56)$$

This RIN is proportional to τ_p, β, n_{sp}^{-2}, and R^{-3}. At far above the threshold region, the signal wave induced shot noise is dominant, as shown by

$$\text{RIN} \simeq 2\beta\tau_{PM} / (\eta n_{sp} R). \quad (57)$$

The RIN in this region is proportional to τ_{PM}, β, n_{sp}^{-1}, and R^{-1}. It is noticeable that the RIN depends on photodetector quantum efficiency.

C. Photon Number Probability Density and Variance in Intensity Fluctuations

The probability distribution for the photon number was calculated for the superposition of the constant amplitude coherent wave and the Gaussian noise waves [29], [30]. The photon number probability density is of the form

$$\text{Prob}(n) = \frac{1}{1 + \langle n_T \rangle} \left[\frac{\langle n_T \rangle}{1 + \langle n_T \rangle} \right]^n \exp\left(- \frac{\langle n_s \rangle}{1 + \langle n_T \rangle} \right) \cdot L_n \left(- \frac{\langle n_s \rangle}{\langle n_T \rangle + \langle n_T \rangle^2} \right) \quad (58)$$

where $\langle n_s \rangle$ is the signal photon number, $\langle n_T \rangle$ is the noise photon number, and $L_n(x)$ is the Laguerre polynomial.

This result can be directly applied to the photon number probability density of semiconductor lasers through introducing the equivalent signal photon number and noise photon number in the following manner:

$$\langle n_s \rangle = \frac{E_0^2}{2\hbar\Omega} = \frac{n_{sp}}{\beta} (R + \Delta R) - \frac{1}{2(R + \Delta R)} \quad (59)$$

$$\langle n_T \rangle = \frac{\overline{C_n^2}}{2\hbar\Omega} = \frac{1}{2(R + \Delta R)}. \quad (60)$$

The first and second moments of the photon number are given by [29]

$$\langle n \rangle \equiv \sum n \, \text{Prob}(n) = \langle n_s \rangle + \langle n_T \rangle \quad (61)$$

$$\langle n^2 \rangle \equiv \sum n^2 \, \text{Prob}(n) = \langle n_s + n_T \rangle^2 + 2\langle n_s \rangle \langle n_T \rangle + \langle n_T \rangle^2 + \langle n_s + n_T \rangle. \quad (62)$$

The variance σ^2 is defined by

$$\sigma^2 \equiv \langle n^2 \rangle - \langle n \rangle^2 = 2\langle n_s \rangle \langle n_T \rangle + \langle n_T \rangle^2 + \langle n_s + n_T \rangle \quad (63)$$

where the first term is beat noise between the signal and noise waves, the second term is beat noise between the noise waves, and the third term is signal wave- and noise waves-induced shot noise. The relative variance in the intensity fluctuation $\rho \equiv \sigma^2 / \langle n \rangle^2$ is given by

$$\rho = \left[\frac{n_{sp}}{\beta} - \frac{1}{4(R + \Delta R)^2} + \frac{n_{sp}}{\beta} (R + \Delta R) \right] \Big/ \left[\frac{n_{sp}^2}{\beta^2} (R + \Delta R)^2 \right]. \quad (64)$$

The relative variance ρ is alternatively obtained by integrating (55) over $\omega = 0$ to $\omega = \infty$, which brings the same result as (68).

D. FM Noise Spectrum

In this section, the FM noise spectrum, that is, the spectral density function of the instantaneous frequency deviation $\delta\Omega = \Omega - \Omega_0$ will be derived.

The laser field (40) is written as

$$E = [E_0 + C_n(t)] \cos(\Omega t + \theta) \quad (65)$$

where

$$\theta(t) = -\tan^{-1} \left[\frac{S_n(t)}{E_0 + C_n(t)} \right] = - \frac{S_n(t)}{E_0 + C_n(t)}. \quad (66)$$

The second equality of (66) is valid only when the phase diffusion is not large, that is when the measuring time interval is much shorter than the coherence time for the laser field. The same assumption was used when deriving (42) and (43). The instantaneous frequency deviation $\delta\Omega$ is given by

$$\delta\Omega \equiv \frac{d\theta}{dt} = \frac{-\dot{S}_n(t)}{E_0 + C_n(t)} = - \frac{N_c(t)}{2\Omega [E_0 + C_n(t)]}. \quad (67)$$

Consequently, the spectral density function of $\delta\Omega$ can be calculated using (44) and (49) such that

$$W_{\delta\Omega}(\omega) = \frac{W_{NC}(\omega)}{4\Omega^2 [E_0^2 + \overline{C_n(t)^2}]} = \beta g_N(\Omega_0 + \omega) / [\pi\tau_p (R + \Delta R)]. \quad (68)$$

The FM noise spectrum (68) shows a flat frequency response up to the cutoff frequency for the gain envelope function $g_N(\Omega_0 + \omega)$ which is typically 10^{12}–10^{13} Hz for GaAs lasers. This is the most striking difference between the FM noise spectrum and the AM noise spectrum (55), which has a much lower and bias level-dependent cutoff frequency ω_c.

E. Power Spectrum and Spectral Linewidth

The power spectrum of the laser output is mainly due to the FM noise. The contribution of the AM noise spreads over a

broad frequency range, and the integrated power spectrum is smaller than that for FM noise [2], [3]. Therefore, the power spectrum determined by the FM noise will be derived in this section.

The laser field is expressed as

$$E = [E_0 + C_n(t)] \cdot \mathrm{Re}\,[v(t) \exp(j\Omega t)], \tag{69}$$

where

$$v(t) = \exp[j\theta(t)]. \tag{70}$$

The phase θ is a random Gaussian process, although it is not stationary. The autocorrelation function of $v(t)$ is given by

$$C_v(\tau) = \langle v(t)\, v(t+\tau)^* \rangle = \exp\left[-2 \int_0^\infty W_{\delta\Omega}(\omega) \left[\frac{\sin\left(\frac{\omega\tau}{2}\right)}{\omega}\right]^2 d\omega\right]. \tag{71}$$

Since $W_{\delta\Omega}$ is constant in the integration, (71) is written as

$$C_v(\tau) = \exp\left[-\frac{\pi}{2} W_{\delta\Omega}(0)\, \tau\right]. \tag{72}$$

The power spectrum $W_0(\Omega - \Omega_0)$ can be represented using the spectral density function of $C_v(\tau)$ as follows.

$$W_0(\Omega - \Omega_0) = \frac{1}{2\pi} \int_{-\infty}^{\infty} C_v(\tau) \exp(-j\Omega\tau)\, d\tau = \beta \Big/ \left[2\pi\tau_p(R + \Delta R) \left\{\left(\frac{\beta}{2\tau_p(R+\Delta R)}\right)^2 + (\Omega - \Omega_0)^2\right\}\right]. \tag{73}$$

The oscillation power spectrum has a Lorentzian shape, with a full linewidth at half-maximum of

$$\Delta\nu_{1/2} = \frac{\beta}{4\pi\tau_p(R + \Delta R)}. \tag{74}$$

By comparing (68) and (74), it is possible to obtain

$$\Delta\nu_{1/2} = \tfrac{1}{2}\, W_{\delta\Omega}(\omega \approx 0). \tag{75}$$

The FM noise spectrum and spectral linewidth are proportional to β, τ_p^{-1}, and R^{-1}, but are independent of n_{sp}.

The instantaneous frequency probability density, Prob(Ω), can be given as a function of the spectral linewidth $\Delta\nu_{1/2}$. This last identity is calculated in the Appendix.

V. Fokker-Planck Equation

A. Derivation of the Equation

Since the noise driving source $\tilde{F}(t)$ in the generalized van der Pol equation (12) is of a Marcovian type, the distribution function of the photon amplitude $W(B, t)$ can be described by the Fokker-Planck equation [6], [7]. Here the photon amplitude $B = B_1 + jB_2$, is treated as a classical random variable. The noise driving source is similarly treated as a classical variable $\tilde{F} = F_1 + jF_2$.

The distribution function of the photon amplitude $W(B, t)$ obeys the following equation:

$$\frac{\partial W}{\partial t} = -\sum_{i=1}^{2} \frac{\partial}{\partial B_i}(d_i W) + \frac{1}{2} \sum_{i,j=1}^{2} \frac{\partial^2}{\partial B_i \partial B_j}(D_{ij} W) \tag{76}$$

where the drift constant d_i and the diffusion constant D_{ij} are defined as

$$d_i = \lim_{T \to 0} \frac{1}{T} \langle B_i(t+T) - B_i(t) \rangle, \tag{77}$$

$$D_{ij} = \lim_{T \to 0} \frac{1}{T} \langle [B_i(t+T) - B_i(t)]\, [B_j(t+T) - B_j(t)] \rangle. \tag{78}$$

From the generalized van der Pol equation (12), one obtains

$$B_i(t+T) - B_i(t) = \int_t^{t+T} \left\{\left[G - K - \frac{dS(n)}{dn} B^* B\right] B + \tilde{F}(t')\right\} dt'. \tag{79}$$

Using (79) and $\langle \tilde{F}(t) \rangle = 0$ in (77) and (78), it is possible to get

$$d_i = \left(G - K - \frac{dS(n)}{dn} B^* B\right) B_i = \frac{1}{2\tau_p}(R n_{sp} - \beta B^* B)\, B_i \tag{80}$$

$$D_{ij} = \lim_{T \to 0} \frac{1}{T} \langle \tilde{F}_i(t+T)\, \tilde{F}_j(t) \rangle = \delta_{ij} \frac{n_{sp}}{\tau_p}. \tag{81}$$

The Fokker-Plank equation for semiconductor lasers is, from (76), (80), and (81), of the form

$$\frac{\partial W}{\partial t} + C_1 \,\mathrm{div}\,[(C_2 - |B|^2) BW] = C_3 \Delta W \tag{82}$$

where the operator, div, and the Laplacian Δ act on B. The coefficients C_1, C_2, and C_3 are given by

$$C_1 = \beta/2\tau_p \tag{83}$$

$$C_2 = R n_{sp}/\beta \tag{84}$$

$$C_3 = n_{sp}/4\tau_p. \tag{85}$$

It is convenient to use polar coordinates $B = re^{j\phi}$. The Fokker-Planck equation is then transformed into

$$\frac{\partial W}{\partial t} + C_1 \cdot \frac{1}{r} \frac{\partial}{\partial r}[(C_2 - r^2) r^2 W] = C_3 \left[\frac{1}{r} \frac{\partial}{\partial r}\left(r \frac{\partial W}{\partial r}\right) + \frac{1}{r^2} \frac{\partial^2 W}{\partial \vartheta^2}\right]. \tag{86}$$

A theoretical analysis of the Fokker-Planck equation (86) was performed by Risken in this form [6], [7]. All results which were found by Risken can immediately be used for semiconductor lasers.

B. Probability Density and Joint Distribution Functions

The stationary distribution function for the photon amplitude $W(r)$ in (86) reads

$$W(r) = W_0 \exp\left[-\frac{C_1}{4C_3} r^2(r^2 - 2C_2)\right]$$
$$= W_0 \exp\left[-\frac{\beta}{2n_{sp}} r^2 \left(r^2 - \frac{2Rn_{sp}}{\beta}\right)\right]. \quad (87)$$

The photon number probability density, $\text{Prob}(n = r^2)$ can then be given by

$$\text{Prob}(n) = P_0 \cdot \exp\left[-\frac{\beta}{2n_{sp}} n \left(n - \frac{2Rn_{sp}}{\beta}\right)\right] \quad (88)$$

where the normalization constant is calculated from

$$\int_0^\infty \text{Prob}(n)\, dn = 1$$

as

$$P_0^{-1} = \sqrt{\pi}\, \kappa\, [1 + \text{erf}\,(\kappa R)]\, \exp(\kappa^2 R^2) \quad (89)$$

$$\kappa = \sqrt{\frac{n_{sp}}{2\beta}}. \quad (90)$$

The mean photon number $\langle n \rangle$ is calculated by using (88) in the following manner:

$$\langle n \rangle \equiv \sum n\, \text{Prob}(n) = \frac{n_{sp}}{\beta}(R + P_0). \quad (91)$$

In order to calculate the correlation function $\langle B(t+T)^* B(t) \rangle$ the joint distribution probability that $B(t)$ lies in the interval $B' \leqslant B(t) \leqslant B' + dB'$ and that $B(t+T)$ lies in the interval $B \leqslant B(t+T) \leqslant B + dB$ has to be dealt with first. At well above the threshold region, this joint distribution can be broken down into

$$F(r, \phi; r', \phi', \tau) = F_1(r, r', \tau) \cdot F_2(\phi, \phi', \tau), \quad (92)$$

where

$$F_1(r, r', \tau) = \pi^{-1}\, [1 - \exp(-4C_1C_2\tau)]^{-1/2} \cdot \exp\left[-\frac{y^2 + y'^2 - 2yy' \exp(-2C_1C_2\tau)}{1 - \exp(-4C_1C_2\tau)}\right], \quad (93)$$

$$F_2(\phi, \phi', \tau) = (2\pi)^{-2}\, \vartheta_3\left(\frac{\phi - \phi'}{2\pi}, \frac{C_3\tau}{C_2\pi}\right). \quad (94)$$

Here, ϑ_3 is the third Jacobian theta function. The abbreviation

$$y = \sqrt{2R}\, (r - \langle r \rangle) \quad (95)$$

is used for convenience.

C. Variance and Spectrum for Intensity Fluctuation

The correlation function for the intensity fluctuation $K(\tau)$ is calculated from (93) as

$$K(\tau) = \langle [r^2(t+\tau) - \langle r^2 \rangle]\, [r^2(t) - \langle r^2 \rangle] \rangle$$
$$= \frac{n_{sp}}{\beta} \exp\left(-\frac{Rn_{sp}}{\tau_p} \cdot \tau\right). \quad (96)$$

Equation (96) shows that variance and bandwidth of intensity fluctuation are given by $\sigma^2 = n_{sp}/\beta$ and $\omega_c = Rn_{sp}/\tau_p$. This is in agreement with the results at well above the threshold region given in (64) and (53). The relative variance, including shot noise, is given by

$$\rho = \frac{K(0) + \langle r^2 \rangle}{\langle r^2 \rangle^2} = \beta(R + P_0 + 1)/[n_{sp}(R + P_0)^2]. \quad (97)$$

The spectrum of intensity fluctuation is provided by

$$\text{RIN} = 2\tau_p\beta/[\pi n_{sp}^2 (R + P_0)^3\, \{1 + (\omega/\omega_c)^2\}] + \text{shot noise term}, \quad (98)$$

where the cutoff frequency ω_c is calculated through taking the first value of P_0 into account, which is

$$\omega_c = \frac{n_{sp}}{\tau_p}(R + P_0). \quad (99)$$

D. Spectral Linewidth

The correlation function for the phase is calculated by (94) such that

$$C_v(\tau) \equiv \langle e^{-i\varphi(t+\tau)} e^{i\varphi(t)} \rangle = \exp\left(-\frac{\beta}{4\tau_p R}\tau\right). \quad (100)$$

The spectral linewidth at half-maximum of the Lorentzian power spectrum is, taking into account the finite value of P_0,

$$\Delta\nu_{1/2} = \frac{\beta}{4\pi\tau_p(R + P_0)}. \quad (101)$$

This result is in agreement with (74), which was obtained by assuming that the laser field is expanded to the coherent signal wave E_0 and noise waves C_n, S_n.

VI. Rate Equations with a Fluctuating Operator

A. Derivation of the Rate Equation

The Statz-deMars type rate equation, i.e., the photon number representation of the Langevin equation, is obtained from (13), (16), (19), and (20) for semiconductor lasers as

$$\frac{d}{dt} n = -\frac{n}{\tau_p} + A\Gamma \frac{N_c}{V_e} + A\Gamma \left(\frac{N_c}{V_e} - N_0\right) n + F_n(t). \quad (102)$$

The equation for the total electron number N_c reads

$$\frac{d}{dt} N_c = P - \frac{N_c}{\tau_s} - A\Gamma \left(\frac{N_c}{V_e} - N_0\right) n - A\Gamma \frac{N_c}{V_e} + F_c(t). \quad (103)$$

The correlation function for the photon and carrier fluctuation operators have already been given by (15), (17), and (18).

The carrier and photon numbers are expressed as the sum of the mean value and fluctuation around them such that

$$n = \bar{n} + \Delta n$$
$$N_c = \bar{N}_c + \Delta N_c.$$

Using these equations with (102) and (103), and neglecting the products of the small fluctuation terms, one obtains

$$\frac{d}{dt}\Delta N_c = A_1 \Delta N_c + A_2 \Delta n + F_c(t) \tag{104}$$

$$\frac{d}{dt}\Delta n = A_3 \Delta N_c + A_4 \Delta n + F_n(t) \tag{105}$$

where

$$A_1 = -\frac{1}{\tau_s}(1+\beta\bar{n}) + \frac{1}{\tau_s^2}\frac{d\tau_s}{dN_c}\frac{\bar{N}_c}{V_e}, \tag{106}$$

$$A_2 = -\beta\frac{\bar{N}_c}{\tau_s} + A\Gamma N_0, \tag{107}$$

$$A_3 = \frac{\beta}{\tau_s}(1+\bar{n}), \tag{108}$$

$$A_4 = \beta\frac{\bar{N}_c}{\tau_s} - A\Gamma N_0 - \frac{1}{\tau_p}. \tag{109}$$

The Fourier transform of (104) and (105) gives

$$\Delta N_c(\omega) = \frac{A_2 F_n(\omega) + (j\omega - A_4) F_c(\omega)}{(A_1A_4 - A_2A_3 - \omega^2) - j\omega(A_1 + A_4)}, \tag{110}$$

$$\Delta n(\omega) = \frac{A_3 F_c(\omega) + (j\omega - A_1) F_n(\omega)}{(A_1A_4 - A_2A_3 - \omega^2) - j\omega(A_1 + A_4)}. \tag{111}$$

Here the spectral density of the photon and carrier fluctuation terms are given by

$$\langle F_n(\omega)^2\rangle = \frac{\bar{n}}{\tau_p} + \frac{\beta\bar{N}_c}{\tau_s}(1+\bar{n}) + A\Gamma N_0\bar{n}, \tag{112}$$

$$\langle F_c(\omega)^2\rangle = P + \frac{\bar{N}_c}{\tau_s} + \frac{\beta\bar{N}_c}{\tau_s}(1+\bar{n}) + A\Gamma N_0\bar{n}, \tag{113}$$

$$\langle F_c(\omega)\,F_n(\omega)\rangle = -\frac{\beta\bar{N}_c}{\tau_s}(1+\bar{n}) - A\Gamma N_0\bar{n}. \tag{114}$$

Equations (110) and (111), together with (112)-(114), are basic equations for the quantum noise analysis presented in this section. This set of equations automatically includes the carrier noise (113), photon noise (112), and competition between the two noises (114). Therefore, it can describe the laser noise properties over the whole range of the pumping level, including below and just at the threshold, and also over the range of the relaxation oscillation frequencies. However, the actual noise properties below and just above the threshold, as well as in the resonant relaxation frequency range, are affected by the existence of spurious longitudinal modes and the lateral carrier diffusion effect, which will be discussed later. Multimode rate equations with fluctuation operators were treated by Jackel *et al.* [32] and by Mukai *et al.* [27].

B. Photon Noise and Carrier Noise Spectra

The relative intensity noise spectrum is calculated from (111) as

$$\mathrm{RIN} \equiv \frac{\langle \Delta n(\omega)^2\rangle}{\bar{n}^2} = \frac{1}{\bar{n}^2}\left[\frac{A_3^2\langle F_c(\omega)^2\rangle + (\omega^2 + A_1^2)\langle F_n(\omega)^2\rangle - 2A_1A_3\langle F_c(\omega)\,F_n(\omega)\rangle}{(A_1A_4 - A_2A_3 - \omega^2)^2 + \omega^2(A_1 + A_4)^2}\right]. \tag{115}$$

Here, the mean photon number $\bar{n}$ and the mean carrier number $\bar{N}_c$ are calculated from the following transcendental equation

$$P - (1+\beta)\frac{\bar{N}_c}{\tau_s} - \left(\beta\frac{\bar{N}_c}{\tau_s} - A\Gamma N_0\right) \times \frac{\beta\bar{N}_c/\tau_s}{1/\tau_p - (\beta(\bar{N}_c/\tau_s) - A\Gamma N_0)} = 0 \tag{116}$$

where

$$\bar{n} = \frac{\beta(\bar{N}_c/\tau_s)}{1/\tau_p - (\beta(\bar{N}_c/\tau_s) - A\Gamma N_0)}.$$

The relative carrier noise spectrum is similarly obtained as

$$\frac{\langle \Delta N_c(\omega)^2\rangle}{\bar{N}_c^2} = \frac{1}{\bar{N}_c^2} \times \left[\frac{A_2^2\langle F_n(\omega)^2\rangle + (\omega^2 + A_4^2)\langle F_c(\omega)^2\rangle - 2A_2A_4\langle F_c(\omega)\,F_n(\omega)\rangle}{(A_1A_4 - A_2A_3 - \omega^2)^2 + \omega^2(A_1 + A_4)^2}\right]. \tag{118}$$

C. Spectrum of FM Noise Due to Spontaneous Emission

The phase diffusion constant $D(\Delta\theta)$ caused by spontaneous emission is determined by the ratio of the out-of-phase noise photon n_{sn} coupled to the lasing mode, to the total signal photon inside a laser cavity. The total noise photon coupled to the lasing mode is given by the second term on the right in (102). The probabilities that these noise photons are in-phase and out-of-phase with respect to the signal photon are equal. The phase diffusion constant is given by

$$D(\Delta\theta) \equiv \frac{n_{sn}}{\bar{n}} = \left\{2\left[\frac{1}{\tau_p} - \left(\beta\frac{\bar{N}_c}{\tau_s} - A\Gamma N_0\right)\right]\right\}^{-1}. \tag{119}$$

The spectral linewidth $\Delta\nu_{1/2}$ and the FM noise spectrum are given by

$$\Delta\nu_{1/2} = \frac{1}{2}W_{\delta\Omega}(0) = \left\{4\pi\left[\frac{1}{\tau_p} - \left(\beta\frac{\bar{N}_c}{\tau_s} - A\Gamma N_0\right)\right]\right\}^{-1}. \tag{120}$$

The value of $1/\tau_p - (\beta(\bar{N}_c/\tau_s) - A\Gamma N_0)$ indicates how the actual saturated gain $(\beta(\bar{N}_c/\tau_s) - A\Gamma N_0)$ approaches the cavity loss constant $1/\tau_p$. It can be concluded that the spectral linewidth is determined by the difference between the theoretical threshold gain and the actual saturated gain.

D. Spectrum of FM Noise Due to Carrier Modulation Noise

The difference between the FM noise spectrum in semiconductor lasers from spectra in other lasers is that in semiconductor lasers both the carrier modulation noise and current modulation noise due to the quantum effect cause additional FM noise. The additional line broadening due to the refractive-index dispersion effect is treated by Haug and Haken [8], and very recently by Henry [34]. The two treatments employ the adiabatic elimination of the equation describing a carrier density fluctuation and use only the equation for photon field variables. Therefore, it seems that they cannot describe the effects of the carrier and photon noise competition on FM noise spectrum and line shape.

The frequency modulation $\Delta\Omega$ due to the carrier modulation $\Delta N_c(t)$ is given by

$$\Delta\Omega = \Omega_0(C_{BB} + C_{FC}) \frac{\Gamma}{\overline{n_{\text{eff}}}} \cdot \frac{\Delta N_c(t)}{V_e}. \tag{121}$$

Here, Ω_0 is the oscillation center frequency, and C_{BB} and C_{FC} are the coefficients representing the contribution of the carrier density change to the refractive-index change caused, respectively, by the band-to-band transition effect and free carrier plasma dispersion effect [33]. The estimation of values C_{BB} and C_{FC} will be discussed in an accompanying paper. $\overline{n_{\text{eff}}}$ is the refractive-index of the GaAs active layer. The FM noise spectrum $W^c_{\delta\Omega}$ due to the carrier modulation noise is given by

$$W^c_{\delta\Omega} = \left[\frac{\Omega_0(C_{BB} + C_{FC})}{\overline{n_{\text{eff}}} V_0}\right]^2 \langle \Delta N_c(\omega)^2 \rangle \tag{122}$$

where $\langle \Delta N_c(\omega)^2 \rangle$ is calculated from (118).

E. Spectrum of FM Noise Due to Current Modulation Noise

The junction current is modulated by the quantum noise fluctuation of the carrier. In the low frequency range, this current noise induces diode temperature fluctuation, and consequently, causes frequency modulation.

The junction current noise is introduced in (103) by the form

$$P = [\bar{I} + \Delta I(t)]/e. \tag{123}$$

Using (123) in (104) gives

$$\frac{d}{dt}\Delta N_c = \frac{\Delta I(t)}{e} + A_1 \Delta N_c + A_2 \Delta n + F_c(t). \tag{104'}$$

The Fourier transform of (104) gives

$$\Delta I(\omega) = e\,[(j\omega - A_1)\Delta N_c(\omega) - A_2 \Delta n(\omega) - F_c(\omega)]. \tag{124}$$

The relative current noise spectrum is calculated to be

$$\frac{\langle \Delta I(\omega)^2 \rangle}{\bar{I}^2} = \frac{e^2 A_1^2}{\bar{I}^2}\left[\frac{A_2^2 \langle F_n(\omega)^2 \rangle + (\omega^2 + A_4^2)\langle F_c(\omega)^2 \rangle - 2A_2A_4 \langle F_c(\omega) F_n(\omega) \rangle}{(A_1A_4 - A_2A_3 - \omega^2)^2 + \omega^2(A_1 + A_4)^2}\right] \tag{125}$$

where the small contribution of the current noise directly induced by the photon noise and the usual shot noise $F_c(t)$ are ignored.

Frequency modulation $\Delta\Omega$ due to temperature modulation $\Delta T(t)$ as induced by the junction current modulation $\Delta I(t)$ is of the form

$$\Delta\Omega = -\Omega_0(\alpha_L + \alpha_n)\,\Delta T(t). \tag{126}$$

Here, α_L is the linear thermal expansion coefficient, and α_n is the thermal refractive-index change coefficient. Temperature modulation is calculated by the Fourier and Laplace transform method for the time-dependent thermal equation [35]. The theoretical and experimental determination of the values $\Delta\Omega/\Delta I$ will be discussed in an accompanying paper [19]. The FM noise spectrum $W^I_{\delta\Omega}$ due to the current modulation noise is then given by

$$W^I_{\delta\Omega}(\omega) = (\Delta\Omega/\Delta I)^2 \langle \Delta I(\omega)^2 \rangle. \tag{127}$$

VII. Photon Density Matrix Equation

A. Derivation of the Equation

The equation of motion for the photon density matrix diagonal element takes the form

$$\begin{aligned}\frac{d\rho_n}{dt} = &-\frac{(n+1)A}{1+(n+1)s}\rho_n + \frac{nA}{1+ns}\rho_{n-1} \\ &+ \frac{(n+1)B}{1+(n+1)s}\rho_{n+1} - \frac{nB}{1+ns}\rho_n \\ &+ (n+1)C\rho_{n+1} - nC\rho_n\end{aligned} \tag{128}$$

where

$$A = \frac{n_{sp}}{\tau_p}(R+1) \tag{129}$$

$$B = \frac{1}{\tau_p}(n_{sp} - 1) \tag{130}$$

$$C = \frac{1}{\tau_p}. \tag{131}$$

Value A-B corresponds to the unsaturated gain α in the van der Pol equation (32). The saturation parameter s is equal to the spontaneous emission coefficient β, as was discussed in Section III, that is represented by

$$s = \beta. \tag{132}$$

The equation of motion for the mean photon number $\langle n \rangle = \Sigma n\rho_n$, the second moment $\langle n^2 \rangle = \Sigma n^2\rho_n$, and the rth moment $\langle n^r \rangle = \Sigma n^r \rho_n$ are given by

$$\frac{d\langle n \rangle}{dt} = \left\langle \frac{n+1}{1+(n+1)s} \right\rangle A - \left\langle \frac{n}{1+ns} \right\rangle B - \langle n \rangle C, \tag{133}$$

$$\frac{d\langle n^2\rangle}{dt} = \left\langle \frac{2n^2+3n+1}{1+(n+1)s} \right\rangle A - \left\langle \frac{2n^2-n}{1+n\cdot s} \right\rangle B - 2\langle n^2\rangle C + \langle n\rangle C, \tag{134}$$

$$\frac{d\langle n^r\rangle}{dt} = \sum_{j=0}^{r-1} \binom{r}{j} \left[\left\langle \frac{(n+1)n^j}{1+(n+1)s} \right\rangle A + (-1)^{r+j} \left\langle \frac{n^{j+1}}{1+ns} \right\rangle B + (-1)^{r+j} \langle n^{j+1}\rangle C \right]. \tag{135}$$

For gaseous and solid-state lasers with $n_{sp} = 1$, terms proportional to B are dropped from (128), (133)-(135). This special case corresponds to the results derived by Scully and Lamb [10].

B. Photon Number Probability Density

The master equation (128) is reduced to two equivalent systems of first order difference equations

$$\frac{nA}{1+ns}\rho_{n-1} - \frac{nB}{1+ns}\rho_n - nC\rho_n = 0 \tag{136}$$

$$\frac{(n+1)A}{1+(n+1)s}\rho_n - \frac{(n+1)B}{1+(n+1)s}\rho_{n+1} - (n+1)C\rho_{n+1} = 0. \tag{137}$$

These equations can be solved by using (136) and (137) iteratively, that is

$$\rho_n = N_0 \left(\frac{A-B}{C}\right)^n \prod_{k=0}^{n} \frac{1}{1+ks} = \frac{N_0}{s!} \cdot \frac{Z^n}{\left(\frac{1}{s}+n\right)!}. \tag{138}$$

Here,

$$Z = \frac{A-B}{sC} = \frac{Rn_{sp}+1}{\beta}. \tag{139}$$

The normalization factor N_0 is determined by the condition $\Sigma\rho_n = 1$.

C. Mean Value and Variance of Photon Number

The mean photon number $\langle n\rangle$ is calculated by

$$\langle n\rangle \equiv \sum n\rho_n = \frac{n_{sp}}{\beta}(R+\rho_0). \tag{140}$$

The result is in agreement with (91), obtained from the Fokker-Planck equation. The relative variance of the photon number is given by

$$\rho \equiv \frac{\langle n^2\rangle - \langle n\rangle^2}{\langle n\rangle^2} = \frac{\beta(R+1)}{n_{sp}(R+\rho_0)^2}. \tag{141}$$

This result is again in agreement with (97), as obtained from the Fokker-Planck equation.

D. Spectral Linewidth

Even when the diagonal elements ρ_n of the density matrix are in a steady state, as shown by (138), the off-diagonal elements in the density matrix have exponential decay functions [11], which are

$$\rho_{n,n+k}(t) = \rho_{n,n+k}(0)\exp\left(-\tfrac{1}{2}k^2Dt\right). \tag{142}$$

Here,

$$D = \frac{1}{2}C\frac{n_{sp}}{\langle n\rangle} = \frac{\beta}{2\tau_p(R+\rho_0)}. \tag{143}$$

The expected value of the electric field for this element is given by

$$E(t) = E_0\exp\left(-\tfrac{1}{2}Dt\right)\cos\Omega_0 t. \tag{144}$$

The spectral profile for this field is Lorentzian, and its linewidth is given by

$$\Delta\nu_{1/2} = \frac{\beta}{4\pi\tau_p(R+\rho_0)}. \tag{145}$$

This result is in agreement with (101), as obtained from the Fokker-Planck equation.

VIII. Conclusion

Quantum noise properties for semiconductor lasers were studied through the use of four different theoretical formulations: the van der Pol equation; the Fokker-Planck equation; the rate equation; and the photon density matrix master equation.

AM quantum noise properties were characterized by: 1) the AM noise spectrum at low frequency RIN($\omega \approx 0$); 2) the resonance enhancement of AM noise near the relaxation oscillation frequency RIN($\omega \approx \omega_r$); 3) the bandwidth of AM noise spectrum ω_c; 4) the variance of intensity fluctuation ρ; and 5) the photon number probability density Prob(n). FM quantum noise properties were characterized by the FM noise spectrum caused by: 1) the spontaneous emission coupled to a lasing mode $W_{\delta\Omega}^{sp}(\omega)$; 2) the carrier modulation noise $W_{\delta\Omega}^{c}(\omega)$; 3) the current modulation noise $W_{\delta\Omega}^{I}(\omega)$; 4) the instantaneous frequency probability density Prob(Ω); and 5) the power spectrum or the spectral linewidth $\Delta\nu_{1/2}$. Theoretical formulations for these quantum noise properties, derived from the just-mentioned four different approaches are summarized in Table I. Numerical comparisons between these different formulations are described in an accompanying paper, as also are experimental results with AlGaAs lasers.

Theoretical formulations for the AM and FM noise spectra presented in this paper enable calculation of the signal-to noise ratio and carrier-to-noise ratio degradation due to quantum noise. The *C/N* degradation in optical heterodyne detection caused by local oscillator AM noise, and *S/N* degradation in FSK and PSK systems caused by FM noise in both the transmitter and local oscillator are specially important.

Error rate calculations for coherent optical transmission systems that have been based on completely coherent waves and Gaussian probability densities [36] should be modified to incorporate the effects described here. This will be treated in more detail in a future work, together with the effects of convolution with detector dark current induced shot noise of Poisson process, and the receiver amplifier thermal noise of Gaussian process, and also photon number probability density deformation due to optical attenuation and the detection band limit.

TABLE I
THEORETICAL FORMULATIONS FOR AM AND FM NOISE PROPERTIES IN SEMICONDUCTOR LASERS. ———: NOT DERIVED IN THIS WORK

Theoretical Methods	van der Pol eq.	Fokker-Planck eq.	Rate eq.	Density Matrix eq.
AM noise				
RIN($\omega \approx 0$)	Eq.(55)	Eq.(98)	Eq.(115)	———
RIN($\omega \approx \omega_r$)	———	———	Eq.(115)	———
bandwidth ω_c	Eq.(53)	Eq.(99)	Eq.(115)	———
variance ρ	Eq.(64)	Eq.(97)	———	Eq.(141)
Prob(n)	Eq.(58)	Eq.(88)	———	Eq.(138)
FM noise				
spectrum $W_{\delta\Omega}^{SP}(\omega)$	Eq.(68)	Eq.(101)	Eq.(120)	Eq.(145)
spectrum $W_{\delta\Omega}^{C}(\omega)$	———	———	Eq.(122)	———
spectrum $W_{\delta\Omega}^{I}(\omega)$	———	———	Eq.(127)	———
spectral linewidth $\Delta\nu_{1/2}$	Eq.(74)	Eq.(101)	Eq.(120)	Eq.(145)
Prob(Ω)	Eq.(A5) with Eq.(74)	Eq.(101)	Eq.(120)	Eq.(145)

APPENDIX
INSTANTANEOUS FREQUENCY PROBABILITY DENSITY

The probability distribution of the output intensity Prob(I), after passing through an optical frequency discriminator corresponds to the instantaneous frequency probability density when the relation of the output power versus the optical frequency can be assumed to be linear. This ideal optical frequency discriminator is, for instance, realized by a Michelson interferometer operating around its center frequency $\Omega_0\tau = 2N\pi + \pi/2$, where Ω_0 is the optical frequency and τ is the delay time introduced by the arm length difference in the interferometer. Normalized optical power from the Michelson interferometer is written as

$$I(t) = 1 + \sin\left[\Delta\theta(\tau)\right]. \tag{A-1}$$

In order to determine the probability density function Prob(I), the probability $P_\tau(\Delta\theta)$ that the phase has changed by $\Delta\theta$ in the time interval τ should be calculated. The phase change has a Gaussian probability density [27]

$$P_\tau(\Delta\theta) = \frac{1}{\sqrt{2\pi D\tau}} \exp\left(-\frac{\Delta\theta^2}{2D\tau}\right) \tag{A-2}$$

where $D = 2\pi\Delta\nu_{1/2}$ is the phase diffusion constant. The output intensity I is a multivalued function of $\Delta\theta$ as indicated by (A-1). Therefore, the probability density Prob(I) dI is the sum of all probabilities that $\Delta\theta$ is an interval $d(\Delta\theta)$ around $\sin^{-1}(I-1)$. This is shown by

$$\begin{aligned}\text{Prob}(I)\,dI &= \frac{d(\Delta\theta)}{(2\pi D\tau)^{1/2}} \sum_{k=-\infty}^{\infty} \left\{\exp\left[-\frac{(\Delta\theta + 2k\pi)^2}{2D\tau}\right] + \exp\left[-\frac{(\Delta\theta - 2k\pi)^2}{2D\tau}\right]\right\} \\ &= \frac{d(\Delta\theta)}{\left(\frac{1}{2}D\tau\right)^{1/2}} \exp\left(-\frac{\Delta\theta^2}{2D\tau}\right) \cdot \vartheta_3\left[\frac{i\pi\Delta\theta}{D\tau}, \exp\left(\frac{-2\pi^2}{D\tau}\right)\right]\end{aligned} \tag{A-3}$$

where $\vartheta_3(\kappa, y)$ is the third Jacobian theta function. The output intensity deviation ΔI corresponds to the optical frequency deviation $\Delta\Omega$ from the center frequency Ω_0 as follows:

$$\Delta I = \tau \cdot \Delta\Omega. \tag{A-4}$$

The instantaneous frequency probability density, Prob(Δf), is calculated from (A-3) and (A-4) as

$$\text{Prob}(\Delta f) = A_0 \exp\left[-\Delta f^2/(\Delta\nu_{1/2}/\pi\tau)^2\right] \cdot \vartheta_3\left[-\frac{i\pi\Delta f}{\Delta\nu_{1/2}}, \exp\left(-\frac{\pi^2}{2\pi\Delta\nu_{1/2}\tau}\right)\right]. \tag{A-5}$$

Equation (A-5) indicates that the instantaneous frequency probability density has a Gaussian profile near the central region, but that it has a much broader tail due to the additional theta function. The bandwidth of the Michelson interferometer with a decay time τ is $1/2\pi\tau$. Equation (A-5) can then be written in a general form as a function of the spectral linewidth of $\Delta\nu_{1/2}$ and detection bandwidth B_0.

$$\text{Prob}(\Delta f) = A_0 \exp\left(-\frac{\Delta f^2}{2\Delta\nu_{1/2}B_0}\right) \cdot \vartheta_3\left[-\frac{i\pi\Delta f}{\Delta\nu_{1/2}}, \exp\left(-\frac{\pi^2 B_0}{\Delta\nu_{1/2}}\right)\right]. \tag{A-6}$$

ACKNOWLEDGMENT

The author wishes to thank T. Kimura and A. Kawana for their useful suggestions. He also wishes to thank P. Meissner for his critical comments concerning the photon number probability density calculation.

REFERENCES

[1] Y. Yamamoto and T. Kimura, "Coherent optical fiber transmission systems," *IEEE J. Quantum Electron.*, vol. QE-17, pp. 919–935, June 1981.
[2] H. Haken, *Laser Handbook, Vol. 1*, F. T. Arrechi, Ed. New York: North-Holland.
[3] —, *Encyclopedia of Physics*, vol. XXV/2c, S. Flugge, Ed. Berlin: Springer-Verlag.
[4] D. E. McCumber, "Intensity fluctuations in the output of cw laser oscillators I," *Phys. Rev.*, vol. 141, pp. 306–322, 1966.

[5] H. Haug, "Quantum mechanical rate equations for semiconductor lasers," *Phys. Rev.*, vol. 184, pp. 338-348, 1969.
[6] H. Risken, "Distribution and correlation functions of a laser amplitude," *Z. Phys.*, vol. 186, pp. 85-98, 1965.
[7] —, "Correlation function of the amplitude and of the intensity fluctuation for a laser model near threshold," *Z. Phys.*, vol. 191, pp. 302-313, 1966.
[8] H. Haug and H. Haken, "Theory of noise in semiconductor laser emission," *Z. Phys.*, vol. 204, pp. 262-275, 1967.
[9] A. Yariv and W. M. Caton, "Frequency, intensity, and field fluctuations in laser oscillators," *IEEE J. Quantum Electron.*, vol. QE-10, pp. 509-515, 1974.
[10] M. O. Scully and W. E. Lamb, Jr., "Quantum theory of an optical maser: I General theory," *Phys. Rev.*, vol. 159, pp. 208-226, 1967.
[11] —, "Quantum theory of an optical maser: II Spectral profile," *Phys. Rev.*, vol. 166, pp. 246-249, 1968.
[12] —, "Quantum theory of an optical maser: III Theory of photoelectron counting statistics," *Phys. Rev.*, vol. 179, pp. 368-374, 1969.
[13] K. Shimoda, H. Takahashi, and C. H. Townes, "Fluctuations in amplification of quanta with application to maser amplifiers," *J. Phys. Soc. Japan*, vol. 12, pp. 686-700, 1957.
[14] M. Lax and W. H. Louisell, "Quantum noise XII: Density operator treatment of field and population fluctuations," *Phys. Rev.*, vol. 185, pp. 568-591, 1969.
[15] M. Lax and W. H. Louissel, "Quantum noise IX: Quantum Fokker-Planch solution for laser noise," *IEEE J. Quantum Electron.*, vol. QE-3, pp. 47-58, 1967.
[16] W. A. Smith, "Laser intensity fluctuations when the photon number at threshold is small," *Opt. Commun.*, vol. 12, pp. 236-239, 1974.
[17] D. Meltzer, W. Davis, and L. Mandel, "Measurements of photoelectric counting distributions for a laser near threshold," *Appl. Phys. Lett.*, vol. 17, pp. 242-245, 1970.
[18] M. Lax and M. Zwanziger, "Exact photocount statistics: Lasers near threshold," *Phys. Rev.*, vol. A7, pp. 750-771, 1973.
[19] Y. Yamamoto, S. Saito, and T. Mukai, "AM and FM quantum noise in semiconductor lasers—Part II: Comparison of theoretical and experimental results for AlGaAs lasers," *IEEE J. Quantum Electron.*, this issue, pp. 47-58.
[20] H. Haug, "Quantum mechanical theory of fluctuations and relaxation in semiconductor lasers," *Z. Phys.*, vol. 200, pp. 57-68, 1967.
[21] E. O. Kane, "Thomas Fermi approach to impure semiconductor band structure," *Phys. Rev.*, vol. 131, pp. 79-88, 1963.
[22] B. I. Halperin and M. Lax, "Impurity band tails in the high density limit: I Maximum counting method," *Phys. Rev.*, vol. 148, pp. 722-740, 1966.
[23] H. C. Casey, Jr. and F. Stern, "Concentration-dependent absorption and spontaneous emission of heavily doped GaAs," *J. Appl. Phys.*, vol. 47, pp. 631-643, 1976.
[24] R. A. Smith, *Wave Mechanics of Crystalline Solids.* London: Chapman and Hall, 1961, p. 406.
[25] W. P. Dumke, "Optical transitions involving impurities in semiconductors," *Phys. Rev.*, vol. 132, pp. 1998-2002, 1963.
[26] Y. Yamamoto, "Noise and error rate performance of semiconductor laser amplifiers in PCM-IM optical transmission systems," *IEEE J. Quantum Electron.*, vol. QE-16, pp. 1073-1081, Oct. 1980.
[27] T. Mukai and Y. Yamamoto, "Noise in an AlGaAs semiconductor laser amplifier," *IEEE J. Quantum Electron.*, vol. QE-18, pp. 564-575, Apr. 1982.
[29] G. Lachs, "Theoretical aspects of mixtures of thermal noise and coherent radiation," *Phys. Rev.*, vol. 138, pp. 1012-1015, 1965.
[30] R. J. Glauber, *Quantum Optics and Electronics*, C. DeWitt *et al.*, Eds. New York: Gordon Breach, 1965.
[31] J. A. Armstrong, "Theory of interferometric analysis of laser phase noise," *J. Opt. Soc. Amer.*, vol. 56, pp. 1024-1031, 1966.
[32] H. Jackel, "Light intensity fluctuations and dynamic behavior of AlGaAs heterostructure diode lasers in the frequency range of 10 MHz to 8 GHz," Ph.D. dissertation, Technical University of Zurich, Zurich, Switzerland, 1980.
[33] F. R. Nash, "Mode guidance parallel to the junction plane of double heterostructure GaAs lasers," *J. Appl. Phys.*, vol. 44, pp. 4696-4707, 1973.
[34] C. H. Henry, "Theory of the linewidth of semiconductor lasers," *IEEE J. Quantum Electron.*, vol. QE-18, pp. 259-264, Feb. 1982.
[35] M. Ito and T. Kimura, "Stationary and transient thermal properties of semiconductor laser diodes," *IEEE J. Quantum Electron.*, vol. QE-17, pp. 787-795, May 1981.
[36] Y. Yamamoto, "Receiver performance evaluation of various digital optical modulation-demodulation systems in the 0.5-10 μm wavelength region," *IEEE J. Quantum Electron.*, vol. QE-16, pp. 1251-1259, Nov. 1980.

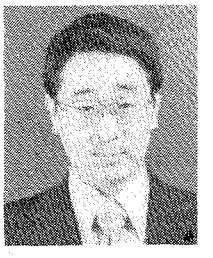

Yoshihisa Yamamoto (S'75-M'80) was born in Tokyo, Japan, on November 21, 1950. He received the B.S. degree from the Tokyo Institute of Technology, Tokyo, Japan, in 1973, and the S.M. and Ph.D. degrees from the University of Tokyo, Tokyo, Japan, in 1975 and 1978, respectively.

Since joining the Musashino Electrical Communication Laboratory, Nippon Telegraph and Telephone Public Corporation, Tokyo, Japan, in 1978, he has been engaged in research on photodetectors for optical communication, optical amplifiers, and coherent optical transmission systems.

Dr. Yamamoto is a member of the Institute of Electronics and Communication Engineers of Japan and the Japan Society of Applied Physics.

AM and FM Quantum Noise in Semiconductor Lasers—Part II: Comparison of Theoretical and Experimental Results for AlGaAs Lasers

YOSHIHISA YAMAMOTO, MEMBER, IEEE, SHIGERU SAITO, MEMBER, IEEE, AND TAKAAKI MUKAI

Abstract—Four different theoretical formulations for AM and FM quantum noise properties in semiconductor lasers are compared with each other for AlGaAs lasers. These formulations are based on van der Pol, Fokker-Planck, rate, and photon density matrix equations. Experimental results with AM noise spectra, FM noise spectra, and spectral linewidths for four different types of AlGaAs lasers are also delineated and compared with the theoretical predictions. The spontaneous emission coefficient β and population inversion parameter n_{sp}, which are basic parameters for determining the quantum noise properties of semiconductor lasers, were calculated by the density of states with Kane function interpolated to Halperin-Lax bandtail and the Stern's improved matrix element. Experimental AM and FM quantum noise properties show good agreement with the theoretical predictions derived through use of estimated β and n_{sp} values.

I. Introduction

THE AM and FM quantum noise properties for semiconductor lasers were formulated in the preceding paper [1] through implementation of the four different theoretical approaches: a classical van der Pol equation; a Fokker-Planck equation, a rate equation, and a photon density matrix master equation. These formulations are numerically compared in this paper with AlGaAs laser parameters being taken into account. Experimental studies of AM and FM quantum noise properties for AlGaAs semiconductor lasers and a comparison between experimental and theoretical results are also described in detail.

Variance in intensity fluctuation for semiconductor lasers was originally measured by Armstrong and Smith, through a Hanbury Brawn-Twiss experiment [2]. AM noise spectra for an AlGaAs laser have been measured by a single detector technique, [3], [4] and the results compared with a rate equation analysis based on an approximate parabolic band model [4]. AM noise spectra for an AlGaAs semiconductor laser amplifier biased below the lasing threshold were also measured under external signal injection, and the results compared with multimode rate equations based on an approximate exponential bandtail model [5]. A photon counting experiment was performed for an AlGaAs laser just above the lasing threshold [12]. The obtained photon number probability density has also been compared with a Fokker-Planck equation analysis [13].

Several experimental studies concerning the power spectrum and spectral linewidth for semiconductor lasers have been reported. The Lorentzian line shape was directly observed by means of optical heterodyne detection for a 10.6 μm PbSnTe laser [6] and a 0.85 μm AlGaAs laser [7]. The spectral linewidth was also mentioned by coherent length measurement using 4.15 km fiber [8], delayed self-heterodyne detection [9], Fabry-Perot interferometry [10], visibility measurement with a Michelson interferometer [12], and FM-AM noise conversion [11]. FM noise spectra, however, have not yet been studied, to the authors' knowledge.

The purpose of this paper is to provide systematic comparisons between theoretical and experimental results for AM noise, FM noise, and power spectrum for AlGaAs lasers. Four different types of AlGaAs lasers were used in the experiment. The experimental dependences of the above three quantum noise properties mentioned above on laser structure, bias level, and output power are compared with the four different theoretical formulations derived in the preceding paper [1]. The material parameters, describing stimulated emission, spontaneous emission, and anomalous dispersion, used in the theoretical noise analyses are obtained by the calculation using the Stern band model and several independent experiments.

II. Spontaneous Emission Coefficient, Population Inversion Parameter, Effective Carrier Lifetime, and Refractive Index Dispersion

A. Evaluation of Structural and Material Parameters

The spontaneous emission coefficient β and population inversion parameter n_{sp} are two basic parameters for determining the AM and FM quantum noise properties of semiconductor lasers. The effective carrier lifetime is shortened from the spontaneous lifetime due to its dependence on carrier density. The refractive index is also dependent on carrier density through the anomalous dispersion and the free carrier plasma dispersion. These two processes are also deeply related to the quantum noise properties. In this section, these parameters illustrated in Fig. 1 will be determined for four different types of AlGaAs lasers which are used in the noise measurement.

The spontaneous emission coefficient β, which is alternatively called the saturation parameter s, is of the form [1]

Manuscript received February 22, 1982; revised August 10, 1982.

The authors are with the Musashino Electrical Communication Laboratory, Nippon Telegraph and Telephone Public Corporation, Musashino-shi, Tokyo, Japan.

0018-9197/83/0100-0047$01.00 © 1983 IEEE

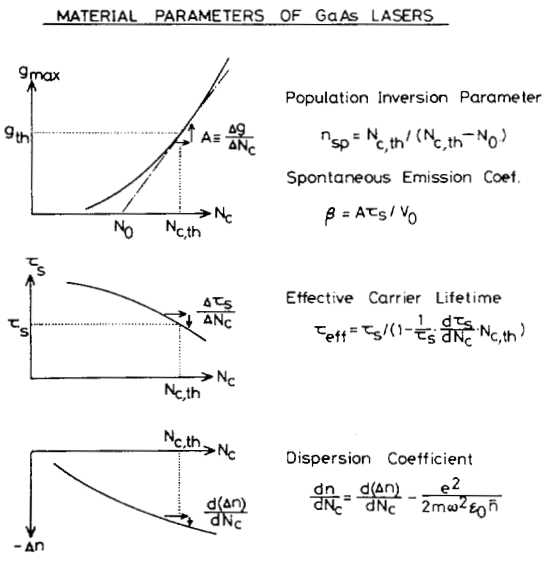

Fig. 1. Definitions of five material parameters A, N_O, τ_s, $d\tau_s/dN_e$, and dn/dN_e.

$$\beta = A\tau_s/V_o \tag{1}$$

where $A = dG/dN_e$ is the differential gain constant in m^3/s, τ_s is the spontaneous lifetime, and V_o is the optical mode volume. The population inversion parameter $n_{sp} = N_e/(N_e - N_o)$ is given by

$$n_{sp} = 1 + A\Gamma\tau_p N_o \tag{2}$$

for above the lasing threshold. Here, Γ is the optical mode confinement factor for the active layer, N_o is the carrier density where stimulated emission rate exceeds absorption rate, and τ_p is the photon lifetime. The effective carrier lifetime τ_{eff} is given by

$$\tau_{\text{eff}} = \tau_s \Big/ \left(1 - \frac{1}{\tau_s}\frac{d\tau_s}{dN_e}\cdot N_{e,\text{th}}\right). \tag{3}$$

The refractive index dispersion is given by the sum of the band-to-band anomalous dispersion and the free carrier plasma dispersion as follows:

$$\frac{dn}{dN_e} = \frac{d(\Delta n)}{dN_e} - \frac{e^2}{2m\omega^2\epsilon_0\bar{n}}. \tag{4}$$

The five material parameters A, N_o, τ_s, $d\tau_s/dN_e$, and dn/dN_e, and the three structural parameters V_o, Γ, and τ_p are necessary to calculate these parameters.

Material parameters A and N_o are determined by the relation of the peak gain coefficient $g_{\max}$ to the carrier density N_e as shown in Fig. 1. Peak gain coefficient versus carrier density for GaAs, is calculated by using the density of states with Kane function interpolated to Halperin-Lax bandtail and the Stern's improved matrix element [14]. The numerical results are shown in Fig. 2 as a function of the background doping level.

The gain coefficient was experimentally measured with external signal injection into the semiconductor laser, biased at below the lasing threshold [15], [16]. The transmitted signal power was maximum when the signal frequency was matched to the Fabry-Perot resonant frequency and was minimum when the signal frequency was detuned to fit

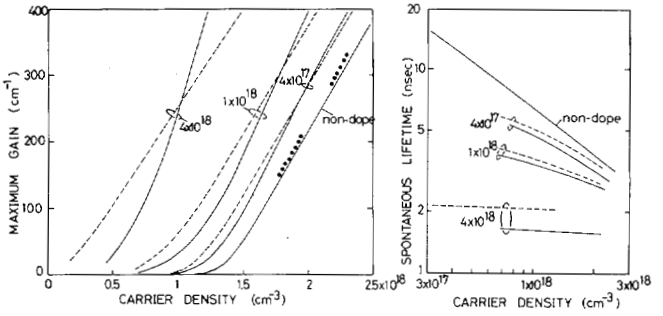

Fig. 2. Theoretical and experimental peak gain coefficient $g_{\max}$ versus the minority carrier density N_e for GaAs lasers. ————: p-type, – – – – –: n-type, •: experimental results for GaAs lasers with non-doped active layer.

between the two axial mode frequencies. The output signal power ratio v leads to the gain coefficient as follows:

$$g = \frac{1}{\Gamma}\left\{\frac{1}{L}\ln\left[\frac{1}{R_M}\left(\frac{\sqrt{v}-1}{\sqrt{v}+1}\right)\right] + \alpha_{fc}\right\} \tag{5}$$

where L is cavity length, R_M is facet reflectivity, and α_{fc} is free carrier absorption loss. The optical mode confinement factor Γ and facet reflectivity R_M are calculated through the use of the laser waveguide structure parameters [16]. The free carrier absorption loss α_{fc} is given as a function of the majority carrier density in an active layer [17]. The carrier density N_e is, on the other hand, estimated from the nominal current density J_{nom} ($A/cm^2 \cdot \mu m$), like $N_e = \tau_s \times J_{\text{nom}} \times 10^{10}/e$. Here, e is the electron charge. The leak current estimated by the measured maximum quantum efficiency is extracted. As will be mentioned later, the spontaneous lifetime τ_s is dependent on the carrier density N_e. Therefore, the procedure to determine N_e needs to be solved in a manner consistent with the relation between τ_s and N_e. Experimental results for g versus N_e, thus obtained, are plotted in Fig. 2 for a 900 μm cavity length channeled substrate planar (CSP) AlGaAs laser and a 300 μm CSP laser. The active layers of all these lasers are undoped.

Agreement between the theoretical and experimental results for g versus N_e is fairly good. Parameters A and N_o can be estimated from these results as shown in Table I for the four AlGaAs lasers used in the noise measurement.

The spontaneous lifetime τ_s versus the carrier density N_e is shown in Fig. 2 as a function of background doping level. The values of τ_s and $d\tau_s/dN_e$ at the clamped threshold carrier density are shown in Table I.

Fig. 3 shows the calculated gain spectra and the related refractive index anomalous dispersion as a function of minority carrier density. The anomalous dispersion is calculated by the following Kramers-Kronig integral of theoretical gain spectra.

$$\Delta n(E) = -\frac{P}{2\pi^2}\int_0^\infty \frac{1}{E'+E}\left[\frac{\Delta g(E') - \Delta g(E)}{E'-E}\right]dE'. \tag{6}$$

The theoretical results of Δn versus N_e are shown in Fig. 4 as a function of background doping. The total refractive index dispersion including free carrier plasma dispersion coefficient at the clamped threshold carrier density is shown in Table I.

The optical mode volume V_o is given by the product of the cavity length L and the cross-sectional area of the lasing mode,

TABLE I
THE STRUCTURAL AND MATERIAL PARAMETERS AND THE SPONTANEOUS EMISSION COEFFICIENTS AND POPULATION INVERSION PARAMETERS FOR AlGaAs LASERS

	900μm CSP	300μm CSP	300μm BH	200μm TJS
Active Layer	non-doped	non-doped	non-doped	p-doped ($p_0=1\times10^{18}$ cm^{-3})
V_0 (m^3)	1.3x10-15	4.0×10^{-16}	2.1×10^{-16}	1.5×10^{-16}
Γ	0.2	0.2	0.2	0.5
τ_p (psec)	1.9	1.3	1.3	1.1
A (m^3/sec)	2.81×10^{-12}	2.82×10^{-12}	2.82×10^{-12}	3.3×10^{-12}
N_0 (m^{-3})	1.36×10^{24}	1.36×10^{24}	1.36×10^{24}	1.05×10^{24}
τ_s (nsec)	2.4	2.2	2.2	2.0
$d\tau_s/dN_e$ ($sec m^3$)	-0.8	-0.5	-0.5	-0.4×10^{-33}
dn/dN_e (m^3)	-6.5	-3.0	-3.0	-8.5×10^{-27}
β theoretical	5.2×10^{-6}	1.6×10^{-5}	3.0×10^{-5}	4.4×10^{-5}
n_{sp} theoretical	4.1	2.5	2.5	3.7
β experimental, derived from				
<n>	3.3×10^{-6}	1.1×10^{-5}	2.2×10^{-5}	3.5×10^{-5}
I_s	———	1.0×10^{-5}	1.5×10^{-5}	2.2×10^{-5}
$\Delta\lambda_{1/2}$	6.4×10^{-6}	2.5×10^{-5}	———	4.0×10^{-5}

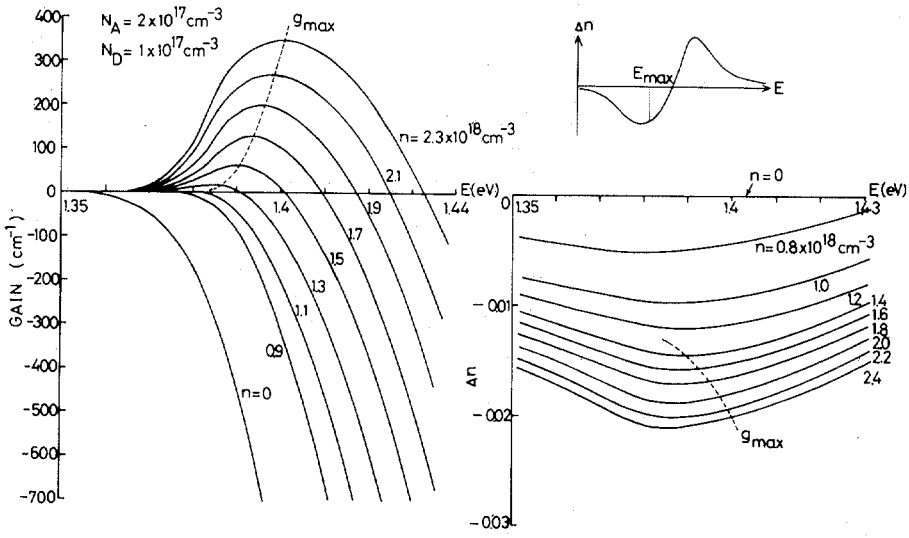

Fig. 3. Calculated gain spectra and refractive index dispersion due to anomalous dispersion.

which is estimated by the far field pattern divergent angles in the lateral and vertical directions. Photon lifetime is defined as $\tau_p = [c\{1/L \ln 1/R_M + \alpha_{fc}\}]^{-1}$.

Material and structural parameters that were thus determined, as well as calculated β and n_{sp} values using these parameters, are summarized in Table I for the four AlGaAs lasers.

B. Mean Photon Number and Saturation Output Power

Output optical power at well above the lasing threshold is determined by the photon number in a single lasing mode in the following manner:

$$P_o = \hbar\Omega\langle n\rangle/\tau_{PM} \tag{7}$$

where $\tau_{PM} = [(c/2L) \ln (1/R_M)]^{-1}$ is the photon lifetime due to the output coupling from the facet. The mean photon number at well above the threshold can be derived from [1]

$$\langle n\rangle = \frac{n_{sp}}{\beta} \cdot R \tag{8}$$

where $R = I/I_{th} - 1$ is the pumping parameter. Fig. 5 shows the theoretical photon number, which is calculated using the estimated β and n_{sp} values in (8), as a function of the bias level R. Experimental results for a 900 μm CSP laser, 300 μm CSP laser, and 300 μm buried heterostructure (BH) laser are also presented.

The spontaneous emission coefficients β estimated from the

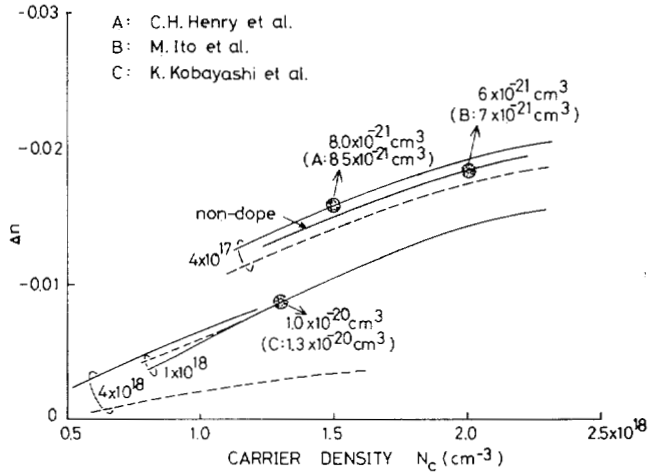

Fig. 4. Calculated refractive index change Δn versus minority carrier density.

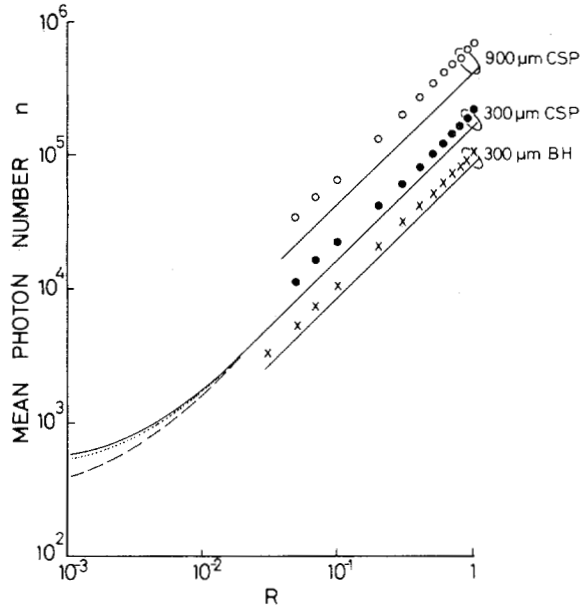

Fig. 5. Total photon number n in a laser mode versus bias level R for three different types of GaAs lasers. ————: rate equation; — — — —: van der Pol equation and Fokker-Planck equation; - - - - - - - - - -: photon density matrix equation; ○ ● ×: experimental results.

measured photon number, are summarized in Table I for the four AlGaAs lasers. Here theoretical n_{sp} values are used to derive β from (8). The discrepancy between the theoretical and the experimental β values is within a factor of two for all the lasers.

The saturation output power I_s at which the gain coefficient is decreased by 3 dB from the unsaturated value is given by (29) of [1]

$$I_s = \frac{c\hbar\Omega}{A\tau_s} = c\hbar\Omega/(\beta V_o) \quad [\mathrm{W/m^2}]. \tag{9}$$

This value was experimentally determined by gain saturation measurement of semiconductor laser amplifiers through varying the external injection signal level [16]. The saturated single pass gain G_s and the saturated overall gain G_c of a Fabry-Perot type amplifier are given by

$$G_s = \exp\left[\{\Gamma g^o/(1 + I/I_s) - \alpha_{fc}\} L\right] \tag{10}$$

$$G_c = (1 - R_M)^2 G_s/(1 - R_M G_s)^2. \tag{11}$$

Here, g^o is the unsaturated gain coefficient, which is measured with the small injection signal derived above. The mode power density I inside a laser cavity is given as a function of the photon number in this manner:

$$I = \frac{c\hbar\Omega\langle n\rangle}{V_o}. \tag{12}$$

Using (9) and (12) with (10), it is possible to obtain the saturated single pass gain

$$G_s = \exp\left[\{\Gamma g^o/(1 + \beta\langle n\rangle) - \alpha_{fc}\} L\right]. \tag{13}$$

Fig. 6 presents experimental results comparing overall signal gain normalized by the unsaturated overall signal gain G_c/G_c^o, with photon number $\langle n\rangle$ for a 300 μm CSP laser, 300 μm BH laser, and a 200 μm TJS laser. The bias levels for the laser amplifiers were adjusted to give an unsaturated overall signal gain of 20 dB. The mode photon number $\langle n\rangle$ is estimated from the amplified signal output power using (7).

The spontaneous emission coefficients β estimated from the gain saturation experiment shown in Fig. 6, are summarized in Table I. The spontaneous emission coefficients β thus determined, are again in agreement with the theoretical β values to within a factor of two.

III. AM Quantum Noise

AM quantum noise properties of semiconductor lasers are characterized by AM noise spectra, variance in intensity fluctuation, and photon number probability density. In this section, theoretical and experimental comparisons of these values are discussed.

A. AM Noise Spectrum

The experimental setup for measuring AM noise spectra is shown in [5, Fig. 2]. The noise power $P(\omega)$, displayed on a spectral analyzer, is given by

$$P(\omega) = [\eta_D^2\langle i_n^2\rangle_{\mathrm{AM}}\langle g\rangle^2 + 2e\eta_D\langle i_{ph}^o\rangle\langle g^2\rangle]\, R_L B_o G(\omega) + P_{\mathrm{thermal}}(\omega) + P_{\mathrm{dark\ current}}(\omega). \tag{14}$$

Here, η_D is the quantum efficiency of Si-APD, including the coupling loss between semiconductor lasers and Si-APD; $\langle g\rangle$ is the avalanche multiplication factor of Si-APD; $\langle i_{ph}^o\rangle = e\langle n\rangle/\tau_{PM}$ is the assumed initial photocurrent at $\eta_D = 1$; R_L is the load resistance; B_o is the resolution frequency width of a spectrum analyzer; $G(\omega)$ is the frequency response of the electronic amplifier, including the frequency response of Si-APD; $P_{\mathrm{thermal}}(\omega)$ is the electronic amplifier thermal noise; and $P_{\mathrm{dark\ current}}(\omega)$ is the Si-APD dark current shot noise. The mean square value of g is given by [18]

$$\langle g^2\rangle = \left[k\langle g\rangle + \left(2 - \frac{1}{\langle g\rangle}\right)(1 - k)\right]\langle g\rangle^2 \tag{15}$$

where k is the ionization coefficient ratio between electron and hole. The value of k in the Si-APD used in the experiment is 0.02 [19].

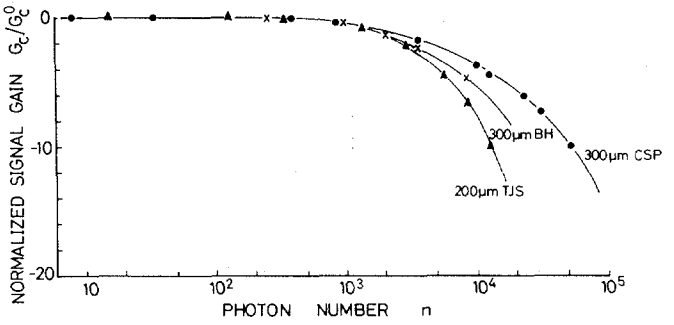

Fig. 6. Experimental results with normalized signal gain G_c/G_c^o versus photon number n inside a laser cavity for three different types of GaAs laser amplifiers. Unsaturated signal gain was 20 dB.

The normalized AM noise spectrum, defined by the noise power generated in a unit of load resistance per unit bandwidth normalized by the dc electric power [1], is given by

$$\text{RIN} = \frac{\langle i_n^2\rangle_{\text{AM}} + 2e\langle i_{ph}^o\rangle}{\langle i_{ph}^o\rangle^2}$$

$$= \frac{P(\omega) - P_{\text{thermal}}(\omega) - P_{\text{dark current}}(\omega)}{R_L B_o G(\omega)\eta_D^2\langle g\rangle^2\langle i_{ph}^o\rangle^2}$$

$$+ \frac{2e}{\langle i_{ph}^o\rangle}\left[1 - \frac{\langle g^2\rangle}{\eta_D\langle g\rangle^2}\right]. \tag{16}$$

The spectrum for $G(\omega)$ was measured by using AlGaAs LED light to illuminate the Si-APD, which induced shot noise with a white spectrum. The quantum efficiency of Si-APD was 0.7 at an 825 nm wavelength. Coupling loss between the semiconductor lasers and Si-APD was -4.5 dB.

Fig. 7 shows experimental results for RIN at low frequency, versus the bias level R for the 300 μm CSP laser. Theoretical results calculated with the rate equation (115), van der Pol equation (55), and the Fokker-Planck equation (98), as derived in the preceding paper [1], are also plotted with the theoretical β and n_{sp} values in Fig. 7.

The RIN decreases by R^{-3} with the bias level between $10^{-2} \leqslant R \leqslant 1$, where the beat noise between signal and noise photons is the dominant noise source. Experimental results are in good agreement with the rate equation analysis. The van der Pol and Fokker-Planck equations give slightly lower RIN's than the rate equation analysis because the carrier modulation noise induced AM noise and the coupling effect of the carrier noise and photon noise were not taken into account. This is not the inherent drawback of the Fokker-Planck equation. The quantum mechanical Fokker-Planck equation for field and carrier operators, of course, is the exact expression for quantum noise. The above discrepancy stems from the adiabatic elimination of carrier variables introduced to derive simple Fokker-Planck equation (98) of [1]. The RIN in this bias region is proportional to $\tau_p\beta/n_{sp}^2$.

The RIN at the high bias level $R \geqslant 1$, on the other hand, decreases more slowly with bias level and the dependence on bias level approaches R^{-1}. At this bias level, signal photon induced shot noise is the main noise source. The RIN is proportional to $\beta\tau_{PM}/n_{sp}$.

Although experimental results are in good agreement with single-mode rate equation analysis for the bias level $R \geqslant 10^{-2}$,

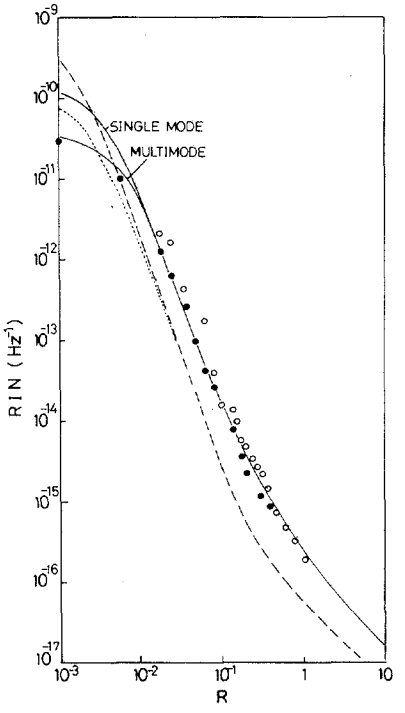

Fig. 7. RIN spectrum at low frequency versus bias level R for 300 μm CSP laser. ————: rate equation; — — — —: van der Pol equation and Fokker-Planck equation; ----------: photon density matrix equation; ○: experimental results in this work; and ●: experimental results from Jackel *et al.* [4].

experimental results at bias level $R \leqslant 10^{-2}$ differ from those with the single-mode rate equation. The multimode rate equation analysis [5] is, on the other hand, satisfactory at this bias level, as can be seen in Fig. 7. Similar results were obtained for the 900 μm CSP and 200 μm TJS lasers.

Fig. 8 shows experimental and theoretical results concerning the excess noise factor χ defined by

$$\chi = \langle i_n^2\rangle_{\text{AM}}/(2e\langle i_{ph}^o\rangle), \tag{17}$$

for the 300 μm CSP laser. The excess noise factor χ indicates how the actual laser field approaches the completely coherent wave with Poisson distribution and a theoretical shot noise limit. Fig. 8(a) and (b) employs the normalized bias level R and the output optical power as an abscissa, respectively. The AM noise level of the semiconductor laser is about one order of magnitude larger than the theoretical shot noise limit even at a high bias level. The dependences of AM excess noise factor on background doping level and threshold gain are shown in Fig. 9. To decrease AM excess noise, heavily n-doped active layer and large threshold gain, which, for instance, is realized by decreasing the mode confinement factor, are preferable. This is mainly because the population inversion parameter n_{sp} is small in n-doped GaAs and decreased with threshold gain as shown in Fig. 2.

Experimental and theoretical results concerning RIN frequency characteristics for the 300 μm CSP laser are shown in Fig. 10. The experimental results with flat response at low frequency, as well as the cutoff characteristics at high frequency are well described by the rate equation analysis. The discrepancy between the experimental results and single-mode rate equation analysis near the relaxation oscillation fre-

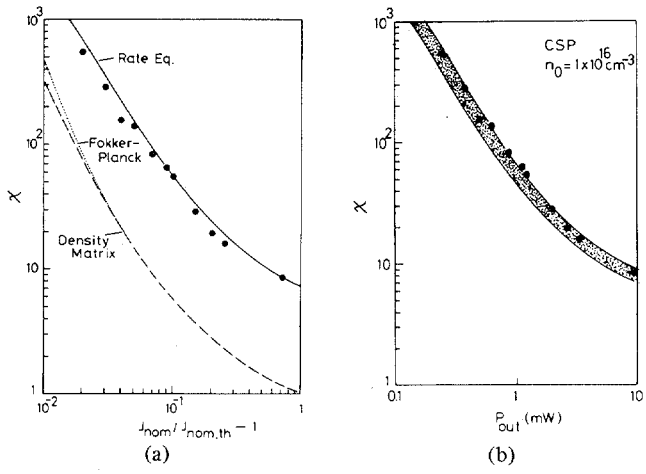

Fig. 8. (a) AM excess noise factor χ versus normalized bias level R for 300 μm CSP laser. (b) AM excess noise factor χ versus optical output power for 300 μm CSP laser. ————: rate equation analysis, •: experimental results.

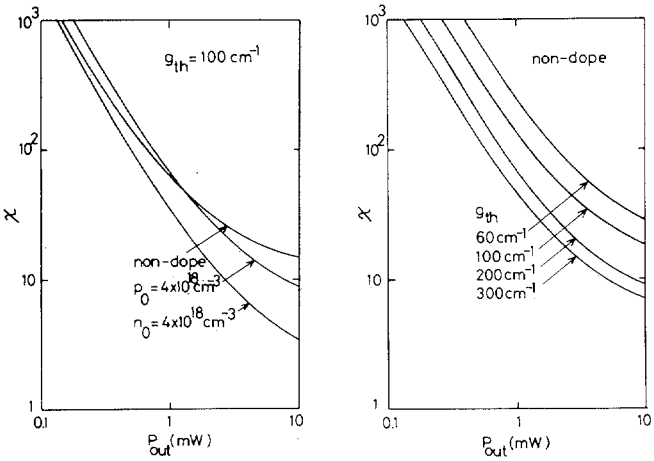

Fig. 9. AM excess noise factor χ versus optical output power as functions of background doping level and threshold gain.

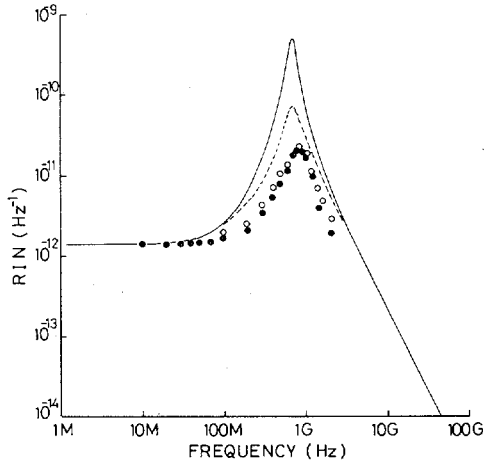

Fig. 10. AM noise spectrum for 300 μm CSP laser biased at R = 0.02. ————: single-mode rate equation; — — — —: multimode rate equation; ○: experimental results in this work; and •: experimental results from Jackel *et al.* [4].

quency stems from spurious longitudinal modes and lateral carrier diffusion effects, both of which are neglected in the single-mode rate equation analysis shown by a solid line. The multimode rate equation analysis [5] shown by the dotted line agrees better with the experimental results.

Fig. 11 shows the 3 dB down cutoff frequency for RIN against the bias level R for the 300 μm CSP laser. Calculations were performed using the rate equation, van der Pol equation, and the Fokker-Planck equation. The three theoretical methods gave similar results. The cutoff frequency is proportional to $n_{sp}R/\tau_p$ and is from several tens to several hundred GHz, even at the $R \leqslant 1$ bias level.

B. Variance of Intensity Fluctuation

Variance in intensity fluctuation ρ for the 300 μm CSP laser is presented in Fig. 12 as a function of the bias level R. Three theoretical curves, based on the van der Pol equation (64), Fokker-Planck equation (97), and photon density matrix equation (141) of [1], show similar results. The theoretical shot noise limit is also plotted in Fig. 12. The Fokker-Planck equation analysis differs from the other two in the $R \geqslant 1$ bias level, since the signal wave induced shot noise is not included in the Fokker-Planck method.

The photon distribution changes at threshold from a Bose-Einstein distribution below threshold to a Poisson distribution at well above the threshold. This smooth transition is seen by the value H_2 defined as

$$\langle n^2\rangle - \langle n\rangle^2 = \langle n\rangle (1 + H_2\langle n\rangle). \tag{18}$$

The value of H_2 is unity for the Bose-Einstein distribution, and zero for the Poisson distribution. The value of H_2 is calculated in terms of the variance ρ and the mean photon number $\langle n\rangle$ as

$$H_2 = \rho - 1/\langle n\rangle. \tag{19}$$

Fig. 13 shows the experimental and theoretical values for H_2 in relation to the bias level R for the 300 μm CSP laser.

C. Photon Number Probability Density

The probability density for the photon number Prob(n) in the 300 μm CSP laser is shown in Fig. 14 as a function of the bias level R. The probability densities for the photon number, calculated by the Fokker-Planck and density matrix equations, give similar results. The Poisson distribution with the same mean photon number is plotted by dotted lines for reference. The probability density, on the other hand, approaches the Bose-Einstein distribution with decreasing bias level.

IV. FM Quantum Noise

FM quantum noise properties for semiconductor lasers are characterized by FM noise, power spectra, spectral linewidth, and instantaneous frequency probability density. In this section, theoretical and experimental comparisons of these values are presented.

A. FM Noise Spectrum

The experimental setup for measuring FM noise spectra is shown in [11, Fig. 1]. The FM noise from the AlGaAs semiconductor laser field is converted to AM noise by the optical frequency discriminator, which consists of a Michelson interferometer. The output of the optical frequency dis-

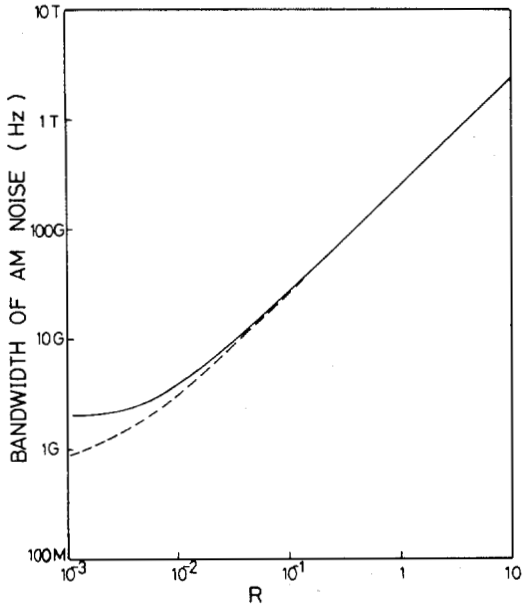

Fig. 11. Theoretical 3 dB down cutoff frequency for AM noise spectrum with 300 μm CSP laser, versus bias level R. ————: rate equation; – – – – –: van der Pol equation and Fokker-Planck equation.

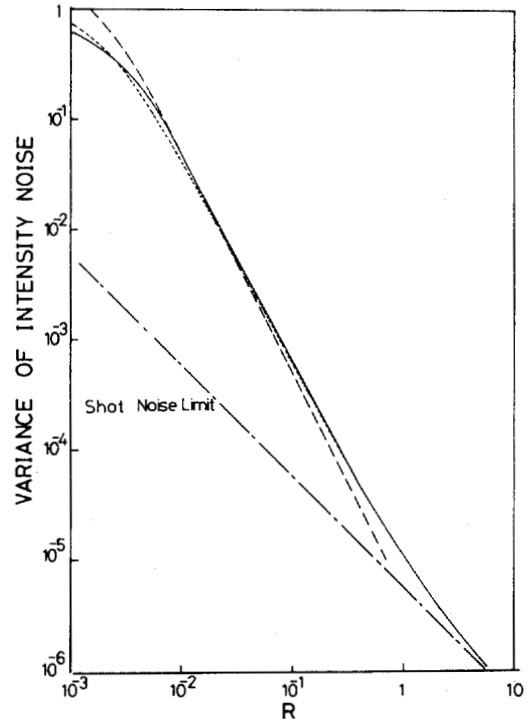

Fig. 12. Theoretical variance in intensity fluctuation ρ versus bias level R for 300 μm CSP laser. ————: van der Pol equation; – – – – –: Fokker-Planck equation analysis; ----------: photon density matrix equation; —·—·—·—: theoretical shot noise level.

criminator contains both the original AM noise and FM-AM conversion noise. The noise power $P(\omega)$, displayed on a spectrum analyzer, is defined by

$$P(\omega) = [\eta_D^2(\langle i_n^2\rangle_{\mathrm{AM}} + \langle i_n^2\rangle_{\mathrm{FM}})\langle g\rangle^2 + 2e\eta_D\langle i_{ph}^o\rangle\langle g^2\rangle] \cdot R_L B_o G(\omega) + P_{\mathrm{thermal}}(\omega) + P_{\mathrm{dark\ current}}(\omega). \quad (20)$$

Here, the excess noise $\langle i_n^2\rangle_{\mathrm{FM}}$ due to FM-AM conversion is given as a function of the FM noise spectrum $W_{s\Omega}(\omega)$,

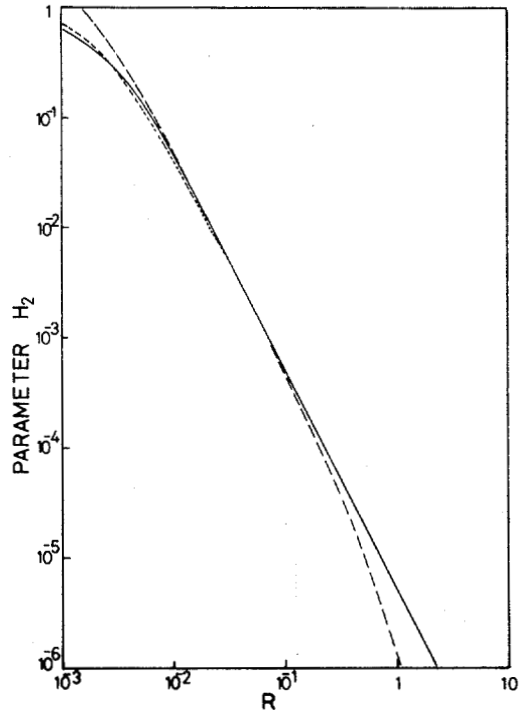

Fig. 13. Parameter H_2 versus bias level R for 300 μm GaAs CSP laser. ————: van der Pol equation; – – – – –: Fokker-Planck equation; ----------: photon density matrix equation analysis.

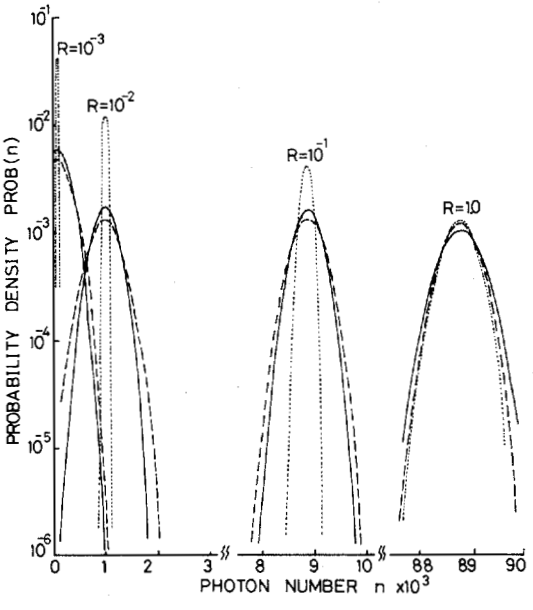

Fig. 14. Photon number probability density Prob(n) for 300 μm CSP laser as a function of the bias level R. ————: photon density matrix equation; – – – – –: Fokker-Planck equation; ----------: Poisson distribution.

$$\frac{\langle i_n^2\rangle_{\mathrm{FM}}}{\langle i_{ph}^0\rangle^2} \equiv K_d W_{s\Omega}(\omega) = 2\pi^2\tau^2 W_{s\Omega}(\omega)/[1 + (\omega\tau)^2]. \quad (21)$$

Here, K_d is the Michelson interferometer constant and τ is the delay time due to the arm length difference.

The frequency discriminator constant K_d is estimated by the measured delay time τ. The value of K_d is directly measured by the demodulation experiment with the sinusoidally frequency modulated AlGaAs laser. The oscillation frequency for the AlGaAs laser is directly modulated by the injection

current modulation [20]. The maximum frequency shift Δf_s at modulation frequency f_m was determined by the sideband to carrier intensity ratio of the optical spectrum observed by the Fabry-Perot interferometer; as is shown in Fig. 15(a). The FM-AM converted optical signal was detected by Si-APD and displayed on the spectrum analyzer. This is shown in Fig. 15(b). Demodulated output, divided by Δf_s, gives the spectrum of the frequency discriminator constant. The discriminator constant K_d thus determined is in good agreement with the estimated K_d value using the measured τ value. Fig. 15(c) shows the output signal obtained by direct detection of frequency modulated semiconductor laser output. A spurious AM signal due to injection current modulation and the AM noise spectrum can be seen. These are smaller than the FM signal and FM noise by 25 and 10 dB, respectively.

Fig. 16 contains experimental results concerning the FM noise spectrum for the 900 μm CSP laser. Theoretical FM noise spectra, calculated by the rate equation, are seen in this figure. They are results of the spontaneous emission coupled to the lasing mode, the carrier modulation noise induced refractive index fluctuation, and the current modulation noise induced temperature fluctuation. The FM noise spectrum at low frequency is mainly determined by the current modulation noise. Resonant enhancement of the FM noise spectrum at the relaxation oscillation frequency stems from the carrier modulation effect. To the authors' knowledge, the existence of these two noises has not been mentioned thus far. The FM noises spectrum in the other frequency range is determined by spontaneous emission noise and carrier modulation noise.

A theoretical and experimental comparison of the FM noise spectra for the 900 μm CSP laser is shown in Fig. 17. Fig. 18 shows a theoretical and experimental comparison of the resonant peak frequency of the FM noise spectrum versus the bias level R for the 900 μm CSP laser. The resonant peak frequency for the AM noise spectrum is also plotted in Fig. 18. Similar results are obtained for the 300 μm CSP and 200 μm TJS lasers.

B. Power Spectrum and Spectral Linewidth

The experimental setup for measuring the power spectrum through optical heterodyne detection is shown in [21, Fig. 1]. Two identical AlGaAs lasers, which oscillate in a single longitudinal mode with almost identical wavelengths, are installed in a temperature controlled chamber, and biased at almost the same bias level R. The oscillation frequencies for the two lasers were detuned in relation to each other by about 1 GHz. Rough frequency tuning was performed by adjusting the diode temperature, and fine tuning was done by changing the bias current. Two additional optical isolators were inserted to eliminate undesired reflection feedback from the optical elements into the lasers. The same optical isolators were also used in the FM noise spectrum measurement, since FM noise properties are sensitive to the external feedback [7], [22], [23].

The observed beat spectrum was shown in Fig. 19 as a function of the bias level for the 300 μm CSP laser. The experimental results are in good agreement with the theoretical Lorentzian line shape shown by a solid line. The power spec-

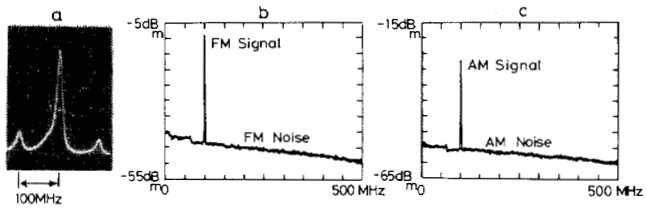

Fig. 15. (a) Optical spectrum of directly frequency modulated GaAs laser output as observed by scanning Fabry-Perot interferometer. Modulation frequency was 100 MHz. (b) Demodulated FM signal, and FM noise determined by means of Michelson interferometer frequency discriminator. (c) Residual AM signal, and AM noise.

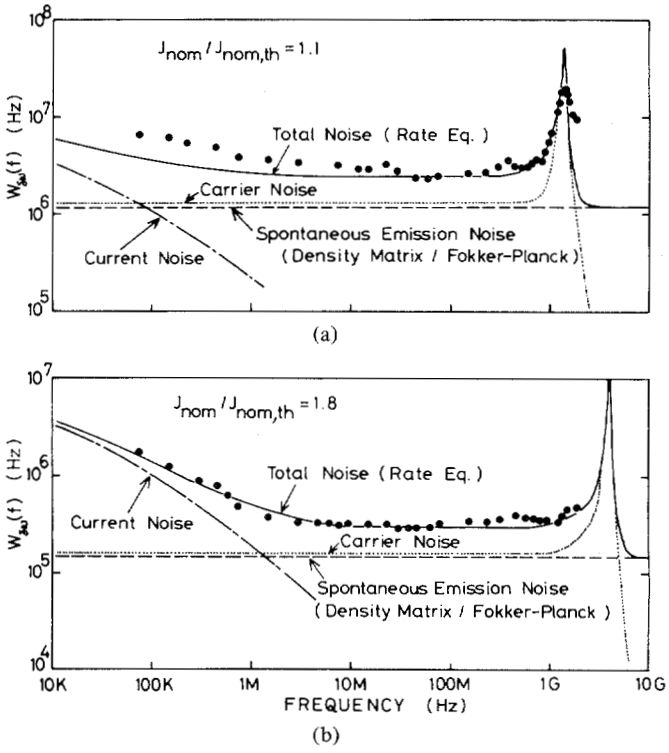

Fig. 16. FM noise spectra for 900 μm CSP laser. ———: spontaneous emission induced FM noise; —·—·—: current noise induced FM noise; ----------: carrier noise induced FM noise; ————: total FM noise; •: experimental results. (a) R = 0.1. (b) R = 0.8.

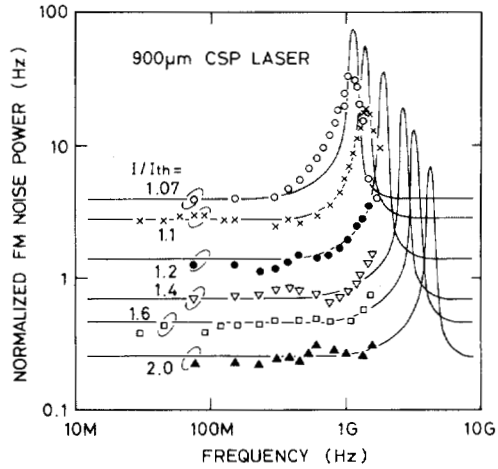

Fig. 17. FM noise spectra of 900 μm GaAs CSP laser for different bias levels. ————: theoretical results using rate equation analysis.

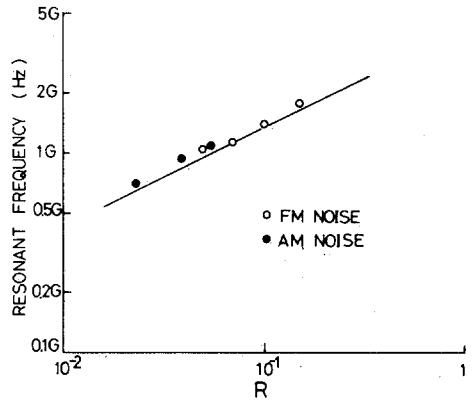

Fig. 18. Resonant peak frequency of FM noise and AM noise versus bias level R for 900 μm CSP laser. ————: theoretical result from rate equation.

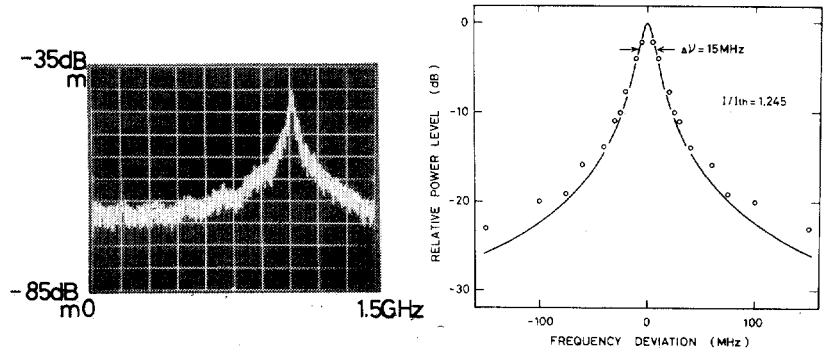

(a)

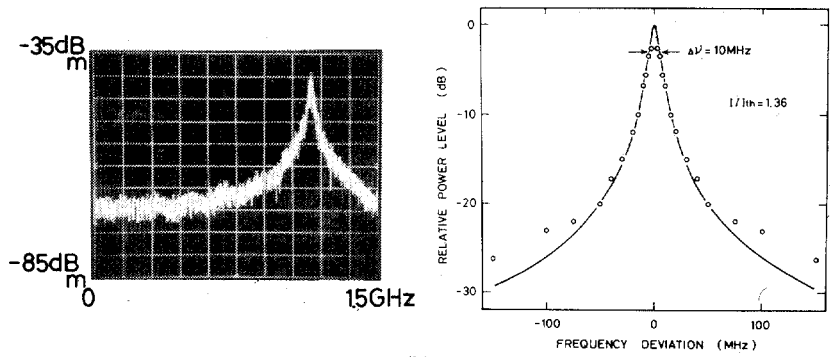

(b)

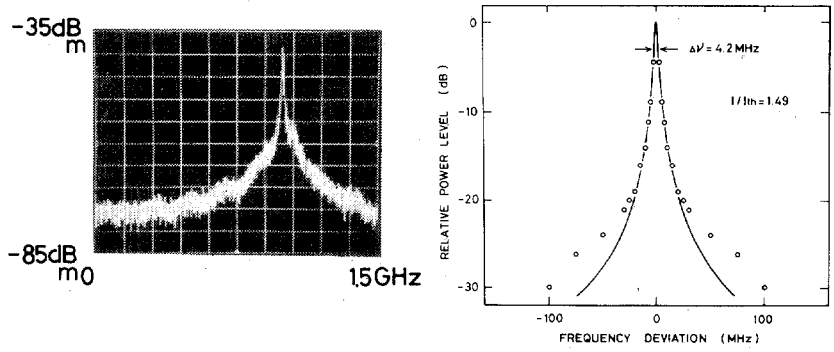

(c)

Fig. 19. Observed beat spectra between two 300 μm CSP lasers biased at same pumping level. ————: Lorentzian line shape. (a) R = 0.245. (b) R = 0.36. (c) R = 0.49.

trum is, to be exact, not the Lorentzian line shape, because the current modulation noise and carrier modulation noise introduce nonuniform FM noise spectra as shown in Fig. 16. The solid lines in Fig. 19 are drawn by choosing the linewidth to give the best fit to the experimental results. The noise floor at about −67 dBm stems from electronic amplifier thermal noise.

The spectral linewidth obtained from the oscillation power spectrum is shown in Fig. 20 as a function of the bias level R for the 300 μm CSP laser. Here the spectral linewidth for one laser is assumed to be half the spectral linewidth of the beat spectrum, since the two lasers are biased at almost the same pumping level and have almost equal spectral linewidths. The spectral linewidth was alternatively measured by the FM noise spectrum using the relation [1]

$$\Delta\nu_{1/2} = \tfrac{1}{2} W_{\delta\Omega}(\omega \approx 0). \tag{22}$$

The spectral linewidth, determined by the flat portion of FM noise spectra is also presented in Fig. 20. The theoretical linewidths calculated with the four different theoretical models are also shown in Fig. 20. Here the theoretical β and n_{sp} values from Table I are used. Experimental results are in good agreement with the rate equation analysis. The van der Pol, Fokker-Planck, and photon density matrix equation analyses give slightly lower results than the rate equation analysis, since carrier modulation noise induced line broadening is not included in them. It is noticeable that both line broadening due to spontaneous emission noise and carrier modulation noise decrease in proportion to R^{-1}.

The theoretical and experimental spectral linewidth for the 900 μm CSP laser, 300 μm CSP laser, and the 200 μm TJS laser are shown in Fig. 21. The difference between three lasers stems from the difference in spontaneous emission coefficients. Spectral linewidth is proportional to $\beta/\tau_p R$ and is as narrow as 250 kHz at $R = 1$ for the 900 μm CSP laser.

Fig. 22(a) and (b) compares the experimental spectral linewidths versus optical output power reported so far for CSP laser and TJS laser. It is uncertain why the linewidth measured by Mooradian *et al.* is broader than other results. Recently, Henry claimed that linewidth broadening due to carrier modulation noise is about thirty times larger than the spontaneous emission noise contribution, which is successful to explain Mooradian's experimental results [25]. The discrepancy between the present theoretical result and Henry's result is mainly due to his omission of mode confinement factor. Henry used the parabolic band model to estimate carrier density and refractive index anomalous dispersion coefficient [26], which results in the overestimation of anomalous dispersion effect. This seems to be partly responsible for the above discrepancy.

The linewidth due to spontaneous emission noise and carrier modulation noise are plotted in Fig. 23 as functions of background doping level and threshold gain. To decrease the linewidth, n-doped active layer and small optical mode confinement factor are preferable.

C. Instantaneous Frequency Probability Density

The probability density for the instantaneous frequency, Prob(Ω), is shown in Fig. 24 as a function of the spectral linewidth $\Delta\nu_{1/2}/B_o$, as normalized by the detection bandwidth. The instantaneous frequency probability density has a Gaussian probability density with $W_{\delta\Omega}B_o$ variance near the central region, but it has a much broader tail than the Gaussian distribution as shown by (A5) of [1].

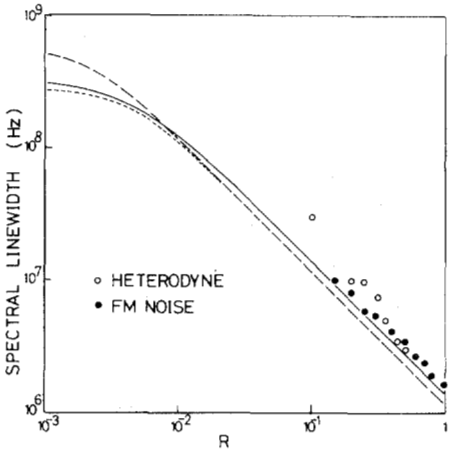

Fig. 20. Spectral linewidth $\Delta\nu_{1/2}$ versus bias level R for 300 μm CSP laser. ————: total FM noise calculated by rate equation; ----------: spontaneous emission noise induced FM noise (rate equation, Fokker-Planck equation, and density matrix equation. — — — —: carrier modulation noise induced FM noise.

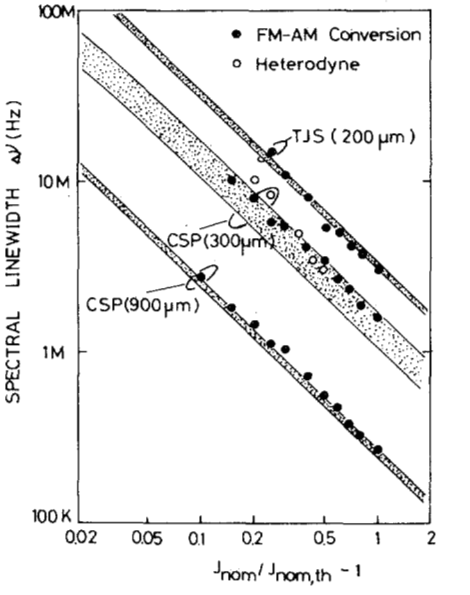

Fig. 21. Spectral linewidth $\Delta\nu_{1/2}$ versus bias level R for three different types of GaAs lasers. ▭: rate equation; △ □ ●: experimental results from FM noise spectrum measurement.

V. Conclusion

AM and FM quantum noise properties for four different types of AlGaAs lasers were studied experimentally. The experimental results were compared with the theoretical predictions using four different formulations derived in the preceding paper [1].

Two basic parameters of the spontaneous emission coefficient β and population inversion parameter n_{sp}, as well as the effective lifetime τ_{eff}, and the refractive index dispersion coefficient dn/dN_e, which determine the AM and FM quantum noise properties, were estimated using the Stern band model and the structural parameters V_o, Γ, and τ_p for the four AlGaAs lasers. The accuracy of the estimated β and n_{sp} values

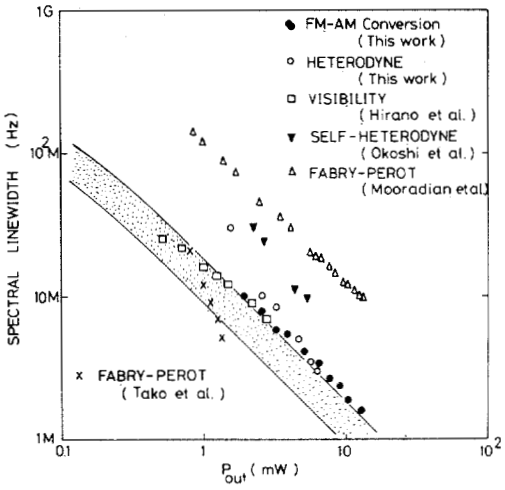

(a)

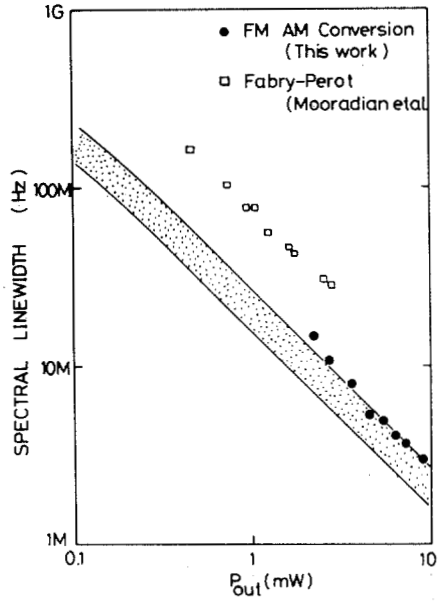

(b)

Fig. 22. Spectral linewidth $\Delta\nu_{1/2}$ versus optical output power for (a) 300 μm CSP laser and (b) 200 μm TJS laser.

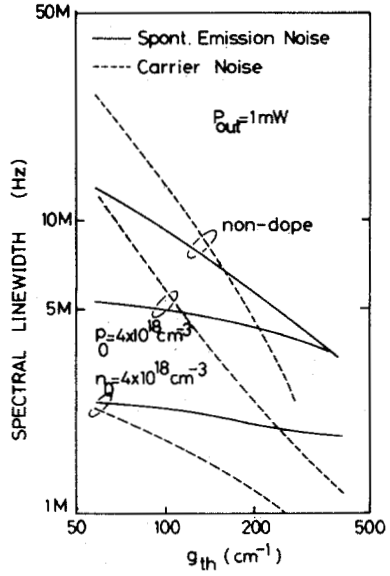

Fig. 23. Linewidths due to spontaneous emission noise and carrier modulation noise versus threshold gain for 300 μm CSP laser.

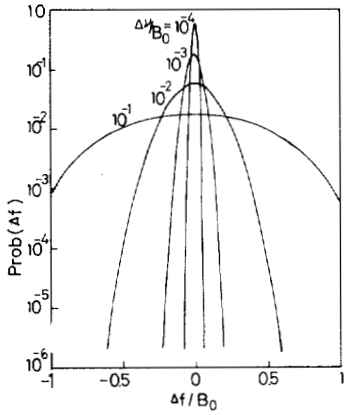

Fig. 24. Instantaneous frequency probability Prob(Ω) as a function of normalized FM noise power $\frac{1}{2}K_d\Delta\nu_{1/2}$.

was confirmed with the independent experimental results concerning mean photon number and saturation output power. Experimental results regarding AM noise spectra, FM noise spectra, and spectral linewidth were in good agreement with the theoretical predictions that used the estimated β and n_{sp} values.

The dependences of the AM noise spectrum, AM noise bandwidth, variance in intensity fluctuation, photon number probability density, and spectral linewidth on material, structural, and pumping parameters are discussed. An active layer with heavily n-doping and small optical mode confinement factor are favorable to decrease both AM and FM quantum noise at a fixed output power. A higher bias level and output power level are, of course, favorable for decreasing quantum noise.

ACKNOWLEDGMENT

The authors wish to thank T. Kimura and A. Kawana for their useful suggestions and discussions.

REFERENCES

[1] Y. Yamamoto, "AM and FM quantum noise in semiconductor lasers—Part I: Theoretical analysis," *IEEE J. Quantum Electron.*, this issue, pp. 34-46.

[2] J. Armstrong and A. W. Smith, "Intensity fluctuations in GaAs laser emission," *Phys. Rev.*, vol. 140, pp. A155-A164, 1965.

[3] T. L. Paoli, "Noise characteristics of stripe-geometry double heterostructure junction laser operating continuously—I. Intensity noise at room temperature," *IEEE J. Quantum Electron.*, vol. QE-11, pp. 276-283, June 1975.

[4] H. Jackel and H. Melchior, "Fundamental limit of the light intensity fluctuations of semiconductor lasers with dielectric transverse mode confinement," presented at the Opt. Commun. Conf., Amsterdam, The Netherlands, 1979.

[5] T. Mukai and Y. Yamamoto, "Noise in an AlGaAs semiconductor laser amplifier," *IEEE J. Quantum Electron.*, vol. QE-18, pp. 564-575, Apr. 1982.

[6] E. D. Hinkley and C. Freed, "Direct observation of the Lorentzian lineshape as limited by quantum phase noise in a laser above threshold," *Phys. Rev. Lett.*, vol. 23, pp. 277-280, 1969.

[7] S. Saito and Y. Yamamoto, "Direct observation of Lorentzian lineshape of semiconductor laser and linewidth reduction with external grating feedback," *Electron. Lett.*, vol. 17, pp. 325-327, 1981.

[8] S. Machida, A. Kawana, K. Ishihara, and H. Tsuchiya, "Interference of an AlGaAs laser diode using 4.15 km single mode fiber cable," *IEEE J. Quantum Electron.*, vol. QE-15, pp. 155-157, 1979.

[9] T. Okoshi, K. Kikuchi, and A. Nakayama, "Novel method for high resolution measurement of laser output spectrum," *Electron. Lett.*, vol. 16, pp. 630-631, 1980.

[10] T. Takakura, K. Iga, and T. Tako, "Measurement of spectral width of a single longitudinal mode semiconductor laser," *Japan. J. Appl. Phys.*, vol. 19, pp. L725-L727, 1980.
[11] Y. Yamamoto, T. Mukai, and S. Saito, "Quantum phase noise and linewidth of a semiconductor laser," *Electron. Lett.*, vol. 17, pp. 327-329, 1981.
[12] A. W. Smith and J. A. Armstrong, "Laser photon counting distributions near threshold," *Phys. Rev. Lett.*, vol. 16, pp. 1169-1172, 1966.
[13] H. Haken, *Encyclopedia of Physics*, vol. XXV/2c, S. Flugge, Ed. Berlin: Springer-Verlag.
[14] H. C. Casey, Jr. and F. Stern, "Concentration-dependent absorption and spontaneous emission of heavily doped GaAs," *J. Appl. Phys.*, vol. 47, pp. 631-643, 1976.
[15] S. Kobayashi and T. Kimura, "Gain and saturation power of resonant AlGaAs laser amplifier," *Electron. Lett.*, vol. 16, pp. 230-232, 1980.
[16] T. Mukai and Y. Yamamoto, "Gain, frequency bandwidth and saturation output power of AlGaAs DH laser amplifiers," *IEEE J. Quantum Electron.*, vol. QE-17, pp. 1028-1034, June 1981.
[17] H. C. Casey, Jr. and M. B. Panish, *Heterostructure Lasers*. New York: Academic, 1978.
[18] R. J. McIntyre, "Multiplication noise in uniform avalanche junctions," *IEEE Trans. Electron Devices*, vol. ED-13, pp. 164-169, 1966.
[19] H. Kanbe, T. Kimura, Y. Mizushima, and K. Kajiyama, "Silicon avalanche photodiodes with low multiplication noise and high speed response," *IEEE Trans. Electron Devices*, vol. ED-23, pp. 1337-1343, 1976.
[20] S. Kobayashi, Y. Yamamoto, M. Ito, and T. Kimura, "Direct frequency modulation in AlGaAs semiconductor lasers," *IEEE J. Quantum Electron.*, vol. QE-18, pp. 582-595, Apr. 1982.
[21] S. Saito, Y. Yamamoto, and T. Kimura, "Optical FSK heterodyne detection experiments using semiconductor laser transmitter and local oscillator," *IEEE J. Quantum Electron.*, vol. QE-17, pp. 935-941, June 1981.
[22] S. Saito, O. Nilsson, and Y. Yamamoto, "Oscillation center frequency tuning, quantum FM noise and direct frequency modulation characteristics in external grating loaded semiconductor lasers," *IEEE J. Quantum Electron.*, vol. QE-18, pp. 961-970, June 1982.
[23] L. Goldberg, H. F. Taylor, A. Dandridge, J. F. Weller, and R. O. Miles, "Spectral characteristics of semiconductor lasers with optical feedback," *IEEE J. Quantum Electron.*, vol. QE-18, pp. 555-564, Apr. 1982.
[24] K. Nemoto, K. Hayashi, and H. Hirano, "Measurement of spectral width of single longitudinal mode semiconductor laser," in *Rec. Nat. Conv.*, IECE Japan, Mar. 1980.
[25] C. H. Henry, "Theory of the linewidth of semiconductor lasers," *IEEE J. Quantum Electron.*, vol. QE-18, pp. 259-264, Feb. 1982.
[26] C. H. Henry, R. A. Logan, and K. A. Bertness, "Spectral dependence of the change in refractive index due to carrier injection in GaAs lasers," *J. Appl. Phys.*, vol. 52, pp. 4451-4461, 1981.

Yoshihisa Yamamoto (S'75-M'80), for a photograph and biography, see this issue, p. 46.

Shigeru Saito (S'76-M'79) was born in Shizuoka, Japan, on September 6, 1951. He received the B.S., M.S., and Ph.D. degrees in electrical communication engineering from Tohoku University, Sendai, Japan, in 1974, 1976, and 1979, respectively.

In 1979 he joined the Musashino Electrical Communication Laboratory, Nippon Telegraph and Telephone Public Corporation, Tokyo, Japan. He has been engaged in research on the coherent optical transmission systems.

Dr. Saito is a member of the Institute of Electronics and Communication Engineers of Japan.

Takaaki Mukai was born in Osaka, Japan, on January 22, 1952. He received the B.S. and M.S. degrees in electronics engineering from Osaka University, Osaka, Japan, in 1975 and 1977, respectively.

In 1977 he joined the Musashino Electrical Communication Laboratory, Nippon Telegraph and Telephone Public Corporation, Tokyo, Japan. He has been engaged in research on the characteristics of semiconductor lasers and optical amplifiers.

Mr. Mukai is a member of the Institute of Electronics and Communication Engineers of Japan and the Japan Society of Applied Physics.

Quantum noise of an injection-locked laser oscillator

H. A. Haus and Y. Yamamoto*
Department of Electrical Engineering and Computer Science and Research Laboratory of Electronics, Massachusetts Institute of Technology, Cambridge, Massachusetts 02139
(Received 21 June 1983)

The quantum noise of an injection-locked laser oscillator is analyzed by the operator Langevin equation. The problem is also treated by the Fokker-Planck equation and the same results are obtained in the same regimes of applicability. The steady-state solution of the Fokker-Planck equation gives the probability distribution of amplitude and phase, the Langevin equation arrives more directly at the spectrum of amplitude and phase. The phase of the injection-locked oscillator is related to the phase of the injection signal and thus constitutes a measurement of phase. In the limit of complete inversion and zero internal loss of the laser resonator, the associated uncertainty is twice that dictated by the uncertainty principle. This result is interpreted by comparing it with the uncertainty introduced by a linear amplifier which can perform a simultaneous measurement of amplitude and phase.

INTRODUCTION

The quantum noise of a laser oscillator has received a great amount of study, both theoretical and experimental. The first treatment of the laser oscillator with operator noise sources is due to Haken.[1–4] Lax and co-workers, in a series of papers, developed and expanded the theory further.[5–9] A density matrix description of the laser oscillator was pioneered by Scully and Lamb[10] and expanded upon in a book by Sargent, Scully, and Lamb.[11] Mandel and Wolf contributed to the theoretical description.[12]

The experimental verification of the quantum noise emitted by lasers started with the study of frequency noise of an He-Ne laser by Javan *et al.*[13] was followed up by laser amplifier noise studies by Klüver.[14] The frequency noise initially observed was governed by the thermal vibrations of the laser cavity length. The amplitude noise near threshold, however, was found to be attributable to quantum noise.[15,16] Quantum noise could be detected in semiconductor diode lasers,[17] since quantum noise predominates over classical noise generating mechanisms in such lasers because of their small dimensions and fast relaxation times. More recently, quantum noise fluctuations were observed in He-Ne laser gyros,[18] the emergence of quantum noise having been made possible by cancellation of classical noise contributions in the measurement of difference frequencies.

Injection locking of lasers for communication purposes[19] has rekindled the interest in quantum noise limitations on this form of modulation. The classical theory of injection locking is discussed in Stratonovich's book.[20] Haken *et al.*[21] studied the quantum theory of locking of modes in a laser oscillator. Chow *et al.*[22] pointed out the narrowing of the laser spectrum due to injection locking. No complete quantum-mechanical treatment of the noise accompanying injection locking exists in the literature. The present paper presents such an analysis. In the limit when the oscillator runs at a very high power level with complete inversion, the mean-square phase fluctuations of the output waveform are found to be

$$(\langle \Delta\phi^2 \rangle_{\rm av})^{1/2} = \frac{1}{\sqrt{2\langle n_s \rangle_{\rm av}}} ,$$

where $\langle n_s \rangle_{\rm av}$ is the average photon number of the injection signal. If the phase of the output is viewed as a measurement of the phase of the locking signal, then this measurement results in a phase uncertainty twice that dictated by the uncertainty principle. This result is compared with a measurement of a coherent state after amplification by an ideal linear amplifier. Such an amplification makes possible the simultaneous measurement of amplitude and phase fluctuations, doubling the uncertainty in the process, as pointed out by Haus and Townes,[23] Arthurs and Kelly,[24] and Caves.[25]

We start in Sec. I with the operator Langevin equation and obtain the fluctuation spectra of amplitude and phase of the locked oscillator in Sec. II. In the limit of complete inversion we determine the minimum phase uncertainty. This result is compared with that of the linear amplifier in Sec. III. The only difference between the two systems is that the relaxation times of amplitude and phase, different in the case of the locked oscillator, become identical in the case of the linear amplifier. We ascertain the fact that the linear amplifier is capable of reaching the ideal limit of a simultaneous measurement.

In Sec. IV we set up the Fokker-Planck equation for the $P(\alpha)$ function of the laser oscillator, supplemented by an injection-locking term due to a c-number source. Section V treats the case of a coherent state coupled to the oscillator via an optical isolator and finds that the Fokker-Planck equation is identical with that of a c-number source, with the amplitude of the c-number source replaced by the eigenvalue of the coherent state. The steady-state distribution $P(\alpha)$ is approximately a two-dimensional Gaussian in amplitude and phase. The equations of motion for the expectation values of amplitude and phase are then related to the analysis of Sec. II. The mean-square amplitude and phase fluctuations are ob-

 ©1984 The American Physical Society

tained in Sec. VI and compared with the results of the Langevin approach. The two approaches are shown to lead to the same result in the same ranges of applicability.

I. QUANTUM-MECHANICAL LANGEVIN EQUATION

In this section, and the subsequent two sections we consider the operator Langevin equation for the injection-locked oscillator (see Fig. 1) and the regenerative amplifier. We start with the Langevin equation for the laser in the absence of an injection signal as derived in Ref. 11. The pertinent equation is (49), p. 334:

$$\dot{a}(t)=-\frac{1}{2}\left[\frac{\omega_0}{Q}-\mathscr{A}+\mathscr{B}a^\dagger a\right]a(t)+G(t)\ , \tag{1.1}$$

where $a(t)$ is the slowly varying envelope of the annihilation operator $a(t)e^{-i\omega_0 t}$.

$\mathscr{A}$ is the linear gain parameter, ω_0/Q is the decay rate of the laser resonator in the absence of the gain medium, $\mathscr{B}$ is the saturation parameter expressing the dependence of the gain on the photon number $a^\dagger a$: the total gain parameter is $\mathscr{A}-\mathscr{B}a^\dagger a$. The function $G(t)$ is the operator noise source with the correlation function[4,11]

$$\langle G^\dagger(t)G(t')\rangle+\langle G(t)G^\dagger(t')\rangle = 2\left[\frac{1}{2}\frac{\omega_0}{Q}+\frac{g^2}{\gamma}(N_2+N_1)\right]\delta(t-t')\ , \tag{1.2}$$

where the first term $\frac{1}{2}\omega_0/Q$ represents the zero-point fluctuation of the photon field and the second term $(g^2/\gamma)(N_2+N_1)$ represents the atomic dipole moment fluctuation. g is the atom-field interaction matrix element and γ is the phase decay constant of the dipole moment. The Marcovian assumption that the dipole moment and energy decay constants are much larger than the photon decay constant ω_0/Q is used to derive (1.1) and (1.2). The noise contribution of the level operator is neglected because it is of higher order in (ga).

The interaction Hamiltonian between a laser photon operator a and an injection signal operator b is assumed to be

$$V=i\hbar(\kappa ba^\dagger e^{-i(\omega-\omega_0)t}-\kappa ab^\dagger e^{i(\omega-\omega_0)t})\ , \tag{1.3}$$

where b is the annihilation operator of the injection signal, ω is the frequency of the injection signal, and ω_0 that of the oscillator. The interaction Hamiltonian is quadratic in the excitation amplitudes of the two systems, laser and injection signal. The coupling is thus linear. Here, again, b is an envelope operator, the natural time dependence $\exp(i\omega t)$ has been factored out. The decay rate ω_0/Q consists of two contributions, one from the unloaded quality factor Q_0, and the other from the external Q, Q_e:

$$\frac{\omega_0}{Q}=\frac{\omega_0}{Q_e}+\frac{\omega_0}{Q_0}\ . \tag{1.4}$$

The external Q expresses the coupling to the mode of the injection signal, the unloaded Q incorporates coupling to any other modes and to the loss. We shall find it convenient to use time constants τ_e and τ_0 defined by

$$\frac{\omega_0}{Q_e}=\frac{2}{\tau_e}\ , \tag{1.5}$$

$$\frac{\omega_0}{Q_0}=\frac{2}{\tau_0}\ . \tag{1.6}$$

The coupling constant κ has been assumed real with no loss of generality, since this choice disposes of an arbitrary phase reference.

The Heisenberg equation of motion:

$$\dot{a}=\frac{i}{\hbar}[\mathscr{H},\ a] \tag{1.7}$$

which led to (1.2) is supplemented by the coupling term (1.3) and results in

$$\dot{a}=\frac{1}{2}\left[\mathscr{A}-\frac{\omega_0}{Q}-\mathscr{B}a^\dagger a\right]a+\kappa b\,e^{-i(\omega-\omega_0)t}+G(t)\ . \tag{1.8}$$

This is the quantum-mechanical Langevin equation of injection locking of an oscillator. The linear laser amplifier, operating below its oscillation threshold, is also described by (1.8) if the gain saturation term $\mathscr{B}a^\dagger a$ is dropped in the above equation. The coupling constant κ can be related to the external Q and the bandwidth B of the injection signal as shown in Appendix A

$$\kappa=2(B/\tau_e)^{1/2}=\left[\frac{2B\omega_0}{Q}\right]^{1/2}\left[1+\frac{\tau_e}{\tau_0}\right]^{-1/2}\ . \tag{1.9}$$

Here B is the Nyquist bandwidth related to the signal sampling time T as follows:

$$B=1/2T\ .$$

II. AMPLITUDE AND PHASE NOISE OF INJECTION-LOCKED OSCILLATOR

The Langevin approach leads directly to the spectra of the amplitude and phase fluctuations, the Fourier transforms of the correlation functions. The Fokker-Planck approach used later on gives the probability densities of the fluctuating quantities. In this section we derive the amplitude and phase spectra of the injection-locked oscillator starting with (1.8).

The operator a generally follows the time dependence of the injection signal, if the locking is successful. Thus, it is convenient to write

$$a(t)=(a_0+\Delta a)e^{-i[(\omega-\omega_0)t+\phi_0+\Delta\phi]} \tag{2.1}$$

and

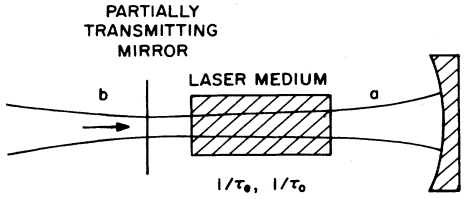

FIG. 1. Schematic of injection-locked laser oscillator.

$$b(t)=(b_0+\Delta b)e^{-i[(\omega-\omega_0)t+\Delta\psi]} . \tag{2.2}$$

Here a_0, b_0, and ϕ_0 are real c numbers. The Hermitian operators Δb and $\Delta\psi$ express the excess amplitude and phase noise of the injection signal, and Hermitian operators Δa and $\Delta\phi$ those of the oscillator excitation. The zero-point fluctuations attributable to the input port are already included in the Langevin noise operator $G(t)$. We shall assume that Δb and $\Delta\psi$ commute and are uncorrelated. $G(t)$ commutes with both and is uncorrelated with either because we assume that a and b are operators pertaining to two different subsystems.

The above quantum-mechanical quasilinearization is an extension of the one used for a laser oscillator by Haken[4] and Lax.[7] Use of (2.1) and (2.2) in the quantum-mechanical Langevin equation (1.4) leads, after separation into orders of the perturbation, to an equation for the c-number amplitude a_0 and phase ϕ_0

$$-i(\omega-\omega_0)a_0-\frac{1}{2}\left[\mathscr{A}-\frac{\omega_0}{Q}-\mathscr{B}a_0^2\right]a_0=\kappa b_0 e^{i\phi_0} . \tag{2.3}$$

The amplitude a_0 is related to b_0 by

$$a_0=\frac{\kappa}{\left[(\omega-\omega_0)^2+\frac{1}{4}\left[\mathscr{A}-\frac{\omega_0}{Q}-\mathscr{B}a_0^2\right]^2\right]^{1/2}}b_0 , \tag{2.4}$$

where the factor multiplying b_0 is the net gain, the enhancement of the injection signal, and

$$\tan\phi_0=\frac{\omega_0-\omega}{\frac{1}{2}\left[\mathscr{B}a_0^2-\mathscr{A}+\frac{\omega_0}{Q}\right]} . \tag{2.5}$$

In the absence of an injection signal, the gain is infinite, and from this fact one may evaluate the value of a_0 of the free-running oscillator

$$a_0^2=\frac{\mathscr{A}-\frac{\omega_0}{Q}}{\mathscr{B}} . \tag{2.6}$$

The injection signal increases a_0 so that

$$\mathscr{A}-\mathscr{B}a_0^2<\omega_0/Q$$

and the gain coefficient is less than the loss coefficient. The increase in amplitude with the injection signal, for small changes Δa_0 from a_0, is given by (2.4) and (2.6)

$$a_0(b_0\neq 0)-a_0(b_0=0)\cong\frac{\kappa\cos\phi_0}{\mathscr{B}a_0^2}b_0 . \tag{2.7}$$

At synchronism, $\omega=\omega_0$, the injection signal b_0 and the response $a_0e^{i\phi_0}$ are in phase, $\phi_0=0$. Increased detuning leads to a reduction of the net gain and an increase of the dephasing, provided that the detuning is within the locking bandwidth $\Delta\omega_L$. The locking bandwidth is obtained from the imaginary part of (2.3) and by noting that $|\sin\phi_0|\leq 1$. We then have

$$|\omega_0-\omega|\leq\frac{\kappa b_0}{a_0}\equiv\Delta\omega_L .$$

The oscillation frequency ω, the phase shift ϕ_0, and the increase Δa_0 of the amplitude are shown schematically in Fig. 2 as functions of the detuning $\omega_0-\omega_i$.

The equations for the amplitude and phase perturbations are

$$\begin{aligned}\Delta\dot{a}=&-\frac{\Delta a}{\tau_a}-(\omega_0-\omega)a_0\Delta\phi+\kappa\cos\phi_0\Delta b+\kappa\sin\phi_0 b_0\Delta\psi\\&+\tfrac{1}{2}(G(t)\exp\{i[(\omega-\omega_0)t+\phi_0]\}\\&+G^\dagger(t)\exp\{-i[(\omega-\omega_0)t+\phi_0]\}) ,\end{aligned} \tag{2.8}$$

where we have used (2.4) and (2.5). Further,

$$\begin{aligned}\Delta\dot{\phi}=&-\frac{\kappa b_0}{a_0}\cos\phi_0(\Delta\phi-\Delta\psi)+(\omega_0-\omega)\frac{\Delta a}{a_0}-\frac{\kappa}{a_0}\sin\phi_0\Delta b\\&+\frac{i}{2a_0}(G(t)\exp\{i[(\omega-\omega_0)t+\phi_0]\}\\&-G^\dagger(t)\exp\{-i[(\omega-\omega_0)t+\phi_0]\}) ,\end{aligned} \tag{2.9}$$

where

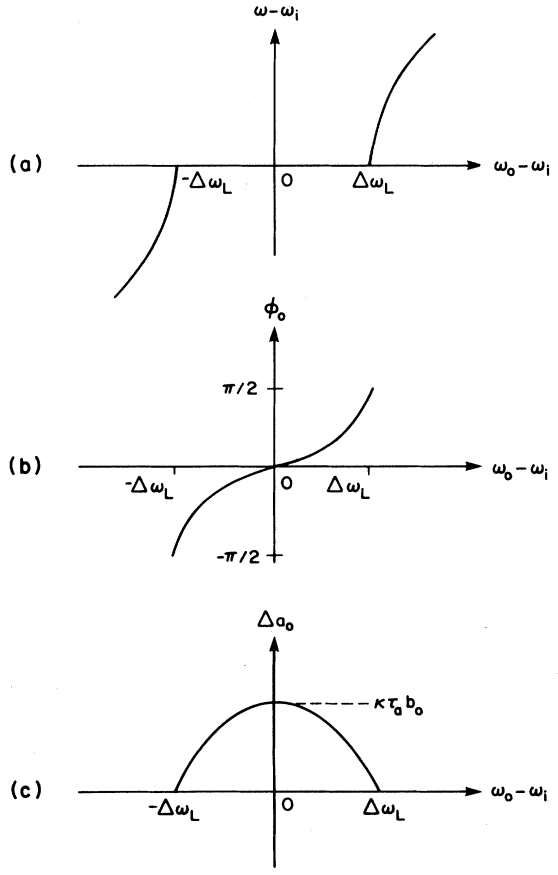

FIG. 2. Oscillation frequency ω, phase shift ϕ_0 and increase in amplitude Δa_0 vs frequency detuning $\omega_i-\omega_0$. ω_i is the input signal frequency, ω_0 is the oscillator frequency without input signal and $\Delta\omega_L$ is the locking bandwidth.

$$\frac{1}{\tau_a}=\mathscr{B}a_0^2 \tag{2.10}$$

is the decay rate of the amplitude perturbation, i.e.,

$$-\frac{1}{2}\left[\mathscr{A}-\frac{\omega_0}{Q}-\mathscr{B}a^2\right]a$$

expanded to first order in Δa, giving $\mathscr{B}a_0^2\Delta a$. The decay rate of the phase is zero in the absence of an injection signal. In the presence of an injection signal it is

$$\frac{1}{\tau_p}=\frac{\kappa b_0}{a_0}\cos\phi_0=\frac{1}{2}\left[\mathscr{B}a_0^2-\mathscr{A}+\frac{\omega_0}{Q}\right] \tag{2.11}$$

and is larger, the larger the injection signal. The phase relaxation time is directly related to the gain at resonance, $a_0=\kappa\tau_p b_0$ at resonance, as can be seen from (2.4) and (2.11).

A useful relation is obtained by combining (2.11) and (2.5):

$$\omega_0-\omega=\frac{1}{\tau_p}\tan\phi_0=\frac{\kappa b_0}{a_0}\sin\phi_0\ . \tag{2.12}$$

The determinantal equation for the homogeneous equation, for an assumed $\exp(-i\Omega t)$ dependence, is

$$\left[-i\Omega+\frac{1}{\tau_a}\right]\left[-i\Omega+\frac{1}{\tau_p}\right]+(\omega_0-\omega)^2=0\ , \tag{2.13}$$

where we have used (2.4) and (2.5). The solution is

$$\Omega=-\frac{i}{2}\left[\frac{1}{\tau_a}+\frac{1}{\tau_p}\right]\pm i\left[\frac{1}{4}\left[\frac{1}{\tau_a}-\frac{1}{\tau_p}\right]^2-(\omega_0-\omega)^2\right]^{1/2}.$$

When the injection signal is not detuned, $\omega_0=\omega$, the eigenfrequencies are imaginary and equal in magnitude to the decay rates $1/\tau_a$ and $1/\tau_p$ of amplitude and phase. The amplitude and phase fluctuations are decoupled. When $\omega_0\neq\omega$, the two fluctuations couple and the decay rates of the resulting solutions are affected by the individual decay rates and degree of detuning.

The Fourier transform of the amplitude fluctuation operator, treated as a periodic function of period T_p is

$$\Delta a(n\,\Delta\Omega)\equiv\lim_{T_p\to\infty}\frac{1}{T_p}\int_{-T_p/2}^{T_p/2}\Delta a(t)e^{in\,\Delta\Omega t}dt\ . \tag{2.14}$$

From here on, we treat

$$\Omega=\lim_{\substack{\Delta\Omega\to 0\\ n\to\infty}} n\,\Delta\Omega$$

as a continuous variable Ω. From (2.8) and (2.9)

$$\Delta a(\Omega)=\frac{\left[-i\Omega+\frac{1}{\tau_p}\right]N_c(\Omega)-(\omega_0-\omega)N_s(\Omega)}{\left[-i\Omega+\frac{1}{\tau_a}\right]\left[-i\Omega+\frac{1}{\tau_p}\right]+(\omega_0-\omega)^2}, \tag{2.15}$$

where the noise sources $N_c(\Omega)$ and $N_s(\Omega)$ are defined, with $n\,\Delta\Omega\equiv\Omega$:

$$N_c(\Omega)=\lim_{T_p\to\infty}\frac{1}{T_p}\int_{-T_p/2}^{T_p/2}dt\,e^{in\,\Delta\Omega t}\{(\cos\phi_0)\kappa\,\Delta b(t)+(\sin\phi_0)\kappa b_0\Delta\psi(t)$$
$$+\tfrac{1}{2}[e^{i\phi_0}G(t)e^{i(\omega-\omega_0)t}+e^{-i\phi_0}G^\dagger(t)e^{-i(\omega-\omega_0)t}]\}\ , \tag{2.16}$$

$$N_s(\Omega)=\lim_{T_p\to\infty}\frac{1}{T_p}\int_{-T_p/2}^{T_p/2}dt\,e^{in\,\Delta\Omega t}\{(\cos\phi_0)\kappa b_0\Delta\psi(t)-(\sin\phi_0)\kappa\,\Delta b(t)$$
$$+\frac{i}{2}[e^{i\phi_0}G(t)e^{i(\omega-\omega_0)t}-e^{-i\phi_0}G^\dagger(t)e^{-i(\omega-\omega_0)t}]\}\ . \tag{2.17}$$

The noise sources consist of the inphase (cosine, subscript c) and quadrature (sine, subscript s) contributions of the excess noise of the signal and the noise source $G(t)$. The former are due to the amplitude Δb and phase $\Delta\psi$ and are weighted by $\cos\phi_0$ and $\pm\sin\phi_0$, respectively; the weighting is interchanged between that for amplitude and phase. Further, the spectrum of the noise source $G(t)$ is shifted from that centered around ω_0, as implied by the noise envelope $G(t)$ of (1.8), to that centered around ω.

The Fourier transform of $\Delta\phi(t)$,

$$\Delta\phi(\Omega)=\lim_{T_p\to\infty}\frac{1}{T_p}\int_{-T_p/2}^{T_p/2}\Delta\phi(t)e^{in\,\Delta\Omega t} \tag{2.18}$$

with $n\Delta\Omega=\Omega$, follows similarly,

$$\Delta\phi(\Omega)=\frac{1}{a_0}\frac{\left[-i\Omega+\frac{1}{\tau_a}\right]N_s(\Omega)+(\omega_0-\omega)N_c(\Omega)}{\left[-i\Omega+\frac{1}{\tau_a}\right]\left[-i\Omega+\frac{1}{\tau_p}\right]+(\omega_0-\omega)^2}\ . \tag{2.19}$$

The spectrum $W_{\Delta a}(\Omega)$ is obtained from (2.15) by taking the average of $\Delta a^\dagger(\Omega)\Delta a(\Omega)$ and by dividing by the frequency interval $\Delta\Omega=2\pi/T$ in the limit as $T\to\infty$, $\Delta\Omega\to 0$:

$$W_{\Delta a}(\Omega)=\lim_{\Delta\Omega\to 0}\frac{1}{\Delta\Omega}\langle\Delta a^{\dagger}(\Omega)\Delta a(\Omega)\rangle=\lim_{\Delta\Omega\to 0}\frac{1}{\Delta\Omega}\frac{1}{|\mathscr{D}|^2}\left[\left[\Omega^2+\frac{1}{\tau_p^2}\right]\langle N_c^{\dagger}(\Omega)N_c(\Omega)\rangle+(\omega_0-\omega)^2\langle N_s^{\dagger}(\Omega)N_s(\Omega)\rangle\right.$$
$$-\left[i\Omega+\frac{1}{\tau_p}\right](\omega_0-\omega)\langle N_c^{\dagger}(\Omega)N_s(\Omega)\rangle$$
$$\left.-\left[-i\Omega+\frac{1}{\tau_p}\right](\omega_0-\omega)\langle N_s^{\dagger}(\Omega)N_c(\Omega)\rangle\right], \tag{2.20}$$

where

$$|\mathscr{D}|^2=\left[\Omega^2-(\omega_0-\omega)^2-\frac{1}{\tau_a\tau_p}\right]^2+\left[\frac{1}{\tau_a}+\frac{1}{\tau_p}\right]^2\Omega^2 . \tag{2.21}$$

The noise source $G(t)$ is uncorrelated with itself; $G^{\dagger}(t)G(t')$ is correlated in an impulselike manner (1.2) and, hence, its spectrum is flat. Denote the spectrum of Δb by

$$W_{\Delta b}(\Omega)=\lim_{\Delta\Omega\to 0}\frac{1}{\Delta\Omega}\langle\Delta b^{\dagger}(\Omega)\Delta b(\Omega)\rangle \tag{2.22}$$

and similarly for $\Delta\psi$. We further assume that the amplitude and phase fluctuations of the injection signal are uncorrelated. Then using (2.16) and (2.17) the spectra of N_c and N_s are

$$\lim_{\Delta\Omega\to 0}\frac{1}{\Delta\Omega}\langle N_c^{\dagger}(\Omega)N_c(\Omega)\rangle$$
$$=(\cos^2\phi_0)\kappa^2W_{\Delta b}(\Omega)+(\sin^2\phi_0)\kappa^2|b_0|^2W_{\Delta\psi}(\Omega)+\frac{1}{4\pi}\left[\frac{1}{2}\frac{\omega_0}{Q}+\frac{g^2}{\gamma}(N_2+N_1)\right], \tag{2.23}$$

$$\lim_{\Delta\Omega\to 0}\frac{1}{\Delta\Omega}\langle N_s^{\dagger}(\Omega)N_s(\Omega)\rangle$$
$$=(\sin^2\phi_0)\kappa^2W_{\Delta b}(\Omega)+(\cos^2\phi_0)\kappa^2|b_0|^2W_{\Delta\psi}(\Omega)+\frac{1}{4\pi}\left[\frac{1}{2}\frac{\omega_0}{Q}+\frac{g^2}{\gamma}(N_2+N_1)\right]. \tag{2.24}$$

The cross spectrum of N_c and N_s is

$$\lim_{\Delta\Omega\to 0}\frac{1}{\Delta\Omega}\langle N_c^{\dagger}(\Omega)N_s(\Omega)\rangle$$
$$=\kappa^2\sin\phi_0\cos\phi_0[W_{\Delta b}(\Omega)-|b_0|^2W_{\Delta\psi}(\Omega)] . \tag{2.25}$$

The spectra of the excess noise of the injection signal may possess structure, whereas the internal noise has a flat spectrum, the last terms in (2.23) and (2.24). The internal noise spectrum has an intensity that is simply related to the inversion as one may ascertain by eliminating the atom-field interaction parameter g^2/γ with the relation[11]

$$\frac{g^2}{\gamma}=\left[2(N_2-N_1)\frac{\omega_0}{Q}\right]^{-1} . \tag{2.26}$$

Combining (2.20) and (2.22)–(2.26) one may write for the amplitude spectrum

$$W_{\Delta a}(\Omega)=\frac{1}{|\mathscr{D}|^2}\left\{\left[\left[\Omega^2+\frac{1}{\tau_p^2}\right]\cos^2\phi_0+(\omega_0-\omega)^2\sin^2\phi_0+\frac{2}{\tau_p}(\omega_0-\omega)\sin\phi_0\cos\phi_0\right]\kappa^2W_{\Delta b}(\Omega)\right.$$
$$+\left[\left[\Omega^2+\frac{1}{\tau_p^2}\right]\sin^2\phi_0+(\omega_0-\omega)^2\cos^2\phi_0-\frac{2}{\tau_p}(\omega_0-\omega)\sin\phi_0\cos\phi_0\right]\kappa^2b_0^2W_{\Delta\psi}(\omega)$$
$$\left.+\frac{1}{2\pi}\left[\Omega^2+\frac{1}{\tau_p^2}+(\omega_0-\omega)^2\right]\frac{\omega_0}{Q}\left[\frac{1}{4}+\frac{1}{4}\frac{N_2+N_1}{N_2-N_1}\right]\right\} . \tag{2.27}$$

The phase spectrum is

$$W_{\Delta\phi}(\Omega)=\frac{1}{|\mathscr{D}|^2a_0^2}\left\{\left[\left[\Omega^2+\frac{1}{\tau_a^2}\right]\cos^2\phi_0+(\omega_0-\omega)^2\sin^2\phi_0+\frac{2}{\tau_a}(\omega_0-\omega)\sin\phi_0\cos\phi_0\right]\kappa^2b_0^2W_{\Delta\psi}(\Omega)\right.$$
$$+\left[\left[\Omega^2+\frac{1}{\tau_a^2}\right]\sin^2\phi_0+(\omega_0-\omega)\cos^2\phi_0-\frac{2}{\tau_a}(\omega_0-\omega)\sin\phi_0\cos\phi_0\right]\kappa^2W_{\Delta b}(\Omega)$$
$$\left.+\frac{1}{2\pi}\left[\Omega^2+\frac{1}{\tau_a^2}+(\omega_0-\omega)^2\right]\frac{\omega_0}{Q}\left[\frac{1}{4}+\frac{1}{4}\frac{N_2+N_1}{N_2-N_1}\right]\right\} . \tag{2.28}$$

Let us consider first the effect of the oscillator noise, assuming zero excess noise of the injection signal. In this case both amplitude and phase spectra simplify greatly. Consider the phase spectrum

$$a_0^2 W_{\Delta\phi}(\Omega)=\frac{\left[\Omega^2+\frac{1}{\tau_a^2}\right]+(\omega_0-\omega)^2}{|\mathscr{D}|^2}\frac{1}{2\pi}\times\frac{\omega_0}{Q}\left[\frac{1}{4}+\frac{1}{4}\frac{N_2+N_1}{N_2-N_1}\right]. \tag{2.29}$$

In the amplitude spectrum $1/\tau_a$ is interchanged with $1/\tau_p$.

$$W_{\Delta a}(\Omega)=\frac{\left[\Omega^2+\frac{1}{\tau_p^2}\right]+(\omega_0-\omega)^2}{|\mathscr{D}|^2}\frac{1}{2\pi}\times\frac{\omega_0}{Q}\left[\frac{1}{4}+\frac{1}{4}\frac{N_2+N_1}{N_2-N_1}\right]. \tag{2.30}$$

Because the two relaxation rates are not the same, the spectra differ.

The phase measurement on the oscillator at a large amplitude $\underline{a}_0$ may be viewed as a measurement of the phase of the injection signal. In the process noise is introduced. The minimum amount of uncertainty, or mean-square phase deviation within the observation time T, must be compatible with the uncertainty principle that does not permit the measurement of phase better than given by the inequality

$$\langle\Delta\phi^2\rangle_{\rm av}\geq\frac{1}{4\langle\Delta n_s^2\rangle_{\rm av}}, \tag{2.31}$$

where $\langle\Delta n_s^2\rangle_{\rm av}$ are the fluctuations of the signal photon number. For a coherent state $\langle\Delta n_s^2\rangle_{\rm av}=\langle n_s\rangle_{\rm av}$ and therefore

$$\langle\Delta\phi^2\rangle_{\rm av}\geq\frac{1}{4\langle n_s\rangle_{\rm av}}.$$

The spectrum of the injection signal is at, and near, the frequency ω. A measurement of the phase must be centered at $\Omega=0$ and have a bandwidth $4\pi B=2\pi/T$ (two-sided spectrum). To detect an undistorted phase signal, the phase response of the locked oscillator must not vary

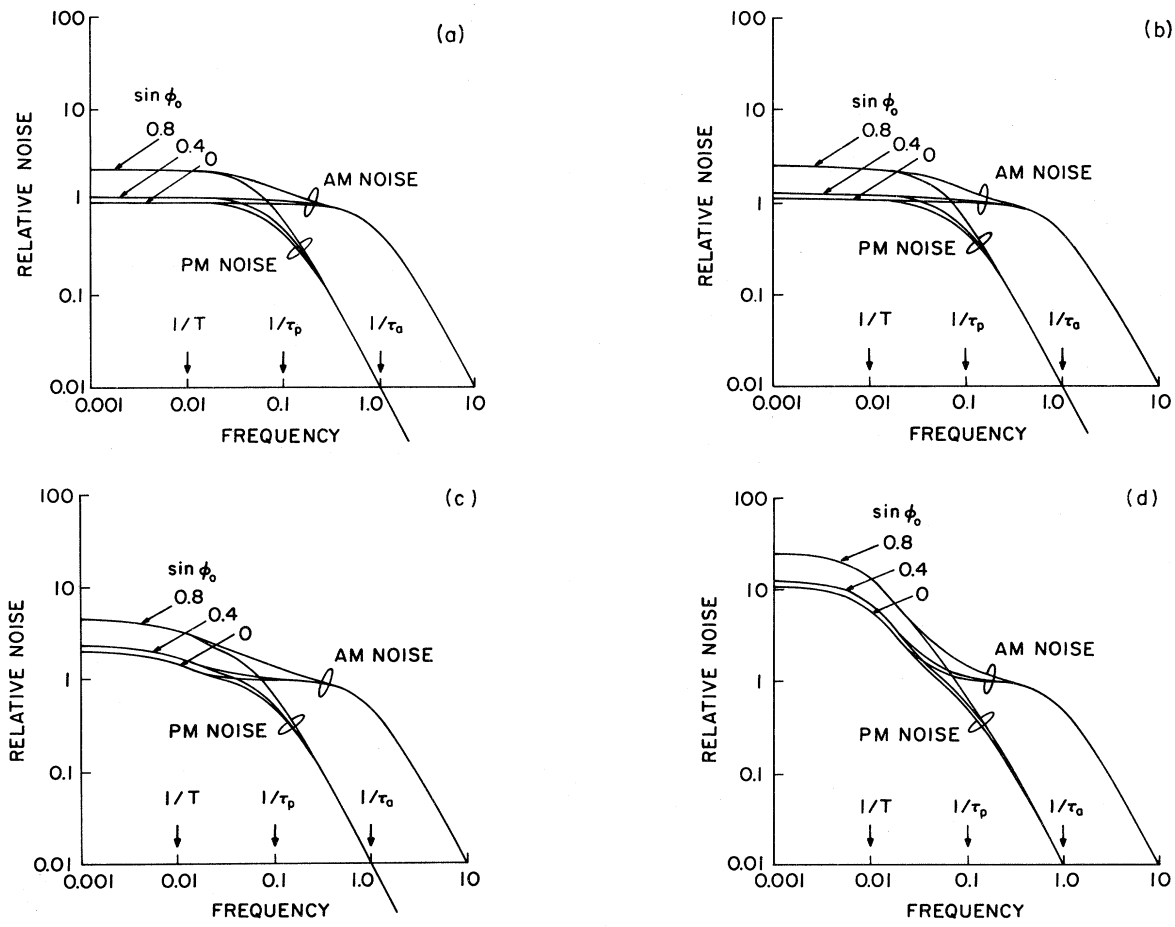

FIG. 3. Spectrum of amplitude and phase noise. Amplitude and phase noise are normalized by $\omega_0\tau_a^2/4\pi Q$ and $\omega_0\tau_p^2\cos^2\phi_0/4\pi Q a_0^2$, respectively. Frequency is normalized by the amplitude noise bandwidth, $1/\tau_a$. Phase noise bandwidth is assumed to be $1/\tau_p=1/10\tau_a$ and signal bandwidth $1/T=1/100\tau_a$. Excess noise of input signal is (a) $\langle\Delta b^2\rangle=b_0^2\langle\Delta\psi^2\rangle=0$, coherent state, (b) $\langle\Delta b^2\rangle=b_0^2\langle\Delta\psi^2\rangle=0.1/4$, (c) $\langle\Delta b^2\rangle=b_0^2\langle\Delta\psi^2\rangle=\frac{1}{4}$, equal to zero-point fluctuation, and (d) $\langle\Delta b^2\rangle=b_0^2\langle\Delta\psi^2\rangle=\frac{10}{4}$.

over the bandwidth $4\pi B$. Therefore, we may evaluate the mean-square fluctuations $\langle \Delta\phi_T^2 \rangle_{\rm av}$ within the observation time T from the product

$$4\pi B W_{\Delta\phi}(\Omega=0) .$$

Using (2.11) and (1.9)

$$\langle \Delta\phi_T^2 \rangle_{\rm av} = 4\pi B W_{\Delta\phi}(\Omega=0)$$

$$= \frac{1}{2\langle n_s \rangle_{\rm av}} \frac{N_2}{N_2-N_1} \left[1+\frac{\tau_e}{\tau_0} \right] \times \frac{[1+\tau_a^2(\omega_0-\omega)^2][1+\tau_p^2(\omega_0-\omega)^2]}{[1+\tau_a\tau_p(\omega_0-\omega)^2]^2} , \quad (2.32)$$

where $\langle n_s \rangle_{\rm av} = b_0^2$ is the average number of signal photons. The frequency-dependent factor has a minimum value of 1 at $(\omega-\omega_0)=0$ and $(\omega-\omega_0)=\infty$ (the latter value is uninteresting because it corresponds to no gain). Thus, the minimum value of $\langle \Delta\phi_T^2 \rangle_{\rm av}$ occurs at $\omega=\omega_0$, when the injection signal has the natural frequency of the oscillator, and is equal to twice the value imposed by the uncertainty principle enhanced by the inversion factor $N_2/(N_2-N_1)$, and the cavity loss factor $[1+(\tau_e/\tau_0)]$. The two factors approach unity for complete inversion of the atomic systems, and for a highly over-coupled cavity $\tau_e/\tau_0 \ll 1$.

Next, consider the noise in the presence of excess amplitude and phase noise of the injection signal. The spectra of amplitude and phase are plotted in Fig. 3 for different detunings and input excess noise spectra. With increasing detuning both the amplitude and phase noise are increased due to amplitude-to-phase conversion and vice versa. The phase noise relaxation rate $1/\tau_p$ is assumed to be $\frac{1}{10}$ times the amplitude relaxation rate $1/\tau_a$ which corresponds to a signal gain of 20 dB. The excess noise is assumed to have the same bandwidth as the signal.

III. AMPLITUDE AND PHASE NOISE OF LINEAR AMPLIFIER

We have found that a locked oscillator measures the phase of the injection signal with an uncertainty twice that of the ideal measurement. This is, at first sight, surprising because one may have expected that the locking of an oscillator constitutes a measurement of the *phase* of the injection signal without a simultaneous measurement of the amplitude. As such, it ought not to incur the 3 dB penalty imposed by a simultaneous measurement.[23-25] In order to understand our result, it is useful to study the linear amplifier.

The fluctuations of the linear amplifier differ from those of the locked oscillator only by the fact that the phase and amplitude relaxation times are identical in the amplifier case

$$\frac{1}{\tau} = \frac{1}{\tau_a} = \frac{1}{\tau_p} = \frac{1}{2} \left[\frac{\omega_0}{Q} - \mathscr{A} \right] \quad (3.1)$$

and the saturation term $\mathscr{B} a_0^2$ is ignored. The result of Sec. II can be taken over with the interpretation of ϕ_0 [compare (2.5)]

$$\tan\phi_0 = (\omega_0-\omega)\tau . \quad (3.2)$$

Introduction of these relations into (2.27) and (2.28) gives

$$W_{\Delta a}(\Omega) = \frac{1}{|\mathscr{D}|^2} \left[\left[\Omega^2\cos^2\phi_0 + \frac{1}{\tau^2\cos^2\phi_0} \right] \kappa^2 W_{\Delta b}(\Omega) + \kappa^2 b_0^2 \Omega^2 (\sin^2\phi_0) W_{\Delta\psi}(\Omega) + \frac{\omega_0}{Q} \left[\Omega^2 + \frac{1}{\tau^2} + (\omega_0-\omega)^2 \right] \frac{1}{2\pi} \left[\frac{1}{4} + \frac{1}{4} \frac{N_2+N_1}{N_2-N_1} \right] \right] \quad (3.3)$$

and

$$a_0^2 W_{\Delta\phi}(\Omega) = \frac{1}{|\mathscr{D}|^2} \left[\left[\Omega^2\cos^2\phi_0 + \frac{1}{\tau^2\cos^2\phi_0} \right] \kappa^2 b_0^2 W_{\Delta\psi}(\Omega) + \kappa^2 \Omega^2 \sin^2\phi_0 W_{\Delta b}(\Omega) + \frac{\omega_0}{Q} \left[\Omega^2 + \frac{1}{\tau^2} + (\omega_0-\omega)^2 \right] \frac{1}{2\pi} \left[\frac{1}{4} + \frac{1}{4} \frac{N_2+N_1}{N_2-N_1} \right] \right] , \quad (3.4)$$

where

$$|\mathscr{D}|^2 = \left[[\Omega+(\omega_0-\omega)]^2 + \frac{1}{\tau^2} \right] \left[[\Omega-(\omega_0-\omega)]^2 + \frac{1}{\tau^2} \right] . \quad (3.5)$$

It is of interest to ascertain the uncertainty in the determination of amplitude and phase of a coherent state, with $W_{\Delta\psi} = W_{\Delta b} = 0$. In this limit, the amplitude spectrum referred to the "input" by division by the power gain

$$G^2 = \frac{\kappa^2}{(\omega_0-\omega)^2 + \frac{1}{\tau^2}}$$

gives, at $\Omega=0$,

$$\frac{W_{\Delta a}(\Omega=0)}{G^2} = \frac{1}{\kappa^2} \frac{\omega_0}{Q} \frac{1}{4\pi} \left[\frac{N_2}{N_2-N_1} \right] . \quad (3.6)$$

The same result is obtained for $b_0^2 W_{\Delta\phi}(\Omega=0)$. Again the use of the definition of the coupling coefficient gives for the amplitude uncertainty $\langle \Delta b_T^2 \rangle_{\rm av}$ measured in a time in-

terval T

$$\langle \Delta b_T^2 \rangle_{\rm av} = \frac{2\pi}{T} \frac{W_{\Delta a}(\Omega=0)}{G^2} = \frac{1}{2} \frac{N_2}{N_2 - N_1} \left[1 + \frac{\tau_e}{\tau_0} \right] \tag{3.7}$$

and for the phase uncertainty

$$\langle \Delta \phi_T^2 \rangle_{\rm av} = \frac{2\pi}{T} W_{\Delta\phi}(\Omega=0) = \frac{1}{2} \frac{1}{b_0^2} \frac{N_2}{N_2 - N_1} \left[1 + \frac{\tau_e}{\tau_0} \right] . \tag{3.8}$$

The product of the two uncertainties is

$$\langle \Delta b_T^2 \rangle_{\rm av} \langle \Delta \phi_T^2 \rangle_{\rm av} = \frac{1}{4} \frac{1}{\langle n_s \rangle_{\rm av}} \left[\frac{N_2}{N_2 - N_1} \right]^2 \left[1 + \frac{\tau_e}{\tau_0} \right]^2 . \tag{3.9}$$

When the inversion is complete this product reaches the ideal limit, imposed on a simultaneous measurement of amplitude and phase. The rms value of the ideal limit is two times larger than that imposed by the Heisenberg principle on an ideal measurement of *either* amplitude *or* phase. This is the penalty incurred by a simultaneous measurement.[23–25]

Injection-locked oscillators also permit the simultaneous measurement of amplitude and phase variations; however, the gains for the in-phase and quadrature components are not the same. It is of interest, therefore, to ascertain whether the locked oscillator obeys the uncertainty principle as it applies to a simultaneous measurement. The amplitude gain follows from (2.7) with $\Omega \to 0$:

$$G_a^2 = \left| \frac{\langle \Delta a \rangle}{\langle \Delta b \rangle} \right|^2 = |\kappa \tau_a \cos\phi_0|^2 = \frac{\kappa^2 \tau_a^2}{1 + (\omega - \omega_0)^2 \tau_p^2} . \tag{3.10}$$

The measurement of b within an observation time T is subject to fluctuations referred to the input by division by G_a^2:

$$\langle \Delta b_T^2 \rangle_{\rm av} = W_{\Delta a}(\Omega=0) \frac{2\pi}{T} \frac{1}{G_a^2} = \frac{1}{2} \frac{N_2}{N_2 - N_1} \left[1 + \frac{\tau_e}{\tau_0} \right] \frac{[1 + (\omega - \omega_0)^2 \tau_p^2]^2}{[1 + (\omega - \omega_0)^2 \tau_a \tau_p]^2} . \tag{3.11}$$

For $(\omega - \omega_0) \to 0$ the above reduces to the result of the linear amplifier. The product $\langle \Delta b_T^2 \rangle_{\rm av} \langle \Delta \phi_T^2 \rangle_{\rm av}$ can be made to approach the ideal limit for a simultaneous measurement in the limit of no detuning, strong overcoupling, and complete inversion. The product increases with increased detuning, because $\tau_p > \tau_a$ for a locked oscillator. [Compare the definitions of $1/\tau_a$ and $1/\tau_p$, (2.10) and (2.11), respectively.]

IV. FOKKER-PLANCK EQUATION FOR c-NUMBER INJECTION SIGNAL

In the preceding sections we used the Langevin approach to obtain expressions for the spectra of the fluctuations. The Fokker-Planck equation leads to the probability distributions of amplitude and phase. The Fokker-Planck equation for the P distribution of Ref. 11, pp. 294–295, Eq. (25), corrected for the erroneously omitted term describing diffusion in the radial direction, reads

$$\frac{\partial P}{\partial t} = -\frac{1}{2} \frac{1}{r} \frac{\partial}{\partial r} \left[r^2 \left[\mathscr{A} - \frac{\omega_0}{Q} - \mathscr{B} r^2 \right] P \right] + \frac{\mathscr{A}}{4} \frac{1}{r} \frac{\partial}{\partial r} \left[r \frac{\partial P}{\partial r} \right] + \frac{\mathscr{A}}{4} \frac{1}{r^2} \frac{\partial^2}{\partial \theta^2} P . \tag{4.1}$$

Here, polar coordinates are used and the α parameter is written

$$\alpha = r e^{i\theta} .$$

Equation (4.1) was obtained by assuming an "injection" of active particles in the upper state. The lower state is populated as the result of the interaction of the particles with the field, resulting in the reduction by $\mathscr{B} r^2$ of the gain parameter $\mathscr{A}$.

The equation of motion is a diffusion equation with a forcing term in the radial direction, the first derivative with respect to r, that tends to confine the P distribution in the radial direction. An initial delta function distribution $P(\alpha) = \delta(\alpha - \alpha_0)$, diffuses from α_0 and, as a function of time, spreads in both θ directions. The natural time dependence $\exp(-i\omega_0 t)$, where ω_0 is the frequency of the oscillator, has been factored out.

Next, recall the origin of the Fokker-Planck equation which was derived through integration by parts of the equation for the density matrix

$$\rho \equiv \int d^2\alpha P(\alpha) |\alpha\rangle\langle\alpha| ,$$

where

$$\dot{\rho} = \int d^2\alpha \frac{\partial P}{\partial t} |\alpha\rangle\langle\alpha|$$

$$= \int d^2\alpha\, \alpha \left[\mathscr{A} - \frac{\omega_0}{Q} - \mathscr{B} |\alpha|^2 \right] P \frac{\partial}{\partial \alpha} |\alpha\rangle\langle\alpha| + \text{c.c.}$$

$$+ \int d^2\alpha\, \mathscr{A} P \frac{\partial^2}{\partial \alpha\, \partial \alpha^*} |\alpha\rangle\langle\alpha| . \tag{4.2}$$

We shall use both (4.1) and (4.2) in extending the analysis to an injection signal.

Suppose that the Hamiltonian used in the derivation of the equation of motion of the density matrix

$$\rho = \int d^2\alpha P(\alpha) |\alpha\rangle\langle\alpha| \tag{4.3}$$

is supplied by the coupling Hamiltonian (1.3). In this section we shall treat the annihilation operator b of the injection signal as a c number. In Sec. V we shall generalize the analysis, treating b as an operator. The time dependence of the density matrix

$$\dot{\rho} = -\frac{i}{\hbar} [\mathscr{H}, \rho] \tag{4.4}$$

is supplemented by

$$[(\kappa b a^\dagger e^{-i(\omega-\omega_0)t}-\kappa b^* a\, e^{i(\omega-\omega_0)t})P(\alpha)\,|\alpha\rangle\langle\alpha|-P(\alpha)\,|\alpha\rangle\langle\alpha|\,(\kappa b a^\dagger e^{-i(\omega-\omega_0)t}-\kappa b^* a e^{i(\omega-\omega_0)t})]$$
$$=P(\alpha)\left[\kappa b^* e^{i(\omega-\omega_0)t}\frac{\partial}{\partial\alpha^*}+\kappa b\, e^{-i(\omega-\omega_0)t}\frac{\partial}{\partial\alpha}\right]|\alpha\rangle\langle\alpha|\,, \quad (4.5)$$

where we have used the identities[11]

$$a\,|\alpha\rangle\langle\alpha|=\alpha\,|\alpha\rangle\langle\alpha|\,,$$
$$a^\dagger|\alpha\rangle\langle\alpha|=\left[\frac{\partial}{\partial\alpha}+\alpha^*\right]|\alpha\rangle\langle\alpha|\,,$$
$$|\alpha\rangle\langle\alpha|\,a=\left[\frac{\partial}{\partial\alpha^*}+\alpha\right]|\alpha\rangle\langle\alpha|\,,$$
$$|\alpha\rangle\langle\alpha|\,a^\dagger=\alpha^*\,|\alpha\rangle\langle\alpha|\,.$$

Equation (4.5) introduced into (4.2) to supplement the interaction Hamiltonian, subsequent integration by parts, lead to the Fokker-Planck equation:

$$\frac{\partial P}{\partial t}=-\left\{\frac{\partial}{\partial\alpha}\left[\alpha\left[\mathscr{A}-\frac{\omega_0}{Q}-\mathscr{B}\,|\alpha|^2\right]P\right]+\text{c.c.}\right\}$$
$$+\mathscr{A}\frac{\partial^2}{\partial\alpha\,\partial\alpha^*}P-\left[\kappa b^* e^{i(\omega-\omega_0)t}\frac{\partial}{\partial\alpha^*}P+\text{c.c.}\right]. \quad (4.6)$$

One may now introduce polar coordinates to clarify the meaning of the above equation. Define the argument of b as $-\psi$, $b=|b|\,e^{-i\psi}$

$$\frac{\partial P}{\partial t}=-\frac{1}{2}\frac{1}{r}\frac{\partial}{\partial r}\left[r^2\left[\mathscr{A}-\frac{\omega_0}{Q}-\mathscr{B}r^2\right]P\right]+\frac{\mathscr{A}}{4}\frac{1}{r}\frac{\partial}{\partial r}\left[r\frac{\partial P}{\partial r}\right]$$
$$+\frac{\mathscr{A}}{4}\frac{1}{r^2}\frac{\partial^2}{\partial\theta^2}P-\kappa\,|b|\,\left[\frac{1}{r}\frac{\partial}{\partial r}r\cos[\theta+(\omega-\omega_0)t+\psi]P-\frac{1}{r}\frac{\partial}{\partial\theta}\sin[\theta+(\omega-\omega_0)t+\psi]P\right]. \quad (4.7)$$

By introducing a new angular variable

$$\phi\equiv(\omega_0-\omega)t-\psi-\theta \quad (4.8)$$

we may transform (4.7) into

$$\frac{\partial}{\partial t}P(r,\phi,t)=-\frac{1}{2}\frac{1}{r}\frac{\partial}{\partial r}\left[r^2\left[\mathscr{A}-\frac{\omega_0}{Q}-\mathscr{B}r^2\right]P\right]+\frac{\mathscr{A}}{4}\frac{1}{r}\frac{\partial}{\partial r}\left[r\frac{\partial}{\partial r}P\right]+\frac{\mathscr{A}}{4}\frac{1}{r^2}\frac{\partial^2}{\partial\phi^2}P$$
$$+(\omega-\omega_0)\frac{\partial P}{\partial\phi}-\kappa\,|b|\,\left[\frac{1}{r}\frac{\partial}{\partial r}(r\cos\phi\,P)-\frac{1}{r}\frac{\partial}{\partial\phi}(\sin\phi\,P)\right]. \quad (4.9)$$

This is the desired locking equation.

Before we proceed with its analysis we want to show that it is of more general validity than its derivation implies. We have assumed that the injection signal was a c-number source. Yet, we are interested in a full quantum-mechanical analysis of a locked oscillator. One may question, therefore, whether the results obtained from (4.9) ignore some quantum noise effects. This is not the case. In Sec. V we shall show that Eq. (4.9) is valid, if the injection signal is a coherent state of another system separated from the oscillator by an isolator at zero temperature so that the coherent state can be defined independent of the evolution of the excitation in the oscillator. Of course, the isolator is responsible, in part, for the zero-point fluctuations of the injection source. The parameter b in (4.9) has to be interpreted as the eigenvalue β of the coherent state of the injection signal, $b=\beta$.

V. FOKKER-PLANCK EQUATION FOR OPERATOR INJECTION SIGNAL

In Sec. IV, we have treated the injection signal amplitude b as a c number. Consider now the case when the injection signal is treated as an operator. The density matrix of the combined system is now

$$\rho=P(\alpha,\beta)\,|\alpha\rangle\langle\alpha|\otimes|\beta\rangle\langle\beta|\,,$$

where $|\beta\rangle\langle\beta|$ is the matrix of the states of the injected signal. The coupling term (4.5) has to be generalized to account for the operator nature of b. We note the property of the operator product $b^\dagger a$:

$$b^\dagger a\,|\alpha\rangle\langle\alpha|\otimes|\beta\rangle\langle\beta|=\left[\frac{\partial}{\partial\beta}+\beta^*\right]\alpha\,|\alpha\rangle\langle\alpha|\otimes|\beta\rangle\langle\beta|$$

and analogous relations for the pre- and post-multiplication by $ba^\dagger$ and $b^\dagger a$. The result is

$$(\kappa b a^{\dagger} e^{i(\omega_0-\omega)t}-\kappa a b^{\dagger} e^{i(\omega-\omega_0)t})\,|\alpha\rangle\langle\alpha|\otimes|\beta\rangle\langle\beta|-|\alpha\rangle\langle\alpha|\otimes|\beta\rangle\langle\beta|\,(\kappa b a^{\dagger} e^{i(\omega_0-\omega)t}-\kappa a b^{\dagger} e^{i(\omega-\omega_0)t})$$

$$=\left[-e^{i(\omega-\omega_0)t}\kappa\alpha\frac{\partial}{\partial\beta}+e^{i(\omega_0-\omega)t}\kappa\beta\frac{\partial}{\partial\alpha}+e^{i(\omega-\omega_0)t}\kappa\beta^*\frac{\partial}{\partial\alpha^*}-e^{i(\omega_0-\omega)t}\kappa\alpha^*\frac{\partial}{\partial\beta^*}\right]|\alpha\rangle\langle\alpha|\otimes|\beta\rangle\langle\beta|\,. \quad (5.1)$$

Integration by parts transfer the derivatives onto P, so that the equation of motion for P becomes [compare (4.6)]

$$\frac{\partial P}{\partial t}=\left\{-\frac{\partial}{\partial\alpha}\left[\alpha\left[\mathscr{A}-\frac{\omega_0}{Q}-\mathscr{B}\,|\alpha|^2\right]P\right]+\text{c.c.}\right\}+\mathscr{A}\frac{\partial^2}{\partial\alpha\,\partial\alpha^*}P$$

$$+\left[-\left[\kappa e^{i(\omega-\omega_0)t}\beta^*\frac{\partial}{\partial\alpha^*}-\kappa e^{i(\omega_0-\omega)t}\alpha^*\frac{\partial}{\partial\beta^*}\right]P+\text{c.c.}\right]. \quad (5.2)$$

We can integrate P over all β. Then, the terms containing derivatives with respect to β and β^* integrate to zero. The equation of motion for $\int d^2\beta P$ is

$$\frac{\partial}{\partial t}\int d^2\beta P=\left\{-\frac{\partial}{\partial\alpha}\left[\alpha\left[\mathscr{A}-\frac{\omega_0}{Q}-\mathscr{B}\,|\alpha|^2\right]\int d^2\beta P\right]+\text{c.c.}\right\}$$

$$+\mathscr{A}\frac{\partial^2}{\partial\alpha\,\partial\alpha^*}\int d^2\beta P+\left[-\left[\kappa e^{i(\omega-\omega_0)t}\frac{\partial}{\partial\alpha^*}\right]\int d^2\beta\beta^* P+\text{c.c.}\right]. \quad (5.3)$$

This is the Fokker-Planck equation for an oscillator, described in terms of a P distribution of α states, locked by injection of β states. In general, the oscillator system reacts back onto the injection-signal system. Another equation would have to be written down for it. If an isolator (at zero degrees) is inserted between the oscillator and the injection-signal system, the latter may be treated as unaffected by the former, except of course that energy is being lost by it to the oscillator. One may imagine it to be continually prepared in sequences of β states assigned to time intervals T.

If the injection signal is in a β state, the integral over all β of $\beta^* P$ can be replaced by $\beta^*\int d^2\beta P$. Then, interpreting $\int d^2\beta P$ as the reduced P distribution one finds that (5.3) and (4.6) are in one-to-one correspondence if β is interpreted as b, and P as $\int d^2\beta P$ of the full P distribution. In the sequel we shall use the notation of Sec. IV with the understanding that we are treating the case of locking via a coherent β state.

VI. FLUCTUATIONS DERIVED FROM FOKKER-PLANCK EQUATION

In Sec. IV we have derived the Fokker-Planck equation for a c-number injection signal. In Sec. V we showed that the same equation follows for an injection signal that is in a coherent state; the eigenvalue β of the coherent state can be identified with the amplitude of the c-number source. In this section we shall study the mean-square fluctuations predicted by the Fokker-Planck equation and compare them with the results obtained from the operator Langevin equations. Because we assumed a coherent state injection signal we are covering only the case of zero excess noise of the injection signal.

Consider first (4.1), the equation of the free-running oscillator. In the steady state, $(\partial/\partial t)P=0$, the phase is random, $(\partial/\partial\theta)P=0$. The first derivative with respect to r provides a forcelike restoring action that makes P cluster around the equilibrium value $r=a_0$, for which

$$\mathscr{A}-\frac{\omega_0}{Q}-\mathscr{B}a_0^2=0\,. \quad (6.1)$$

The equation is solved approximately by expanding

$$r\left[\mathscr{A}-\frac{\omega_0}{Q}-\mathscr{B}r^2\right]$$

around $r=a_0$:

$$-r\left[\mathscr{A}-\frac{\omega_0}{Q}-\mathscr{B}r^2\right]=2\mathscr{B}a_0^2(r-a_0)$$

$$=2\left[\mathscr{A}-\frac{\omega_0}{Q}\right](r-a_0)\,. \quad (6.2)$$

The P distribution can be integrated directly from (6.2)

$$P(r)=\frac{1}{\sqrt{2\pi}\sigma_r}\exp-\frac{(r-a_0)^2}{2\sigma_r^2} \quad (6.3)$$

with

$$\sigma_r^2\equiv(4\mathscr{B}a_0^2/\mathscr{A})^{-1}\,. \quad (6.4)$$

The distribution is Gaussian around the average value $r=a_0$. Note that the first derivative term with respect to r provides a stabilizing effect around $r=a_0$ and that its coefficient is positive.

The locking of the oscillator by the injection signal has two effects represented by the new terms, derivatives with respect to r and ϕ. The derivative with respect to ϕ provides a forcelike restoring action on the phase analogous to the restoring "force" on the amplitude of the free-running oscillator. This term can be interpreted by expanding it around ϕ_0, the phase for which the argument of the derivative $(\partial/r\partial\phi)$ vanishes. Write $r=a_0+\delta r$, $\phi=\phi_0+\delta\phi$. Then

$$(\omega-\omega_0)r+\kappa|b|\sin\phi=(\omega-\omega_0)a_0+\kappa|b|\sin\phi_0 +(\omega-\omega_0)\delta r+\kappa|b|\cos\phi_0\,\delta\phi\ . \tag{6.5}$$

The zeroth-order part of the above equation vanishes when

$$\omega_0-\omega=\frac{\kappa|b|\sin\phi_0}{a_0} \tag{6.6}$$

which is identical in form with (2.12).

The second effect of locking is the increase of the amplitude a_0 from the value imposed by (6.1) in the free-running case. Expansion of the terms under the derivative $(1/r)(\partial/\partial r)r$ in (4.1) around a_0 and ϕ_0 gives

$$\frac{1}{2}r\left[\mathscr{A}-\frac{\omega_0}{Q}-\mathscr{B}r^2\right]+\kappa|b|\cos\phi =\frac{1}{2}a_0\left[\mathscr{A}-\frac{\omega_0}{Q}-\mathscr{B}a_0^2\right] +\kappa|b|\cos\phi_0-\mathscr{B}a_0^2\delta r-\kappa|b|\sin\phi_0\,\delta\phi\ . \tag{6.7}$$

The zeroth-order term gives the new equation for the amplitude a_0 as affected by the injection signal and corresponds to (2.7). The perturbation term may be approximated, in the limit of $|b|/a_0\ll 1$, large gain, by

$$-\mathscr{B}a_0^2\delta r-\kappa|b|\sin\phi_0\,\delta\phi=-\frac{1}{\tau_a}\delta r-(\omega-\omega_0)a_0\,\delta\phi\ , \tag{6.8}$$

where we have used (2.10) and (6.6). When (6.5)—(6.8) are introduced into (4.9) one obtains the "linearized" version of the Fokker-Planck equation with $x\equiv\delta r$ and $y\equiv a_0\delta\phi$ as the independent variables. A change of variables to the Cartesian coordinates x and y gives

$$\frac{\partial}{\partial t}P(x,y,t)=\frac{\partial}{\partial x}\left[\frac{1}{\tau_a}x+(\omega_0-\omega)y\right]P +\frac{\mathscr{A}}{4}\left[\frac{\partial^2}{\partial x^2}+\frac{\partial^2}{\partial y^2}\right]P +\frac{\partial}{\partial y}\left[\frac{1}{\tau_p}y-(\omega_0-\omega)x\right]P\ , \tag{6.9}$$

where we have set

$$\frac{\kappa|b|}{a_0}\cos\phi_0=\frac{1}{\tau_p} \tag{6.10}$$

in analogy with (2.11).

The steady-state solution of (6.9) is obtained with the Gaussian ansatz

$$P\propto\exp[-\tfrac{1}{2}(A_{xx}x^2+2A_{xy}xy+A_{yy}y^2)]\ . \tag{6.11}$$

Equating equal powers of x and y one obtains four equations for the three unknowns A_{xx}, A_{yy}, and A_{xy}. These equations are not independent and have the solution:

$$A_{xx}=\frac{4}{\mathscr{A}}\frac{\left[\frac{1}{\tau_p}+\frac{1}{\tau_a}\right]\left[\frac{1}{\tau_a}\left[\frac{1}{\tau_a}+\frac{1}{\tau_p}\right]+2(\omega-\omega_0)^2\right]}{\left[\frac{1}{\tau_a}+\frac{1}{\tau_p}\right]^2+4(\omega-\omega_0)^2}\ , \tag{6.12}$$

$$A_{yy}=\frac{4}{\mathscr{A}}\frac{\left[\frac{1}{\tau_p}+\frac{1}{\tau_a}\right]\left[\frac{1}{\tau_p}\left[\frac{1}{\tau_a}+\frac{1}{\tau_p}\right]+2(\omega-\omega_0)^2\right]}{\left[\frac{1}{\tau_a}+\frac{1}{\tau_p}\right]^2+4(\omega-\omega_0)^2}\ , \tag{6.13}$$

and

$$A_{xy}=\frac{4}{\mathscr{A}}(\omega_0-\omega)\frac{\frac{1}{\tau_a^2}-\frac{1}{\tau_p^2}}{\left[\frac{1}{\tau_p}+\frac{1}{\tau_a}\right]^2+4(\omega-\omega_0)^2}\ . \tag{6.14}$$

The probability distribution is indicated in Fig. 4 in the (r,ϕ) plane. The x and y coordinates parallel to the amplitude and phase perturbations, respectively, are also indicated. When the injection signal is detuned from the

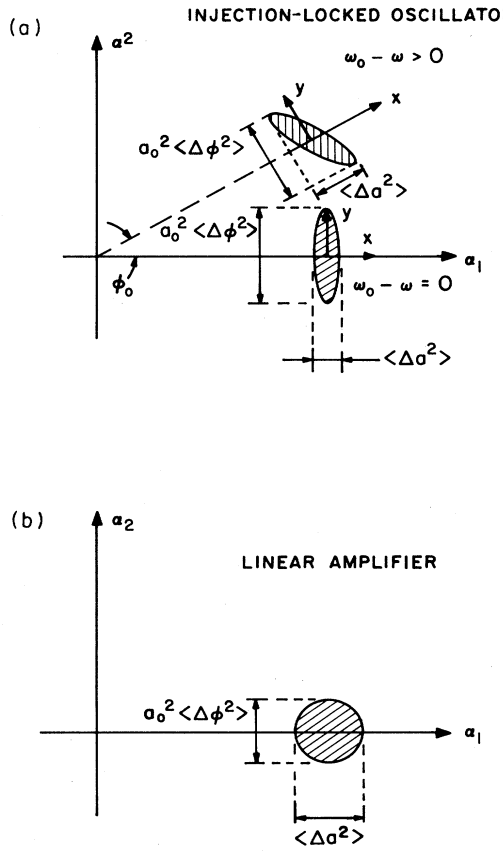

FIG. 4. P distribution of injection-locked oscillator (a) and linear amplifier (b) in α plane.

natural frequency of the oscillator, $\omega \neq \omega_0$, then the two-dimensional Gaussian has principal axes that are not parallel to x and y, respectively; the phase and amplitude fluctuations are correlated.

The present results are easily compared with the results of Sec. II when $\omega=\omega_0$. We shall look at this case in detail. Consider the mean-square phase deviations of (6.9) for $\omega_0-\omega=0$, $A_{xy}=0$,

$$\langle \delta\phi^2 \rangle_{\text{av}} = \frac{1}{A_{yy} a_0^2} = \frac{\mathscr{A}}{4a_0^2}\tau_p \ . \tag{6.15}$$

In the derivation of (4.1) it had been assumed that the laser medium is in the upper state in the absence of saturation. The saturation reduces the gain so that one may identify the unsaturated gain parameter $\mathscr{A}$, divided by the saturated gain, with the ratio of the upper level population N_2, to the difference between upper and lower level populations:

$$\frac{\mathscr{A}}{\mathscr{A}-\mathscr{B}a_0^2} = \frac{N_2}{N_2-N_1}$$

and no level degeneracy has been considered. The saturated gain is approximately equal to ω_0/Q. Thus, we may write for (6.15)

$$\langle \delta\phi^2 \rangle_{\text{av}} = \frac{\omega_0}{Q}\frac{1}{4a_0^2}\tau_p \frac{N_2}{N_2-N_1} \ . \tag{6.16}$$

Next we introduce the average photon number of the injection signal, $|b|^2=\langle n_s \rangle_{\text{av}}$, using the gain at synchronism derived from (2.4)

$$\langle \delta\phi^2 \rangle_{\text{av}} = \frac{\omega_0}{Q}\frac{1}{4\langle n_s \rangle_{\text{av}}}\frac{1}{\kappa^2\tau_p}\frac{N_2}{N_2-N_1} \ . \tag{6.17}$$

The phase fluctuations have a Lorentzian spectral profile (see Sec. II) that occupies a bandwidth proportional to $1/\tau_p$. The phase measurement of the source requires only a bandwidth B equal to $1/2T$, where T is the time of "observation" of the source. Thus, if a filter is introduced that cuts out the unnecessary part of the spectrum, the mean-square fluctuations are reduced by the factor $4B\tau_p=2\tau_p/T$ (see Appendix B) so that one has for the filtered mean-square fluctuations

$$\begin{aligned}\langle \delta\phi_T^2 \rangle_{\text{av}} &= \frac{\omega_0}{Q}\frac{1}{2\langle n_s \rangle_{\text{av}}}\frac{1}{\kappa^2 T}\frac{N_2}{N_2-N_1} \\ &= \frac{1}{2\langle n_s \rangle_{\text{av}}}\left[1+\frac{\tau_e}{\tau_0}\right]\frac{N_2}{N_2-N_1} \ ,\end{aligned} \tag{6.18}$$

where we have used (1.9). This is the same result as (2.32) for $\omega_0-\omega=0$. An analogous investigation of the mean-square amplitude fluctuations $\langle \Delta r^2 \rangle_{\text{av}}$ confirms the result of Sec. III at synchronism. The analysis of locking off synchronism is considerably more complicated and is not presented here. The following issues have to be confronted: (a) The mean-square deviation of the amplitude and phase are equal to the diagonal elements of the inverse of the matrix

$$\begin{bmatrix} A_{xx} A_{xy} \\ A_{xy} A_{yy} \end{bmatrix} \ .$$

(b) The spectrum of the fluctuations off synchronism is given by (2.29) and (2.30), respectively. The filter of bandwidth B selects the portion $4\pi B$ of the overall spectrum at $\Omega=0$. When the analysis is carried out the results of Secs. II and III in the general case, $\omega \neq \omega_0$, are fully confirmed.

We have used the spectral information obtained from the Langevin equations to derive the filtered mean-square fluctuations from the total mean-square fluctuations of the steady-state solution of the Fokker-Planck equation. Alternately, one could have derived the spectrum from the time-dependent solution of the Fokker-Planck equation. The time-dependent Fokker-Planck equation yields the time evolution of an initial impulse of the probability distribution in the x-y plane. The autocorrelation functions

$$\langle x(t)x(t+\tau) \rangle_{\text{av}}$$

and

$$\langle y(t)y(t+\tau)_{\text{av}}$$

can be derived from this information. The spectra are the Fourier transforms of the autocorrelation functions. The same result is obtained as from the Langevin equations, albeit with considerably more effort.

Finally, we note that according to (4.6) we have related the results of the Langevin equation to the mean-square fluctuations of $\alpha=re^{i\theta}$, and not those of the field operator a. In doing so we have ignored the mean-square fluctuations associated with an α state. Because the mean-square fluctuations found are large compared with the mean-square spread associated with an α state, the approximation, applicable in the limit of high gain, is a legitimate one.

VII. DISCUSSION

The operator Langevin equation leads rather directly to the spectra of the amplitude and phase fluctuations of a locked oscillator. The two spectra differ in the case of the oscillator, become identical for the modulated amplifier. The locked oscillator provides a means for the quantum measurement of the phase of the injection signal. It does not give minimum uncertainty. In the limit of complete inversion and negligible internal loss the excess fluctuation is 3 dB higher than the ideal limit. We interpreted this result with the aid of the linear amplifier which does offer an ideal *simultaneous* quantum measurement of amplitude and phase in the limit of complete inversion and negligible internal loss. Such a measurement requires doubling of the minimum uncertainty of each of the complementary variables. The phase noise of the locked oscillator can be understood from another point of view: It can be interpreted as frequency-noise to phase-noise conversion of the oscillator. The spectrum of the frequency modulation noise $W_{\Delta\omega}(\Omega)$ of the self-oscillating laser follows from (2.29), with $1/\tau_p=0$ and $\omega-\omega_0=0$

$$W_{\Delta\omega}(\Omega)=\Omega^2 W_{\Delta\phi}(\Omega)=\frac{\omega_0/Q}{4\pi a_0^2}\frac{N_2}{N_2-N_1} \ . \tag{7.1}$$

The frequency-to-phase conversion factor is obtained from (2.5) and (2.11)

$$\frac{d\phi}{d\omega_0}=-\frac{a_0/\kappa b_0}{\cos\phi_0} . \tag{7.2}$$

Combining (7.1) and (7.2) we find

$$W_{\Delta\phi}(\Omega)=W_{\Delta\omega}(\Omega)\left[\frac{d\phi}{d\omega_0}\right]^2=\frac{\omega_0/Q}{4\pi\kappa^2 b_0^2\cos^2\phi_0}\frac{N_2}{N_2-N_1}$$

and thus

$$\langle\Delta\phi^2\rangle=\frac{2\pi}{T}W_{\Delta\phi}(\Omega)=\frac{1}{2b_0^2\cos^2\phi_0}\frac{N_2}{N_2-N_1}\left[1+\frac{\tau_e}{\tau_0}\right]$$

which is equal to the phase noise of the locked oscillator (6.18) for $\cos\phi_0=1$.

The Fokker-Planck approach gives the probability distribution of amplitude and phase. The uncertainty of a measurement cannot be determined from it directly without information on the spectra of phase and amplitude which is obtained most conveniently from the Langevin approach. Of course, the information on the spectrum is contained in the Fokker-Planck equation as well but requires a greater effort of extrication.

ACKNOWLEDGMENT

This work was supported in part by the U.S. Joint Services Electronics Program under Contract No. DAAG-29-83-K-003.

APPENDIX A: THE EXPECTATION OF EQ. (1.8)

We explore the expectation of Eq. (1.8) as applied to the cavity with no gain

$$\frac{d}{dt}\langle a\rangle=-\left[\frac{1}{\tau_e}+\frac{1}{\tau_0}\right]\langle a\rangle+\kappa\langle b\rangle . \tag{A1}$$

The system is conservative when $1/\tau_0=0$. In this limit one may apply time reversal considerations to the system. Consider the unexcited cavity, with $\langle b\rangle=0$. Thus, $\langle a\rangle$ decays because energy escapes from the resonator at the rate $2/\tau_e$.

The rate of energy escape is $2\hbar\omega_0/\tau_e\,|\langle a\rangle|^2$. This has to equal to the power carried away from the resonator (see Fig. 1). When this solution is time reversed, the power flow is reversed and travels toward the resonator. The buildup rate of energy is now $2/\tau_e$. From (A1)

$$\frac{d}{dt}|\langle a\rangle|^2=\frac{2}{\tau_e}|\langle a\rangle|^2=\frac{\kappa^2|\langle b\rangle|^2}{2/\tau_e} . \tag{A2}$$

But

$$|\langle b\rangle|^2=\frac{2}{\tau_e}\langle a\rangle^2 T , \tag{A3}$$

where T is the sampling time for b. Introducing (A3) into (A2) we find

$$\kappa^2=\frac{2}{\tau_e T} .$$

This is the desired relation.

APPENDIX B: THE FILTERING OF PHASE FLUCTUATIONS

We have stated in the text that a filter of bandwidth B reduces the mean-square fluctuations of the phase by a factor of $4B\tau_p$, where τ_p is the response time of the phase. We prove this statement here.

In Sec. II we find that the spectrum of the phase is Lorentzian of the form

$$H(\Omega)=\frac{1}{1+\Omega^2\tau_p^2} , \tag{B1}$$

where τ_p is the decay time of the phase and $H(\Omega)$ is assigned unity amplitude at $\Omega=0$. The area of $H(\Omega)$ is

$$\int_{-\infty}^{\infty}H(\Omega)d\Omega=\int_{-\infty}^{\infty}\frac{d\Omega}{1+\Omega^2\tau_p^2}=\pi/\tau_p . \tag{B2}$$

A filter with flat response over a bandwidth B ($\ll 1/\tau_p$) in Hz passes a portion $4\pi B$ of the (two-sided) spectrum. Thus, the ratio of the total mean-square fluctuations [integral over all Ω of $H(\Omega)$] to the mean-square fluctuations passed by the filter is

$$\frac{4\pi B}{\pi/\tau_p}=4B\tau_p . \tag{B3}$$

The sampling time T is related to the bandwidth B by the Nyquist criterion

$$B=1/2T .$$

Thus, the fraction $4B\tau_p$ can be written

$$4B\tau_p=2\tau_p/T . \tag{B4}$$

---

*On leave from Musashino Electrical Communication Laboratory, Nippon Telegraph and Telephone Public Corporation, Japan.

[1]H. Haken, Z. Phys. 181, 96 (1964).

[2]H. Haken, Phys. Rev. Lett. 13, 329 (1964).

[3]H. Haken, Z. Phys. 190, 327 (1966).

[4]H. Haken, in *Encyclopedia of Physics, XXXV 12C,* edited by S. Flugge (Addison-Wesley, Reading, Mass., 1974).

[5]M. Lax, Phys. Rev. 145, 110 (1966).

[6]M. Lax, in *Physics of Quantum Electronics,* edited by P. L. Kelley *et al.* (McGraw-Hill, New York, 1966).

[7]M. Lax and W. H. Louisell, Phys. Rev. 185, 568 (1969).

[8]M. Lax and W. H. Louisell, IEEE J. Quant. Electron. QE-3, 47 (1967).

[9]M. Lax and M. Zwanziger, Phys. Rev. A 7, 750 (1973).

[10]M. O. Scully and W. E. Lamb, Jr., Phys. Rev. 159, 208 (1967).

[11]M. Sargent, III, M. O. Scully, and W. E. Lamb, Jr., *Laser Physics,* (Addison-Wesley, Reading, Mass., 1974).

[12]L. Mandel and E. Wolf, Rev. Mod. Phys. 37, 231 (1965).

[13]A. Javan, W. R. Bennett, Jr., and D. R. Herriott, Phys. Rev. Lett. 6, 106 (1961).

[14]J. W. Klüver, J. Appl. Phys. 37, 2987 (1966).

[15]H. A. Haus and J. A. Mullen, Phys. Rev. 128, 2407 (1962).

[16]C. Freed and H. A. Haus, Phys. Rev. 141, 287 (1968).

[17]J. Armstrong and A. W. Smith, Phys. Rev. 140, A155 (1965).

[18]T. A. Dorschner, H. A. Haus, M. Holz, I. W. Smith, and H.

Statz, IEEE J. Quant. Electron. QE-16, 12 (1980).
[19]Y. Yamamoto and T. Kimura, IEEE J. Quant. Electron. QE-17, 919 (1981).
[20]R. L. Stratonovich, *Topics in the Theory of Random Noise* (Gordon and Breach, New York, 1967), Vol. II.
[21]H. Haken, H. Sauermann, Ch. Schmid, and H. D. Vollmer, Z. Phys. 206, 369 (1967).
[22]W. W. Chow, M. O. Scully, and E. W. Van Stryland, Opt. Commun. 15, 6 (1975).
[23]H. A. Haus and C. H. Townes, Proc. IRE 50, 1544 (1962).
[24]E. Arthurs and J. L.Kelly, Jr., Bell Syst. Tech. J. 44, 725 (1965).
[25]C. M. Caves, Phys. Rev. D 26, 1817 (1982).